Deep Contrastive Learning for Feature Representation in Historical Maps

Antonio León Villares

4th Year Project Report
Computer Science and Mathematics
School of Informatics
University of Edinburgh

2023

Abstract

Physical sources of knowledge, such as historical maps, have been increasingly digitised, making them more available to the wider public. However, investigating certain features within these maps remains challenging, particularly if there are a lot of maps. In this project, I investigate how contrastive learning can be used to not only find common features across maps from different time periods, but to numerically score the degree of similarity between these features. Through contrastive learning, I convert patches from maps into vectorised representations in some latent space. These representations can then be used to compute a similarity score between patches, with which the most similar patches can be found, thus allowing a quick and efficient search of specific features across many maps. I develop a novel way of evaluating the capacity of contrastive models to identify positive pairs correctly. Moreover, I employ proxy tasks to better understand how the representations learnt by 2 different contrastive models encode these features. I found that using `SimCLR` leads to more discriminative representations, which are better at finding patch pairs containing the same set of features. Meanwhile, `BYOL` learns representations which are more semantic in nature, and thus can be useful to more broadly explore feature combinations across maps. Finally, I propose a new contrastive framework, `GeoSimCLR`, aimed at encoding both visual and contextual similarity. I compare this with `SimCLR` and `BYOL` by using clustering, which helps reveal how the representations are structured in latent space.

Contents

Chapter 1

Background

1.1 Motivation

With the rise of technology, we have been able to digitise physical sources of knowledge, both textually (books, manuscripts, plays) and visually (images, maps, sketches). Being able to efficiently understand, explore and analyse these digitised sources is particularly critical, should we want to gain important historical knowledge. This is especially true for historical maps, as they contain a plethora of information showcasing how human settlements have varied over time. However, for highly detailed maps, manually searching for changing features is arduous, especially if we want to comprehensively study these changes not only over different time periods, but also using information present from different map styles. Nonetheless, doing so automatically is also highly non-trivial: a system would need to be capable of understanding the difference between permanent features (such as buildings, roads and rivers) and dynamic features (such as text labels, shadings and legend style).

To this end, I believe that deep learning is a sensible way of tackling such a problem, given its demonstrated capacity over the last few years to automatically learn key attributes in images. In particular, in this project I seek to learn common features across temporally-spaced maps from the NLS (National Library of Scotland) through the use of contrastive learning (CL). This technique allows us to translate the notion of image similarity to similarity in some latent representation space, which can be leveraged to explore shared features across different maps. Whilst simpler methods could be employed to extract and compare these features, CL architectures are trained with the objective of assessing the degree of similarity between different images. Lastly, I have taken this as an opportunity to compare the types of attributes which are learnt by two different contrastive methods, not only by seeing how these methods score similarity between regions, but also by employing the latent representations in downstream tasks.

1.2 Related Work

1.2.1 Deep Learning and Maps

Different deep learning techniques have been employed on maps, particularly for text/object detection. The work by Hosseini et al. [1] is of particular relevance, since they used historical maps from the NLS to develop a deep learning, computer vision library. One of their aims was to, for example, identify railways in these maps, for which they used a `ResNet` [2] (Residual Neural Network), trained on augmented versions of patches taken from the maps, for classification (admittedly with around 30 million, very high resolution patches - this might go beyond the scope and computational capacity of this project). They also deal with false positives by gauging contextual information (if a railway was found in an "isolated" patch, this is probably a misclassification). Post-processing steps such as these, which exploit the rich contextual information of maps, could be a useful technique to improve the learnt representations. Another very interesting technique which they apply is that, alongside the patch, they provide a larger "contextual" patch (containing the patch used for classification). Information from the patch and its context can then be used to train a more powerful model. Maps from the NLS have been used in a variety of other publications and projects. For instance, Li [3] applied a CycleGAN [4] to convert OpenStreetMap [5] images into the style of historical maps. Li et al. [6] worked on using OCR, alongside deep neural networks, to extract text from historical maps (amongst which were some from the NLS), and use this to generate meta-labels for the maps, by using geolocation based on the extracted text. In fact, extracting text has been the focus of many map-related projects. In this dissertation by Kai Williams, they developed deep learning models for extracting symbols (i.e trees) and text from the historical maps provided by the NLS.

1.2.2 Contrastive Learning

CL is a form of self-supervised learning (SSL), whereby a model only has access to unlabelled, training data, which it uses to derive labels/representations that can then be used to tackle a downstream supervised or unsupervised task. In this regard, SSL is a crucial technique, since data labelling is a time-intensive and expensive process [7].

Whilst CL has applications in other fields, it has been employed extensively in computer vision tasks, where learning and representing visual similarity might be critical. CL algorithms generally follow a similar workflow. We start with raw, unlabelled images, which are augmented (using a range of transformations, such as cropping, resizing, noise addition, blurring, colour jittering) to generate what are known as positive and negative training pairs. Positive pairs correspond to two different augmentations of the same image, whilst negative pairs are augmentations of different images. The contrastive algorithm learns to think of positive pairs as similar, whilst also learning to think of negative pairs as dissimilar. Generating a good set of positive-negative pairs is crucial for learning useful, contrastive representations, so special care needs to be taken when generating them. For instance, if the positive and negative pairs are easily identifiable as dissimilar, the algorithm might default to learning extremely simple representations, which don't capture the nuanced features that characterise a particular input image [8]. After the positive and negative pairs have been generated, they get passed through the contrastive model, and converted into a vector representation in latent space. The loss for contrastive models encompasses both the level of similarity between positive pairs, alongside the level of dissimilarity between negative pairs. This similarity/dissimilarity is typically defined by the cosine distance of the latent representations, and can be incorporated into the loss in a variety of ways, such as max margin contrastive loss [9], triplet loss [10], n-pair loss (which generalises triplet loss) [11], InfoNCE [12] and NT-Xent Loss (normalised temperature-scaled cross-entropy) [13]. The most well-known CL architectures by far are `SimCLR` [13], `MoCo` [14] and `CPC` [12], which were able to attain nearly supervised-level Top-1 accuracy on `ImageNet` [13]. More recently, `BYOL` [15] was released, which revolutionised the CL paradigm by removing the need for negative samples, whilst obtaining better results than all of the aforementioned methods.

Due to the versatility of CL, it has been employed in a plethora of practical applications beyond benchmarking on `ImageNet` [16]. Medicine has greatly benefited from CL, since human annotated medical images (X-rays, MRIs, CT-Scans, etc...) are scarce [17] [18] [19] [20]. For instance, CL can be applied to obtain better data efficiency in downstream classification tasks, which is particularly important when data is scarce [17]. Furthermore, Chaitanya et al. [20] describes a novel contrastive approach, whereby the contrastive loss is derived by using both global and local features of an image. CL can also be applied beyond the world of images, since it provides a general framework to capture underlying features, which can act as signals. As such, contrastive approaches have been used to develop recommender systems [21], or to represent videos [22], by encoding temporal information between frames.

1.2.3 Contrastive Learning for Geographical Tasks

It is first important to address the fact that many of the CL frameworks described above employ a `ResNet` as an encoder to convert the unlabelled images to latent representations. `ResNets` have also been used for identifying land usage (e.g. is it residential, industrial, agricultural, are there lakes, etc...) from satellite images [23], which indicates its power as an encoder for geographical tasks. However, as demonstrated in Chiang et al. [24], there are many challenges to address when applying a deep Convolutional Neural Network (`CNN`) [25] (such as a `ResNet`) to encode images of historical maps. This is due to the unique nature of maps, which provide a simplified representation of reality. As such, features such as roads, mountains and buildings are represented in a very simplistic manner, as groups of lines. Extracting features from these representations can thus be harder than when faced with the typical images of `ImageNet`, where for each label there are a variety of well-defined, easily-identifiable features. Moreover, this simplicity means that a model can more easily pick up on incorrect features (for example, if a patch of a map cuts off a section of a river, for a `CNN` to identify this correctly will be particularly hard, since it could also be a section of a house). This is particularly the case when small, low-resolution patches are used; for larger, high-resolution patches, `ResNets` should be powerful enough to easily identify the presence of certain features, since such patches inherently contain a lot more information which is harder to misinterpret.

To the best of our knowledge, CL has never been used to learn map representations. However, there have been some uses of CL in geographical applications, particularly from satellite data. Agastya et al. [26] adapted the `SimCLR` architecture to learn representations of images in `BigEarthNet-S2` [27], to then be used for determining the presence of irrigation in images. Perhaps most relevant to the project at hand is the recent work by Ayush et al. [28], who modified the `MoCo` architecture to generate what they called a geography-aware model. They trained 2 models on 2 datasets (a subset of `ImageNet` with geo-tagged metadata, and the remote sensing dataset `fMoW` (Functional Map of the World) [29])). The `fMoW` dataset is of interest because it contains temporally spaced images; this is analogous to the case described here, where we have temporally-spaced and stylistically spaced map images. The authors incorporate these temporal differences to generate positive training pairs within their loss. In addition to generating representations, they also train the model to predict the geo-location of the images. In doing this, they are able to significantly reduce the gap between supervised and SSL performance in a downstream classification task, when compared with the standard `MoCo` architecture. This indicates that using temporal data as "augmentations", alongside training the model to output metadata on the image can be used to bridge the unavoidable gap between supervised and self-supervised performance.

1.3 Goal and Contributions

The goal of this project is to learn representations for historical maps, which can be used to numerically score the degree of similarity between regions, and thus provides an effective way to query different maps in the search for regions with a certain combination of features. To this end, I seek to train 2 different contrastive models, namely `SimCLR` and `BYOL`. To evaluate these models, I propose a set of tasks, known as Positive Pair Identification Tasks. To the best of our knowledge, CL has never been applied for this purpose. Furthermore, I use this as an opportunity to systematically compare the latent representations learnt by the two models. To do this, I explore the degree to which temporal and content information are encoded within these representations. Furthermore, I analyse the effect that different augmentations have on the contrastive similarity scores. Lastly, I develop a new contrastive framework, aimed at encoding both visual and contextual similarity, whose representations I explore by applying clustering.

1.4 Report Structure

I begin this report by explaining the objective of CL, followed by a short explanation on the `SimCLR` and `BYOL` architectures, and how I have adapted them for this project. Afterwards, I explain the data processing pipeline: how I obtained the maps, how they were pre-processed, and how the final dataset was generated for training the contrastive models. Finally, I showcase how the models have been employed, by explaining the experiments performed, the results obtained, and the subsequent conclusions that can be drawn.

Chapter 2

Model Architectures

2.1 Contrastive Learning

Contrastive learning is a learning paradigm by which a model learns to gauge the similarity or dissimilarity between pairs of data points, in a completely self-supervised manner. More explicitly, say we have a set $\mathcal{X}$ of objects (typically images). In contrastive learning, we learn a function f which maps elements in $\mathcal{X}$ to some D-dimensional latent space:

$$f : \mathcal{X} \to \mathbb{R}^D, \quad D \in \mathbb{N}$$

This is done in such a way, so that for some similarity function:

$$\texttt{sim} : \mathbb{R}^D \times \mathbb{R}^D \to \mathbb{R}$$

if x_1, x_2 are similar in $\mathcal{X}$ (that is, they form a positive pair), their embeddings $f(x_1), f(x_2)$ will be similar in latent space (according to `sim`); if on the other hand x_1, x_2 form a negative pair in $\mathcal{X}$, this dissimilarity should also be reflected in latent space.

The most common similarity measure employed in the literature is cosine similarity. Given 2 embeddings in latent space $\underline{z}_1, \underline{z}_2 \in \mathbb{R}^D$, their cosine similarity is given by:

$$\texttt{sim}(\underline{z}_1, \underline{z}_2) = \frac{\underline{z}_1^T \underline{z}_2}{||\underline{z}_1||_2 ||\underline{z}_2||_2} \in [-1, 1]$$

where $\underline{z}_1^T \underline{z}_2$ is the standard dot product, and $|| \cdot ||_2$ is the (Euclidean) `L2` norm. This similarity is nothing but the cosine of the angle between $\underline{z}_1$ and $\underline{z}_2$, whereby perfectly similar vectors are such that $\texttt{sim}(\underline{z}_1, \underline{z}_2) = 1$, whilst perfectly dissimilar vectors are such that $\texttt{sim}(\underline{z}_1, \underline{z}_2) = -1$.

2.2 Models for this Project

For this project I compared the performance of 2 common contrastive architectures, `SimCLR` (**Sim**ple **C**ontrastive **L**earning of **R**epresentations) and `BYOL` (**B**ootstrap **Y**our **O**wn **L**atent). I first provide a general overview, and then explain how I have adapted them to fit the objectives of this project. Lastly, I have deviated slightly from the notation employed by the original `SimCLR` and `BYOL` papers, in order to make the model descriptions more homogeneous and comparable.

2.2.1 `SimCLR`

2.2.1.1 Model Architecture

`SimCLR` learns a representation for an input x, by minimising the contrastive loss between 2 augmentations of x. More specifically, given a set of transformations $\mathcal{T}$, one samples 2 transformations $t_1 \sim \mathcal{T}$ and $t_2 \sim \mathcal{T}$. These include colour jittering, random cropping with flipping (followed by resizing), and random cropping (however, in the original paper they explored the effect of many other transformations, such as random rotations or sobel filtering). t_1 and t_2 are applied to the input to generate augmented views x_1, x_2, which are treated as similar. The augmented views are passed through an encoder f, which generates representation vectors in latent space, $\underline{z}_1 = f(x_1), \underline{z}_2 = f(x_2)$. These representations are projected by a projection head g into some other space, where the contrastive loss is actually computed. Nonetheless, the output of the model (the embedding) will be the representation in latent space *before* passing it through g, since they found that this provided better representations. In the original `SimCLR` (and in most papers utilising this model), f is a pretrained `ResNet50` model. However, instead of using the full network, they take the output of the network at its penultimate layer, which is an average pooling layer. Moreover, the projection head g is a simple multilayer perceptron (`MLP`), with a single hidden layer and ReLU activation.

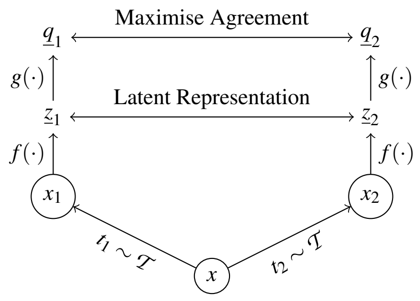
$$\begin{tikzcd}
\underline{q}_1 \arrow[rr, leftrightarrow, "\text{Maximise Agreement}"] & & \underline{q}_2 \\
\underline{z}_1 \arrow[u, "g(\cdot)"] \arrow[rr, leftrightarrow, "\text{Latent Representation}"] & & \underline{z}_2 \arrow[u, "g(\cdot)"'] \\
x_1 \arrow[u, "f(\cdot)"] & & x_2 \arrow[u, "f(\cdot)"'] \\
& x \arrow[ul, "t_1 \sim \mathcal{T}"] \arrow[ur, "t_2 \sim \mathcal{T}"'] &
\end{tikzcd}$$

Figure 2.1: Sketch of the `SimCLR` architecture, adapted from Figure 2 in the original `SimCLR` paper.

2.2.1.2 Loss

`SimCLR` uses NT-XENT as its contrastive loss, as introduced by Sohn [30]. This loss adapts categorical cross-entropy loss, where the contrastive objective is framed as a multi-class classification problem. In particular, this loss seeks representations, such that positive samples have maximised similarity (according to cosine similarity), whilst negative samples have maximised dissimilarity. Given a minibatch of N positive pairs, each positive pair will use the remaining $N-1$ pairs as negative pairs. In particular, if I define:

$$\mathtt{sim\_loss}(\underline{a}, \underline{b}) = \exp\left(\frac{\mathtt{sim}(\underline{a}, \underline{b})}{\tau}\right)$$

the loss for the ith image z^i in the minibatch will be:

$$\ell_i = -\log \frac{\texttt{sim\_loss}(\underline{z}_1^i, \underline{z}_2^i)}{\sum_{k=1}^{N} \mathbb{1}_{k\neq i}\left(\texttt{sim\_loss}(\underline{z}_1^i, \underline{z}_1^k) + \texttt{sim\_loss}(\underline{z}_1^i, \underline{z}_2^k)\right)} - \log \frac{\texttt{sim\_loss}(\underline{z}_1^i, \underline{z}_2^i)}{\sum_{k=1}^{N} \mathbb{1}_{k\neq i}\left(\texttt{sim\_loss}(\underline{z}_2^i, \underline{z}_1^k) + \texttt{sim\_loss}(\underline{z}_2^i, \underline{z}_2^k)\right)}$$

where `sim` is cosine similarity, $\mathbb{1}_{[k\neq i]}$ is an indicator function (evaluates to 1 if and only if $k \neq i$) and τ is a temperature parameter, which modulates the degree of similarity which I want to assign to positive and negative pairs. A higher τ will decrease the similarity terms in the NT-XENT loss, which pushes the model to increase its discriminative power in order to minimise the loss. This means that negative samples will be pushed further apart in representation space, which makes distinguishing between positive and negative pairs easier.

2.2.2 BYOL

2.2.2.1 Model Architecture

Unlike with `SimCLR`, `BYOL` doesn't require negative pairs to learn a representation. To do this, it defines 2 networks: an online network with parameters θ, and a target network with parameters ξ. Critically, ξ is computed as an exponential moving average of θ, and is thus not trained. In particular, for some target decay rate $\tau \in [0,1]$

$$\xi \leftarrow \tau\xi + (1-\tau)\theta$$

`BYOL` solely trains θ, with the purpose of using the online network to predict the output of the target network. To this end, the online network is defined by an encoder f_θ (which converts the input image into a vector), a projector g_θ (which projects the encoded vector into some other space) and a predictor h_θ (which predicts the output vector of the target network from the projected vector). The target network only has an encoder f_ξ and a projector g_ξ. As above, an input image x is augmeneted to produce a positive pair; the first augmentation x_1 is passed through the online network, whilst the second augmentation x_2 is passed through the target network. As with `SimCLR`, once θ has been trained, we only keep f_θ to convert an image into its contrastive embedding. Moreover, the encoders f_θ, f_ξ are also residual networks, whose output will be the final average pooling layer. The projectors g_θ, g_ξ are also `MLPs`, with a single hidden layer and RELU activation, but unlike with `SimCLR`, `BYOL` employs batch normalisation. The predictor h_θ uses the same architecture as g_θ.

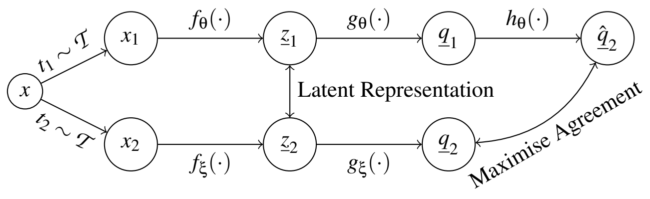

Figure 2.2: Sketch of the `BYOL` architecture, adapted from Figure 2 in the original `BYOL` paper.

2.2.2.2 Loss

Since BYOL requires no negative pairs, and it frames its contrastive problem as a prediction problem, the loss will be the MSE (mean square error) between $\underline{\hat{q}}_2$ and $\underline{q}_2$ (after they have been normalised to unit vectors). Moreover, since the architecture is asymmetric, we do a second pass through the network, but this time with x_2 going through the online network and x_1 going through the target network. Given the ith image z^i in a minibatch of N elements, this is nothing but:

$$\ell_i = 4 - 2\left(\mathtt{sim}(\underline{q}_2^i, \underline{\hat{q}}_2^i) + \mathtt{sim}(\underline{q}_1^i, \underline{\hat{q}}_1^i)\right)$$

where sim is once again cosine similarity.

2.2.3 Project Models

The main difference between my approach and the original SimCLR/BYOL implementations, is that I don't apply any direct data augmentation to generate positive pairs. Instead, much like in the work by Ayush et al. [28], I use temporally-spaced images of historical maps. Due to the time differences, general structure in the images is preserved, but there are certain stylistic changes, such as differences in colour, positioning of legends, legend style, building shading, and so on. I believe that these differences are substantial enough to be considered augmentations, which is why no further processing was performed on these images.

I implemented all the models used in this project (except for the ResNets) from scratch using PyTorch [31]. Whilst there are many implementations of BYOL and SimCLR available online, I wanted to construct a consistent API for the models to make model training and comparison simpler. Beyond this, due to memory constraints I decided to not use ResNet50, and instead opted to consider ResNet18 and ResNet34 (I used the architectures and pretrained weights available from PyTorch: https://pytorch.org/hub/pytorch_vision_resnet/). Note that when using ResNets, images have to be resized to have dimension 224×224, and then normalised in a per-channel basis using:

$$\mu = \mathtt{[0.485,\ 0.456,\ 0.406]} \quad \sigma = \mathtt{[0.229,\ 0.224,\ 0.225]}$$

Furthermore, I wanted to see the effect on learning of using a simple CNN encoder, so somehow following the style of the ResNet encoders, I defined a CNN model which used 5 convolutional layers, with ReLU activation, batch normalisation and max pooling. After the final convolutional layer, average global pooling was applied to generate the encoder output. When using ResNets, I followed the implementation details for SimCLR and BYOL, and used the output of the final global average pooling layer as my latent representation. For both CNN and ResNet models, this results in 512-dimensional embeddings. For the sake of consistency, the MLPs for the SimCLR and BYOL models followed the BYOL structure: a single hidden dimensions, with ReLU activation, and batch normalisation. All the MLPs used 2048 hidden dimensions, and outputted a 256 dimensional vector. Lastly, we used a random seed of 23 for any random process required for this project. In particular, random shuffling was used throughout this whole project when training models, to improve generalisability and convergence.

Chapter 3

Data

In this section, I explain the origin of the historical maps, and how these were processed to generate the data for the project. This data consists of positive pairs, where each pair is composed of patches (square regions from a map) corresponding to the same region but from different maps. I would like to thank Chris Fleet at the NLS for giving me access to all the maps used for this project.

3.1 Obtaining Historical Maps

All the maps used for this project were sourced thanks to the NLS, which contains over 1.5 million sheet maps [32]. From these, approximately 200,000 are available in high resolution at `https://maps.nls.uk`. This project focused on maps of Edinburgh (both the city and surroundings), since there were a lot of these freely available. The NLS contains a plethora of different historical map styles, ranging from the 16th century up until the 20th century. Out of all of these, I wanted to focus on maps which showcased a more modern Edinburgh, as this would provide more applicable results. I also sought georeferenced maps, which have been aligned to a specific geographic coordinate system, as this allowed me to easily visualise temporal differences.

In particular, this project focuses on 25 Inch Ordnance Survey Maps (which I'll call "OS maps" from here onwards). The Ordnance Survey is the national mapping agency of Great Britain [33]. These maps are known as "25 Inch", since every inch of the map corresponds to 25 inches on the ground. These maps are suitable exemplars, since not only are they georeferenced, but I have access to a large number of them: 212 distinct maps, split into 57 distinct regions which together encompass a total area of 278.39 km^2. For each region, either 3 or 4 full maps were made available to me, each of which corresponds to a different time period of production. In particular, I was given 57 maps for the periods 1894-1896, 1906-1908 and 1913-1914; and 41 maps sheets for the period 1933-1947. All these maps are available as `GeoTIFF` files, which are standard `TIFF` (Tag Image File Format) files containing additional metadata, such as bounding boxes and the coordinate system used to georeference the map.

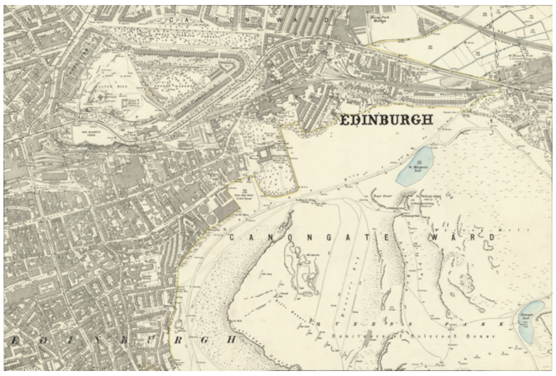
Figure 3.1: An example OS map obtained from the NLS (https://maps.nls.uk/view/82877409).

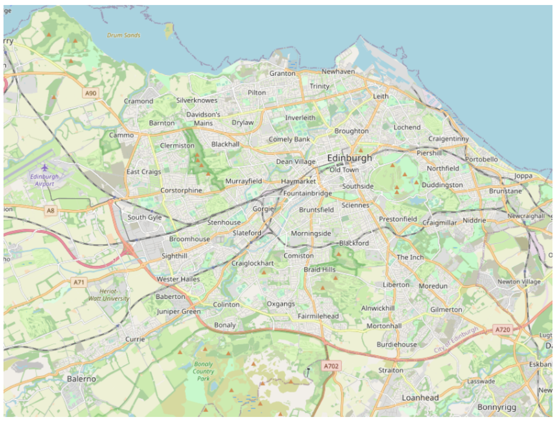
Figure 3.2: The rectangular region encompassed by all the maps. The bottom left corner has longitude-latitude $(-3.38374788940603, 55.8715983250667)$, whilst the top right corner has longitude-latitude $(-3.07422210721001, 56.0020051346329)$. This is an area of $278.39\ km^2$. Image generated using geojson.io (see subsection B.1.1).

The NLS also contains georeferenced maps in different styles, such as "Bartholomew" style maps. However, I chose not to use these, since they had a lower resolution (many OS maps could fit into a single Bartholomew map); they were more blemished than the OS maps (for instance, I found red lines coloured in some Bartholomew maps); and preprocessing them is a lot more challenging, particularly due to their border style (more on this in the next section). Hence, and given that OS maps are more widely used and referenced, I found it unnecessary to produce a dataset containing both OS and Bartholomew maps.

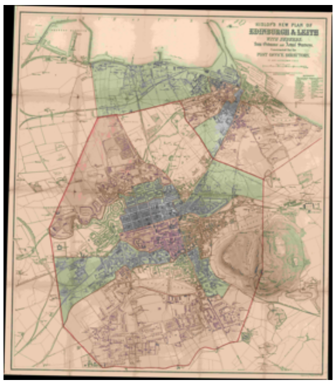
Figure 3.3: An example Bartholomew map. The colourful regions could harm the model's performance. The borders make these maps harder to pre-process. Moreover, this map is oriented vertically, whilst all the OS maps are horizontal.

3.2 Generating Data for Training

3.2.1 Preprocessing the Maps

Before generating a dataset, I pre-processed the maps in 2 steps. Firstly, I rotated and cropped the maps, to rectify scanning issues which would have made map alignment and positive pair generation impossible. Secondly, I downsampled the maps, as their large memory footprint and high resolution would have made them harder to use for training.

3.2.1.1 Rotating and Cropping

The `TIFF` files contained maps which had been rotated during scanning, and then to create a rectangle, padded with white pixels. Since each `TIFF` file had a different rotation and dimensions, aligning 2 maps correctly was impossible.

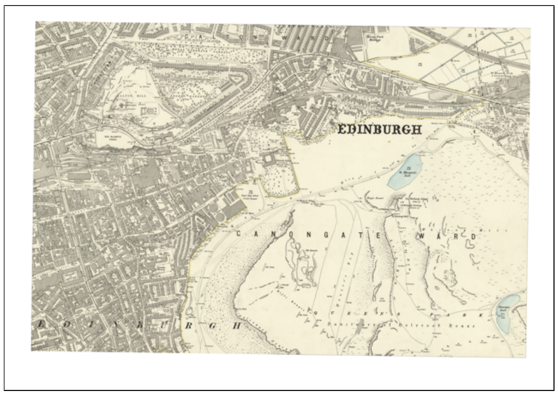

Figure 3.4: The map showcased in Figure 3.1 before any pre-processing. I have added the black frame to show the padding present in the maps before any pre-processing.

However, using `OpenCV` [34] I could rotate the map to make it horizontal, and then easily crop out the padding. Code for this is available at section B.2. Whilst the resulting maps were still of slightly different widths and heights (since the original maps had a dimension mismatch), this difference was negligible, given how large the maps are, and posed no problem for training down the line. Nonetheless, sometimes the boundary between map and padding couldn't be properly located, so not all padding was removed. Such maps were removed from further pre-processing, since this affected less than 10 of the 212 maps, most of which contained very few informative features anyways.

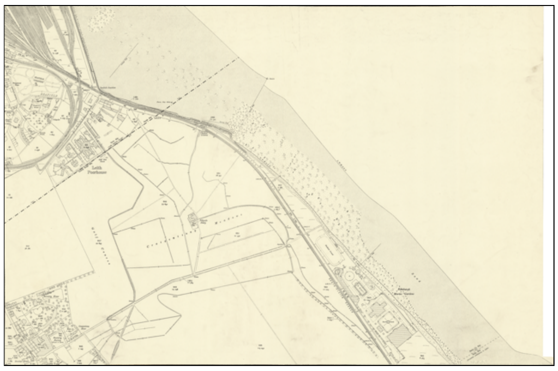

Figure 3.5: A map whose right padding wasn't removed during preprocessing.

3.2.1.2 Downsampling

The metadata and high resolution of the `GeoTIFFs` means that each map occupies 400-600MB of memory, which makes them challenging to work with. Moreover, the high resolution would require me to work with relatively large patches to distinguish features like roads or full buildings, which would lengthen the learning process unnecessarily. Therefore, I decided to downsample the maps by considering kernels of width 2, 3 and 4, where each kernel converts square regions of the kernel's width into a single pixel. I considered **standard downsampling** (pick the minimum, average or median pixel value over the region) and **resizing** (use bilinear, bicubic or nearest-neighbour interpolation).

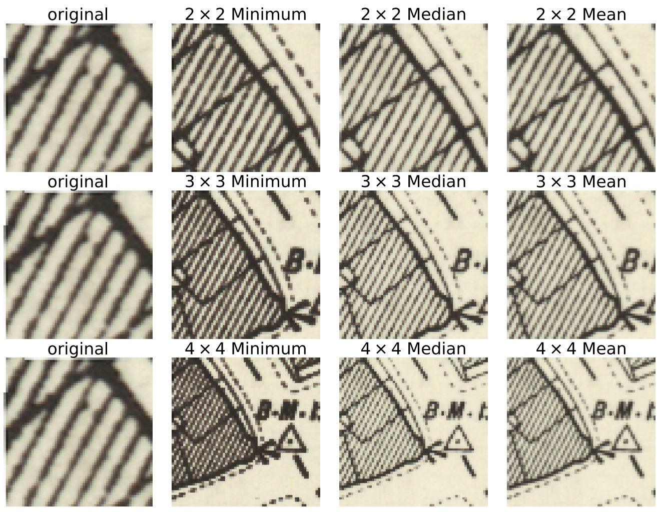

(a) Standard downsampling applied on each map. For the 2×2 kernel, all methods seem to behave similarly. For wider kernels, using the minimum pixels results in a loss of pattern detail, alongside a darkening of the image. Similarly, mean downsampling results in a blurring effect. The median, to a lesser degree, also sees loss of detail, particularly with lightening of pixels.

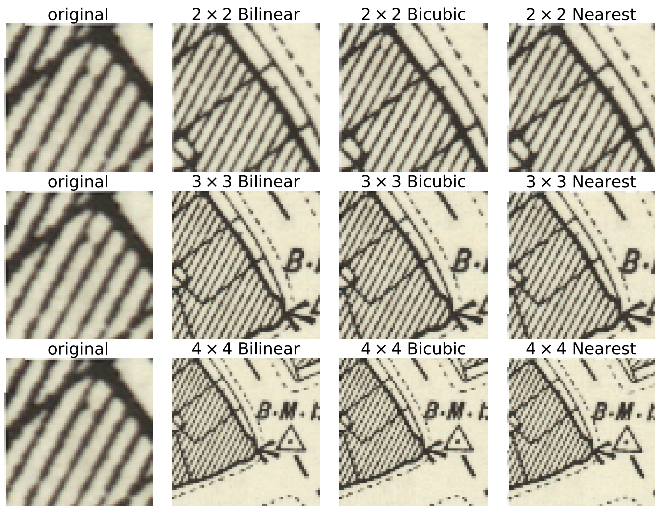

(b) Downsampling via resizing applied on each map. Both bilinear and bicubic interpolation look very similar for all kernel sizes, with good detail preservation. Nearest interpolation also works quite well, but loses some details in the writing for the 4×4 kernel.

Figure 3.6: Downsampling strategies applied to 64×64 patches.

Given the results from Figure 3.6, I chose to apply bilinear interpolation as my downsampling method. I felt that it preserved structure better (letters, shapes, shadings) than the standard downsampling methods; it also looked extremely similar to the bicubic method, and it seems to work better than nearest-neighbour interpolation for bigger kernel sizes. I also felt that using a kernel size of 4 allowed the most flexibility, since then even small patches of size 32×32 contained identifiable features. After all these pre-processing steps, each map occupied around 28MB (this suggest that I successfully isolated the maps from the original `TIFF` files, as before the rotation and padding meant that the `TIFF` files had variable file sizes of 400-600MB); by converting them to `PNG`, we further reduced the file sizes to around 14MB.

3.2.2 Finding Maps of the Same Region

Once the maps had been pre-processed, I had to determine when 2 maps corresponded to the same region, as these would be used to construct the positive pairs. Doing this manually would have been tedious, inefficient and non-scalable, particularly since the file names I was given were rather cryptic (for example, `82878027.tiff`). Whilst this can be done by exploiting the georeference information present in the `GeoTIFFs` (such as the bounding boxes for the maps), I found that the rotations present within the scanned maps had affected the georeferenced data aswell. This could be dealt with fairly easily (as I detail in section A.1), but the method we developed assumed that the georeferenced bounding boxes for maps of the same region were similar, and we couldn't guarantee this. Because of this, I asked the NLS whether they had more reliable metadata about the maps, as this would allow me both identify maps of the same region, but also access other useful pieces of information, such as year of production. Thankfully, this was made available to us as a table (see Table B.1 for further details), and we were able to group maps by region, using the bounding boxes present in the table.

3.2.3 From Maps to Patches

To generate the patches, I used the package `patchify` [35] to split up each map. I created a custom class to represent these patches, in order to store additional data, such as the map from which the patch was extracted and the coordinate of the patch's left pixel in the original map. This helped organise the patches, particularly when working with them in downstream tasks.

It is important to note that `patchify` will discard parts of the map, so as to ensure that every patch which is created has the same shape. For example, if the maps were of size 640×660, and I wanted to create 64×64 patches, `patchify` would "ignore" the column which is 20 pixels wide at the end of the map, and effectively just create 100 patches, by considering a region of size 640×640. `patchify` does include functionality to create overlapping patches, which would mean that we'd be able to potentially use the whole map for patches. This could provide some benefits, in terms of learning more geographically aware embeddings (since neighbouring patches would share features). However, for this project I decided to focus only on non-overlapping patches, as I felt including the overlaps could complicate the analysis and applicability of my results.

Once I had the patches, I developed an alignment algorithm, which would shift patches to maximise their degree of visual alignment, and thus generate positive patch pairs. However, after applying it, I noticed that barely no alignment was required in most cases (this is discussed in detail, alongside the algorithm, in section A.2), so I chose to not use the alignment algorithm. Moreover, misalignments of a few pixels, could constitute some degree of data augmentation, which is an integral part of CL.

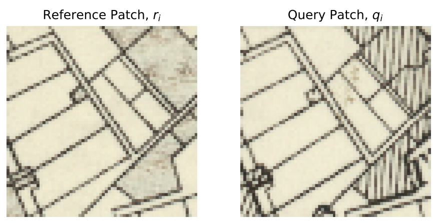

Figure 3.7: In general, upon converting maps into patches, patches tended to align well with one another visually, so we decided to not apply the alignment algorithm.

3.2.4 Generating Datasets from Maps

For training the models, each training sample corresponds to a positive pair of patches (i.e 2 patches representing the same area, but taken from different maps). Since I had 3 or 4 maps for each region, I had 3 or 4 different patches representing the same area. I defined positive pairs by considering all unique combinations of aligned patches. For instance, if I have 4 patches for the same area, this results in 6 positive pairs:

- patch 1 gets associated with patches 2,3 and 4
- patch 2 gets associated with patches 3 and 4 (since a pair already includes patches 1 and 2)
- patch 3 gets associated with patch 4 (it has already been associated with patches 1 and 2)

Similarly, if I had 3 patches, then these would generate 3 positive pairs.

However, I decided to remove some positive pairs from the final datasets, since a lot of patches were blank or contained few discernible features (such as residual segments cut off from buildings/text during the patchifying process). Any patch pair containing at least one of these uninformative patches was removed from the data, as I hoped that a more feature dense dataset would improve the contrastive representations. To achieve this, I once again used `OpenCV`: I converted patches to grayscale, applied Gaussian blur with a 3×3 kernel (and automatic standard deviation), applied the Canny [36] edge detection algorithm, and counted the number of black pixels found in the edges. If these constituted less than 1% of all pixels in the patch, any positive pair containing the patch was removed.

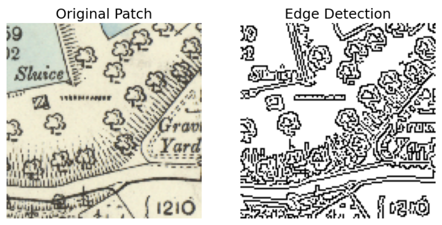

Figure 3.8: Edge detection applied to a patch. This provides a crude measure of information content, and provides a simple heuristic for informative features.

I chose a 1% threshold after visually exploring the patches which were removed, and observing that it generally correlated well with my judgement of whether a patch contains informative features or not:

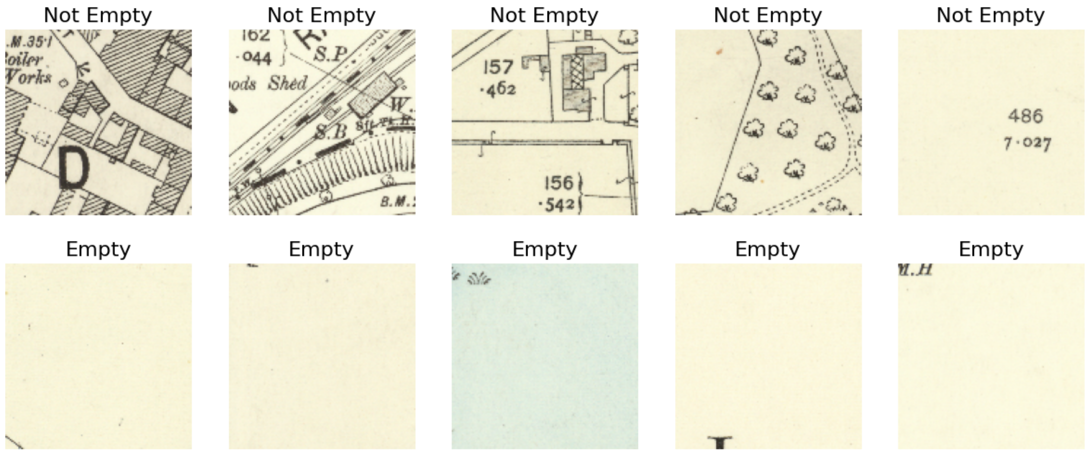

Figure 3.9: Random selection of 10 patches, 5 of which are uninformative according to the algorithm defined above. Notice how patches which are deemed as uninformative can still contain features (such as pieces of text, legends or parts of a road), but these are minimal, and I don't believe they'll contribute to learning more useful representations. On the other hand, non-empty/informative patches are feature rich. Notice how a patch in which full-text appears will generally be recognised as informative.

Whilst exploring the generated dataset, I observed that certain patches contained black lines at the edges, which I believe are lines corresponding to the borders of the maps. I found these to be problematic, since potentially empty patches which have this border would still remain in the dataset, even though the border doesn't constitute an interesting feature to learn. To filter out patches which contain these border pixels, I looked at whether the patches contained continuous vertical/horizontal bands of pixels across the left/right/top/bottom 10% of the image (with edge detection). If any of these bands was completely composed of black pixels *and* these black pixels constituted at least 50% of all edge pixels found in the patch, I removed any patch pair containing said patch. This ensured that if images do have informative content, they remain in the dataset, even if they do have artifacts derived from the border pixels.

Figure 3.10: Examples of patches which have border pixels. Our filtering algorithm will remove the first 4 of these patches, since most of the information that they contain is in the border pixels. However, the last patch will be preserved in the dataset, since it does hold informative value.

I also considered much harsher thresholds (such as 25% instead of 50%), but observed that this only contributed to removing an additional 1,000 positive pairs. Whilst it is true that borders themselves don't contribute an informative features, patches containing borders can still hold useful information (such as the types of features which are typically at the borders of maps). Thus, by choosing a higher threshold, I could be more certain that I was removing patches containing mainly border pixels. See the full implementation in section B.4.

Based on training speed and model performance on preliminary runs, I decided to utilise 128×128 patches. This resulted in a final dataset containing 104,239 positive patch pairs, after removing 44,531 positive patch pairs via the methods outlined above.

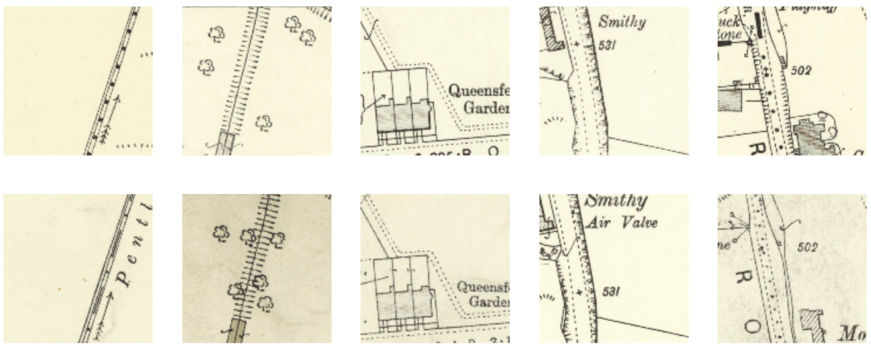

(a) Examples of positive pairs preserved for the final dataset (each column is a positive pair). As can be seen, they contain plenty of information, and the alignment is fairly good.

119
36·96
22·910

(b) Examples of positive pairs removed from the final dataset (each column is a positive pair). As can be seen, empty, uninformative patches are removed. However, due to differences in styling, and the unperfect alignment, certain positive pairs are removed, despite one of the patches containing useful features.

Figure 3.11

3.2.5 Splitting the Dataset

In general, self-supervised learning is used to learn pretrained representations, which can be employed in unrelated downstream tasks, where there is little data for training. As such, large datasets (such as `ImageNet`) are fully used to train the contrastive models. In my case, since I wasn't using any external dataset, and all the downstream tasks which I'd designed employed these historical map patches, I decided to split the 104,239 positive patch pairs into training, validation and testing pairs, using an 80-10-10 split respectively. I used this split both for training the contrastive models, and evaluating them in downstream tasks.

Initially, I thought of applying this split in a straightforward manner, by selecting a corresponding proportion of positive pairs for each of the datasets. However, this has a clear flaw: whilst this prevents the same positive pair from being used in training and evaluation, the nature of the data makes it so that the same patch can appear in training, validation and testing, since every patch appears between 1 and 4 times within different positive pairs in the dataset. This would be problematic, as at evaluation time, our model will have likely already seen some of the patches, so even if it has never directly observed a specific positive pair, this is likely to inflate generalisation performance.

Because of this, I opted for applying the split by using patch indices. Say we have a region r, and that there are 4 OS maps representing said region: $\mathcal{M}^{r,1}, \mathcal{M}^{r,2}, \mathcal{M}^{r,3}, \mathcal{M}^{r,4}$, and let $\mathcal{M}_i^{r,j}$ denote the ith patch of the jth such map, where $j \in \{1,2,3,4\}$. Then, let P^r denote a set of indices, such that if $i \notin P^r$, then $\mathcal{M}_i^{r,j}$ is a patch which was removed from the final dataset in the process outlined in subsection 3.2.4, and otherwise $\mathcal{M}_i^{r,j}$ is a patch which has remained in the dataset. For each region r, I sample 80% of the indices in P^r for training, 10% for validation, and 10% for testing, to generate $P^r_{\texttt{train}}, P^r_{\texttt{validation}}, P^r_{\texttt{test}}$ respectively. Our final training, validation and testing sets are then constructed by, for each region, using the patches corresponding to the indices in $P^r_{\texttt{train}}, P^r_{\texttt{validation}}, P^r_{\texttt{test}}$. This ensures that if there is a positive pair of the form $(\mathcal{M}_i^{r,j_1}, \mathcal{M}_i^{r,j_2})$ in one of the datasets, then the patches $\mathcal{M}_i^{r,j_1}$ and $\mathcal{M}_i^{r,j_2}$ will **only** ever appear within the same dataset. Due to different regions having different degrees of informativeness, after splitting the dataset, the result wasn't a perfect 80-10-10 split:

- 83,648 positive patch pairs for training (80.20% of the full dataset)
- 10,285 positive patch pairs for validation (9.91% of the full dataset)
- 10,306 positive patch pairs for testing (9.90% of the full dataset)

3.2.6 Using Larger Patches

As part of my experiments, I also wanted to see whether increased patch sizes of 224×224 would influence the training results (these patches wouldn't have to be reshaped to pass them through the `ResNet` models, and they should contain more information than the 128×128 patches). Since these patches were larger, since I didn't use overlapping patches, and since the maps have different sizes, the different maps for the same region could get split into a different number of patches. In future work, overlapping patches could be used which ensure that all regions get split into the same number of patches (as otherwise we wouldn't be able to align patches). However, this wasn't the main focus of our investigation, so for simplicity I decided to proceed by only using regions in which all the maps split into the same number of patches. Overall, following the procedure outlined in subsection 3.2.4 followed by the same 80-10-10 split, this resulted in:

- 24,093 positive patch pairs for training (80.53% of the full dataset)
- 2,938 positive patch pairs for validation (9.82% of the full dataset)
- 2,886 positive patch pairs for testing (9.65% of the full dataset)

Chapter 4

Methodology and Results

In this section, I outline the different hyperparameters considered for training, and showcase the 3 proxy tasks I have used to evaluate my models, which should help understand the sort of features being captured by the contrastive representations:

1. **Positive Pair Identification Tasks**: how good are the representations at identifying true positive pairs? How does the similarity vary between patches?
2. **Encoded Features**: what sort of information is encoded within the learnt representations? Does this correspond with what I expect?
3. **Clustering**: is there meaningful structure to the representations in latent space?

This is common when evaluating contrastive models, since then one can see whether the representations capture the underlying structure of the data. For instance, in the `SimCLR` and `BYOL` papers, they used the representations to classify images from `ImageNet`, comparing the performance with a fully supervised model. In this case, evaluation isn't as simple, since I don't have access to any specific labels for each of our patches.

4.1 Training the Models

4.1.1 Hyperparameters

The choice of encoder is critical for CL, so I opted for investigating `ResNet18`, `ResNet34` and a simple `CNN` (as described in subsection 2.2.3) as encoders. I also considered the effect of using pretrained `ResNet` models. Moreover, I varied the learning rate and the batch size (since in the `SimCLR` and `BYOL` papers they claim that larger batches lead to better representations). Finally, `SimCLR` has the temperature parameter in its loss, whilst `BYOL` has the exponential moving average proportion. I refer to both of these hyperparameters with τ; the reader should understand which hyperparameter is being referred to by context.

4.1.2 Training Procedure

In order to select the models for downstream tasks, I performed a total of 20 experiments (see Table C.1), where each hyperparameter was changed at a time, for both a `BYOL` and a `SimCLR` model. These changes were relative to a "base model" for each architecture, which used a pretrained `ResNet18` encoder, with $\tau = 0.99$, a learning rate η of 1×10^{-3},a patch size of 128 and a batch size of 64. Ideally, I would compare every hyperparameter combination, but this would be unfeasible. Given hardware constraints, I conservatively estimated that training **each** of the models for just 5 epochs would take 64 days (this doesn't include using the `CNN` encoder, which require less training time than `ResNet`-based models). See section C.1 for details of this estimate.

All experiments were set to run for 25 epochs on the Informatics Teaching Cluster (given preliminary tests, this was the most that I could afford to do). However, I included early stopping to avoid wasting resources in unnecessary computations. I evaluated each model 150 times per epoch, and stopped training if there was no validation loss improvement in one full epoch, or there was no validation loss improvement in 60 consecutive evaluations after 5 epochs. I wanted to ensure that the models had at least 5 epochs to train, as in preliminary runs models generalised fairly well after 5 epochs. However, if a model got stuck in a local minimum, and its validation loss barely changed within the first 5 epochs, this would have wasted computing resources. All training results can be found in section C.3.

After training, I evaluated each model using the weights which lead to the lowest validation contrastive loss. Even if a lower loss doesn't necessarily correspond with a better model, this might be the fairest way of comparing the models amongst themselves, as I am using the versions which performed best on unseen data.

4.2 Positive Pair Identification Tasks

Evaluating each trained model on the subsequent tasks would have been unrealistic (due to memory and time constraints), so I only compared one `SimCLR` model and one `BYOL` model on downstream tasks. To decide which models to use, I defined a series of **Positive Pair Identification Tasks** (PPIT), which I executed on the validation set. These classification tasks aimed at showcasing the capacity of the contrastive representations in finding true positive patch pairs, which is the principal goal of this project.

4.2.1 Problem Setup

To gauge how well the latent representations comprehend our notion of similarity, we can use them to determine whether 2 patches form a positive pair. Let P, Q be an ordered list of all validation patches (so that (P_i, Q_i) forms a positive validation pair). We construct 2 matrices $X, Y \in \mathbb{R}^{N \times 512}$, where the ith rows of X, Y are defined by:

$$X_{i,:} = \texttt{embed}(P_i) \qquad Y_{i,:} = \texttt{embed}(Q_i)$$

and `embed` takes a patch, embeds it using a contrastive model and normalises it to unit length. Then, define a **similarity score matrix** as $S = XY^T$, where S_{ij} is the similarity score between P_i and Q_j (the cosine similarity between their 2 embeddings). We can find the patch in Q most similar to a $P_i \in P$:

$$\hat{Q}_i = \max_{Q_j \in Q} S_{i,j}$$

or find the patches which are most similar to $P_i \in P$, based on which $Q_j \in Q$ are such that $S_{i,j} \geq \texttt{sim\_thresh}$, where $\texttt{sim\_thresh} \in [-1,1]$.

Due to how I have constructed the positive pairs in the datasets, some patches can appear multiple times in P and Q. For instance, a region present in 4 maps contributes 6 positive patch pairs $(p_1,p_2),(p_1,p_2),(p_1,p_3),(p_2,p_3),(p_2,p_4),(p_3,p_4)$, so p_2 appears twice in P and once in Q. Since a patch has a similarity score of 1 with itself, some entries in S will be 1, which is undesirable, as it isn't indicative of how well the model captures similarity. Hence, I masked such entries (by assigning them a large negative value) to ensure that when finding the most similar patch, a trivial patch isn't returned.

4.2.2 Tasks Considered

The first task involves computing **Top-K Accuracy** in identifying the patch $Q_i \in Q$ which forms a positive pair with patch $P_i \in P$. To do this, for each K, I find the K patches in Q which attain the largest similarity scores with P_i. If Q_i is within these patches, I count this is a correct classification. I considered $K \in \{1,5,10\}$. Using just Top-1 Accuracy wouldn't be that useful of a metric, due to the fact that for each patch I can have multiple positive pairs; I hoped to mitigate this by also considering Top-5 and Top-10. As a variant to Top-K Accuracy, I instead computed accuracy with respect to identifying **all** true positive pairs, which I call **Positive Pair Accuracy**. To this end, say that a single patch $P_i \in P$ forms distinct positive pairs with K patches in Q. I then find the K distinct patches in Q with the highest similarity score with P_i, and compute the proportion of these whcih form a positive pair with P_i. Finally, I take the average of these proportions to compute the **Positive Pair Accuracy**.

4.2.3 Results

Table 4.1: Results for the PPIT for each of the `BYOL` models.

Model	Top-1 Accuracy	Top-5 Accuracy	Top-10 Accuracy	Positive Pair Accuracy
`BYOL` (Base)	**0.22460**	0.73962	0.78999	0.72309
`BYOL` ($\tau = 0.95$)	0.22178	0.74108	0.79290	0.72363
`BYOL` ($\tau = 0.90$)	0.22256	**0.74759**	**0.79679**	**0.73359**
`BYOL` ($\tau = 0.80$)	0.22071	0.74118	0.79028	0.72708
`BYOL` (Not Pretrained)	0.18172	0.55527	0.62722	0.53350
`BYOL` (`ResNet34`)	0.21682	0.72611	0.77647	0.71123
`BYOL` (`CNN`)	0.17151	0.53972	0.58532	0.52460
`BYOL` (Patch Size 224)	*0.25323*	*0.87474*	*0.90572*	*0.86964*
`BYOL` (Batch Size 32)	0.20924	0.66952	0.72280	0.65270
`BYOL` ($\eta = 1 \times 10^{-2}$)	0.0048	0.01575	0.02178	0.0146

Table 4.2: Results for the PPIT for each of the `SimCLR` models.

Model	**Top-1 Accuracy**	**Top-5 Accuracy**	**Top-10 Accuracy**	**Positive Pair Accuracy**
`SimCLR` (Base)	0.22168	0.74166	0.79242	0.72557
`SimCLR` ($\tau = 0.95$)	0.21915	0.73320	0.78785	0.71940
`SimCLR` ($\tau = 0.90$)	0.22538	0.74545	0.79582	0.73155
`SimCLR` ($\tau = 0.80$)	0.22547	0.75158	0.80010	0.73515
`SimCLR` (Not Pretrained)	0.22615	0.75790	0.79922	0.74210
`SimCLR` (`ResNet34`)	0.22421	0.74263	0.79417	0.72679
`SimCLR` (`CNN`)	**0.22654**	**0.76305**	**0.80272**	**0.74905**
`SimCLR` (Patch Size 224)	*0.25528*	*0.88904*	*0.91355*	*0.88462*
`SimCLR` (Batch Size 32)	0.22217	0.73534	0.78882	0.71740
`SimCLR` ($\eta = 1 \times 10^{-2}$)	0.22480	0.75012	0.79689	0.73525

The most noticeable fact about the results shown in Table 4.1 and Table 4.2 is that using 224×224 patches leads to better performance in all the PPIT. However, comparing these accuracies with those for runs using 128×128 patches is unfair: with larger patches, more information is available to distinguish between patches, so better performance doesn't imply better representations. For this project, I focused on the 128×128 patches, since they encompassed all the maps, so derived conclusions should be more representative, although use of larger patches should be further explored in future work.

Looking at Table 4.1, `BYOL` obtains variable results in the PPIT. In some cases, this is because a model suffers from representational collapse: under certain settings, the lack of negative pairs make it so that `BYOL` learns to map all patches to very similar representation. For example, when using $\eta = 1 \times 10^{-2}$, as can be seen in subsubsection D.1.1.9. This harms the model's capacity of identifying when 2 patches are similar. Beyond this, the best `BYOL` model seems to use $\tau = 0.90$, achieving the best results in all metrics except Top-1 Accuracy (where it got the second best result). On the other hand, `SimCLR` obtains relatively similar results across models, probably due to the stabilising effect of the negative pairs. Surprisingly, the `SimCLR` model using a `CNN` encoder obtained the best result in all metrics. Lastly, putting the results of Table 4.1 and Table 4.2 side by side, `SimCLR` models attain slightly higher results across all PPIT metrics. Henceforth, I use the `BYOL` model trained with $\tau = 0.90$ as the "best `BYOL` model", and the `SimCLR` model trained with a `CNN` encoder as the "best `SimCLR` model".

I was worried that early stopping hadn't allowed `ResNet`-based `SimCLR` models to train for enough time and learn good representations. Thus, I retrained the 2 best `ResNet` models (`ResNet18` without pretraining, and with $\tau = 0.80$) for 15 epochs. Despite a slight decrease in training and validation loss, and a small improvement in PPIT performance, the `CNN`-based `SimCLR` model still obtained better results (see section C.4).

4.2.4 Applicability of Results

The metrics from Table 4.1 and Table 4.2 highlight how all the `SimCLR` models, and a majority of the `BYOL` models, are adept at identifying similar patches, even if said patches are unseen by the model. To verify this, I directly inspected the 5 most similar patches found by each model, given some reference patch (more observations available in subsection D.2.1). For the rest of this project, when discussing a patch P_i (which I'll interchangeably name "reference patch" or P_i), I'll refer to a patch Q_j as a "positive patch" if (P_i, Q_j) constitute a positive patch pair, and as a "negative patch" otherwise.

I observed that the learnt contrastive representations are capable of understanding how many different features (roads, buildings, trees, streets, etc...) are composed together to generate a patch. Whilst this might seem fairly trivial, given the variability in styles across the maps, the capacity for generalisation of these models is impressive. For instance, they seem to understand differences between roads with trees to the side, and city roads. Moreover, the models seem to find positive pairs, even if there isn't an immediately obvious visual similarity (see Figure D.4).

Furthermore, I noticed that, generally, `SimCLR` identified all positive patches correctly as the most similar patches (if P_i had 3 positive patches, these were often deemed as the 3 most similar). Contrarily, `BYOL` wasn't as discriminative, and sometimes the most similar patch wasn't part of the correct positive patches. This is somewhat perceptible when looking at positive pair accuracy in Table 4.1 and Table 4.2. However, when looking at the most similar negative patches, `BYOL` was better at finding "the next best patch". For instance, in Figure 4.1 and Figure 4.2 one can observe how `BYOL` has found patches which are more nuanced, and share more features with the reference patch. This indicates that `SimCLR` based models can be better at meticulously retrieving positive pairs, whilst `BYOL` might find more diverse, albeit semantically consistent patches.

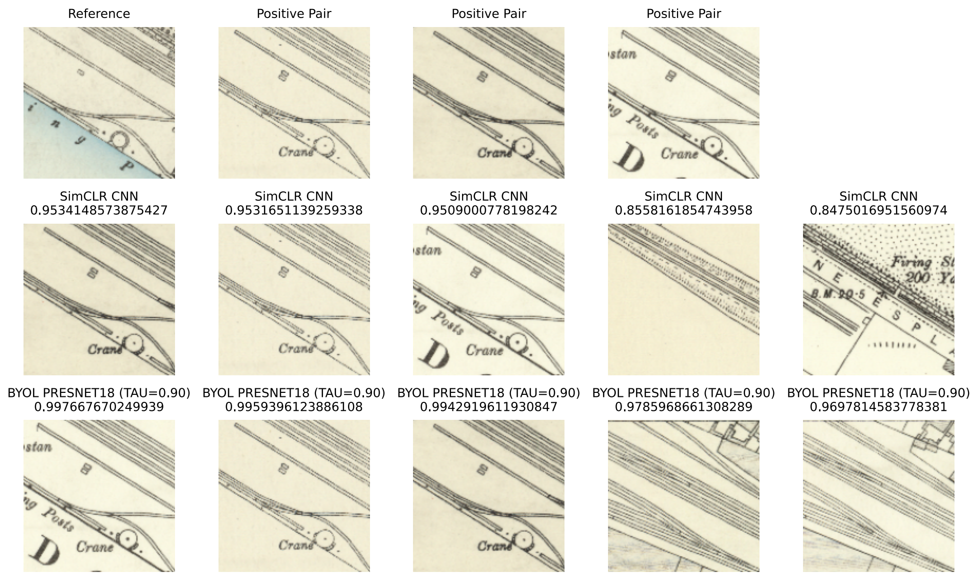
Reference
Positive Pair
Positive Pair
Positive Pair
SimCLR CNN 0.9534148573875427
SimCLR CNN 0.9531651139259338
SimCLR CNN 0.9509000778198242
SimCLR CNN 0.8558161854743958
SimCLR CNN 0.8475016951560974
BYOL PRESNET18 (TAU=0.90) 0.997667670249939
BYOL PRESNET18 (TAU=0.90) 0.9959396123886108
BYOL PRESNET18 (TAU=0.90) 0.9942919611930847
BYOL PRESNET18 (TAU=0.90) 0.9785968661308289
BYOL PRESNET18 (TAU=0.90) 0.9697814583778381

Figure 4.1: Both `SimCLR` and `BYOL` identify the correct positive pairs, and assign to them a notably higher similarity score. However, the most similar negative patches found by `SimCLR` aren't that great: whilst they contain railtracks, they are visibly semantically dissimilar. On the other hand, both positive and negative patches found by `BYOL` contain a high degree of semantic similarity, staying true to the railtrack style and positioning.

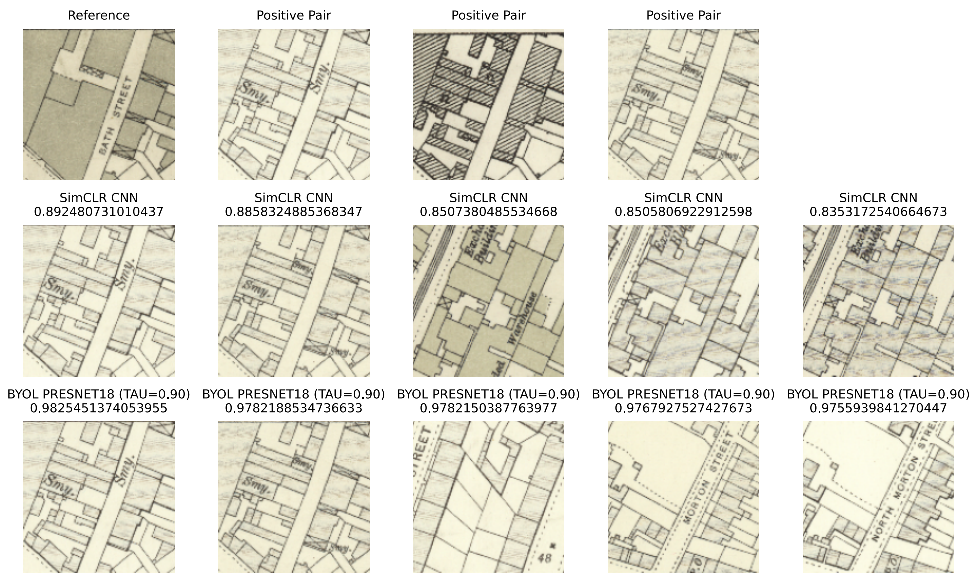
Reference
Positive Pair
Positive Pair
Positive Pair
BATH STREET
SimCLR CNN 0.892480731010437
SimCLR CNN 0.8858324885368347
SimCLR CNN 0.8507380485534668
SimCLR CNN 0.8505806922912598
SimCLR CNN 0.8353172540664673
BYOL PRESNET18 (TAU=0.90) 0.9825451374053955
BYOL PRESNET18 (TAU=0.90) 0.9782188534736633
BYOL PRESNET18 (TAU=0.90) 0.9782150387763977
BYOL PRESNET18 (TAU=0.90) 0.9767927527427673
BYOL PRESNET18 (TAU=0.90) 0.9755939841270447
MORTON STREET
NORTH MORTON STREET

Figure 4.2: Both `SimCLR` and `BYOL` identify 2 of the 3 correct positive patch pairs (although they can't find the darker shaded one, despite having identical building structure to the other positive pairs). `SimCLR` assigns much higher similarity score to the true positive patches, whereas `BYOL` gives fairly consistent scores throughout. The patches found by `BYOL` seem more semantically correct, as most of them show a diagonal road (with text) in the rightmost 2/3 of the patch, with buildings at its sides. On the other hand, `SimCLR` finds visually similar buildings, but which convey different information.

Overall this reveals how the contrastive models can be utilised to "lookup" patches which share a set of features across a variety of different maps, which can allow cartographers or historians to efficiently search for similarities and differences in maps across different eras.

Another potential usage for these methods which I wasn't able to explore in this project is unsupervised map alignment. For instance, say we have patches corresponding to an unseen historical map. Then, I can search through a database of all the contrastive representations embeddings, and for each unknown patch, find the K most similar corresponding patches (here K represents the number of distinct hisotrical time periods encompassed by the maps in the database; in our case $K = 4$). Then, one can take a majority vote between the locations of the found patches, to determine the longitude and latitude to assign to the unknown patches. Measures could be taken to ensure a consistency between the coordinates assigned to adjacent unknown patches (i.e 2 patches adjacent in the map should be assigned adjacent longitudes and latitudes).

4.2.5 Visualising Similarity Scores

To understand the similarity score distributions of the models, I visualised the similarity score matrices from subsection 4.2.1 as grayscale images where pixel intensity corresponds to similarity score. I also randomly sampled 100 rows in S, and plotted the corresponding $10,285 \times 100 = 1,028,500$ scores as a histogram using 100 bins (excluding masked entries).

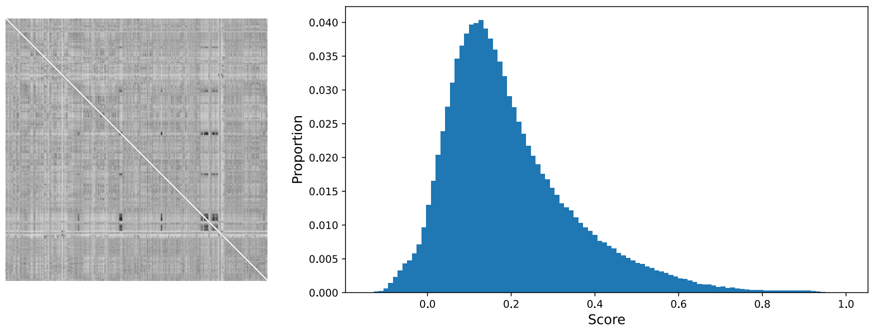

(a) Similarity score distribution for the `SimCLR` model with `CNN` encoder.

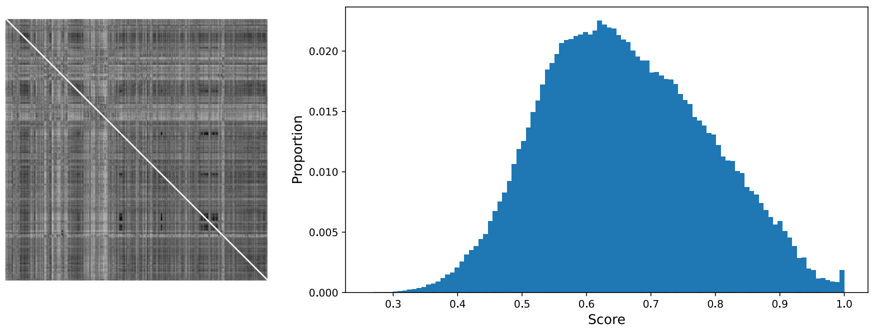

(b) Similarity score distribution for the `BYOL` model with $\tau = 0.90$.

Figure 4.3: Darker colours in the similarity score matrices represent higher similarity scores (closer to 1). Notice the white pseudo-diagonal, generated by the mask applied to ensure that I don't take the similarity score of identical patches into account. The y-axis of the histograms corresponds to the proportion of scores which are part of a certain bin. Distributions for all other models are available at section D.1.

In general, all `SimCLR` models had a strongly left-skewed similarity score distribution (Figure 4.3a exemplifies this). The type of encoder seemed to influence the range of the distributions: with a `ResNet`, similarity scores were in the range $(0.2, 1)$, whilst with a `CNN` scores were in the range $(-0.1, 0.95)$. Moreover, all `ResNet`-based `SimCLR` models had a small peak in the last bin of the distribution (due to assigning scores above 0.99), whilst the `CNN`-based `SimCLR` model is monotonic. Lastly, when the `ResNet` wasn't pretrained, the similarity score distribution became symmetric.

On the other hand, `BYOL` models displayed a more notable distributional difference, although generally they were slightly right-skewed, as shown in Figure 4.3b. For collapsed representations (like when using $\eta = 1 \times 10^{-2}$ or a batch size of 32), the scores were extremely right-skewed, since most pairs obtained a similarity score close to 1. Strangely, both `ResNet34`-based and `CNN`-based `BYOL` models had a bimodal distribution. I also noticed that score distribution ranges followed a similar trend as with `SimCLR` models: a `CNN` encoder lead to wider score ranges (including negative scores), whilst `ResNet` encoders assigned positive scores above 0.2.

Since the distributional differences between `SimCLR` and `BYOL` generally apply independent of hyperparameter choice, they could be due to architecture choice, particularly the use of negative pairs in training. In `SimCLR` they push representations to be more discriminative; however, `BYOL` solely "sees" positive pairs, so representations might move towards pursuing higher similarity, rather than similarity with positive pairs, and dissimilarity with negative pairs. This is noticeable when comparing Figure 4.3a and Figure 4.3b, whereby the BYOL similarity score matrix is darker, indicating it is assigning higher scores to every pair. Moreover, negative pairs could provide a stabilising effect; without them, high learning rates or small batch sizes might lead to local minimum convergence, which for BYOL could be representational collapse.

4.3 Exploring Encoded Features

4.3.1 Classification Tasks

To explore how information was encoded in the representations, I defined two classification tasks, where I classify patches based on time period and amount of information, based solely on their contrastive representations. I used an MLP classifier (call it MLP_C), with a 512-dimensional input, followed by 3 fully-connected, hidden layers (1024, 2048 and 512 hidden units respectively), each with bias and ReLU activation. The output uses a linear layer with bias and softmax activation. I trained for 5 and 50 epochs (to see the effect of longer training time), using a batch size of 128, Adam optimiser, cross-entropy loss and learning rate of 1×10^{-3}. After removing duplicate patches, I obtained 61,647 training patches, 7,689 validation patches and 7,697 testing patches.

4.3.1.1 Temporal Awareness

Positive pairs were constructed using temporally-spaced patches, so I expected temporally invariant contrastive representations. Ideally, such embeddings will encode structural patch elements, and compress out stylistic aspects characteristic of maps from a given time period. I used the NLS metadata to define 4 temporal classes for the maps: before 1900, 1900-1910, 1910-1930, and after 1930. This ensures balanced classes: the first 3 classes contain 57 maps each, whilst the final class contains 41 maps (see section 3.1). Then, I trained MLP_C to predict patch time period from their embedding.

Table 4.3: Training, validation and testing data distribution for the time prediction problem.

Class [Year]	0 [< 1900]	1 [< 1910]	2 [< 1930]	3 [> 1930]
Training Samples (Proportion)	16,426 (26.65%)	16,600 (26.93%)	16,767 (27.20%)	11,854 (19.23%)
Validation Samples (Proportion)	2,033 (26.44%)	2,073 (26.96%)	2,115 (27.51%)	1,468 (19.09%)
Testing Samples (Proportion)	2,063 (26.80%)	2,080 (27.02%)	2,099 (27.27%)	1,455 (18.90%)

If MLP_C obtains an accuracy close to a random classifier (25%), this could indicate that the embeddings are temporally indifferent. However, perhaps the patches don't contain temporal information. Thus, I define an end-to-end classification problem using CNN_C, a simpler CNN encoder than those used by the contrastive models. If CNN_C converts patches into embeddings from which MLP_C successfully predicts time period, this indicates the presence of temporal information in the patches. CNN_C takes in a 128×128 patch, and is comprised of 2 convolutional layers (learning 32 and 64 filters respectively), each with ReLU activation, batch normalisation and max pooling, followed by global average pooling, and a linear layer with bias, which outputs a 512-dimensional embedding. Finally, I defined 3 baselines (uniform random model, random model sampling according to training proportions and a most common class model).

Table 4.4: Results of the time period prediction problem, over 5 and 50 epochs. I include the best training and validation performances, alongside the test performance of the model achieving the best validation accuracy.

Classifier	*Training Accuracy*		*Validation Accuracy*		*Testing Accuracy*	
	5 epochs	**50 epochs**	**5 epochs**	**50 epochs**	**5 epochs**	**50 epochs**
Uniform Random	0.2500		0.2500		0.2500	
Weighted Random	0.2549		0.2547		0.2553	
Most Common Class	0.2720		0.2751		0.2727	
SimCLR Embedding + MLP_C	0.5313	**0.9844**	0.4973	**0.5252**	0.5027	**0.5095**
BYOL Embedding + MLP_C	0.375	0.4141	0.2965	0.3811	0.3077	0.3857
CNN_C Embedding + MLP_C	**0.8672**		**0.6700**		**0.6592**	

The results from Table 4.4 imply that the BYOL model is good at ignoring temporal differences between patches, as its representations perform poorly on the time prediction task. In fact, after training I observed that MLP_C primarily predicted classes 0 and 2 throughout all 3 datasets, implying that it struggled to find features in the BYOL representations to predict the patch's time period. Furthermore, MLP_C doesn't perform well on validation/testing with SimCLR representations, but overfits to the training representations, particularly after 50 epochs. Lastly, when MLP_C uses CNN_C it significantly outperforms both contrastive models, even when run for only 5 epochs.

This indicates that the simple CNN_C finds temporal information in the patches (probably due to the characteristic styles of maps from different time periods). I hypothesise that the contrastive models also somewhat encode temporal information, but this isn't their primary goal. This can be seen from Table 4.4, whereby training for longer allows MLP_C to more fruitfully extract temporal features from the contrastive representations of both models, leading to a sizeable performance improvement.

Given that MLP_C overfits with SimCLR embeddings, but generally predicting the same labels with BYOL embeddings, this indicates that BYOL learns more temporally invariant representations than SimCLR. Perhaps SimCLR better encoding the characteristic stylistic features of the different maps, and is thus better at temporal discimination. Alternatively, BYOL might better abstract away from these features, and is thus learning more semantic representations. Beyond architectural differences, this could be due to the encoder used. Complex ResNets should better generalise to these characteristic features, whereas the simpler CNN encoder might struggle more to ignore the stylistic differences.

This could help explain how in Figure 4.3 (and section D.1), the CNN-based SimCLR model had a wider similarity score distribution, with all similarity scores below 0.95, whilst ResNet-based models had a narrower similarity score distribution, but with many similarity scores above 0.99. If CNN-based models better encode temporal information, stylistic differences between patches might prevent patch pairs from attaining extremely high similarity scores, whereas the higher abstraction capabilities of `ResNets` makes the models perceive more patches as highly similar.

4.3.1.2 Information Awareness

If we apply edge detection to the patches as in subsection 3.2.4, and count the pixels in detected edges, this roughly describes patch informativeness, as patch features are primarily simple lines (generally, more edge pixels will imply more features). Intuitively, a patch with a letter is less informative than a patch with many trees, as it has less learnable features. I use `MLP_C` to classify contrastive representations based on edge-detected pixel count to gauge informativeness encoding in the embeddings.

Initially, I defined the classes using equally spaced ranges for pixel counts (for example, class 2 could be composed of patches with 1000-1500 edge pixels). However, I visualised the edge pixel distribution in training and validation patches, and it was quite left-skewed (since patches with few features are more common). Thence, this approach would have lead to class imbalance, hindering classification. Consequently, I arbitrarily chose to use 5 classes, and found 5 thresholds to split the training data into roughly equally sized subsets (see section C.5 for implementation, and Table 4.5 for the thresholds). Class labels for validation and testing were generated using these thresholds. As in subsubsection 4.3.1.1, I compared the performance with 3 baselines, but didn't use the end-to-end encoder (this task would be trivial even for `CNN_C`).

Table 4.5: Training, validation and testing data for the information prediction problem.

Class [Threshold]	0 [$\leq$ 453]	1 [$\leq$ 969]	2 [$\leq$ 1864]	3 [$\leq$ 2995]	4 [$>$ 2995]
Training Samples (Proportion)	12,352 (20.04%)	12,320 (19.98%)	12,319 (19.98%)	12,335 (20.01%)	12,321 (19.99%)
Validation Samples (Proportion)	1,611 (20.95%)	1,670 (21.72%)	1,533 (19.94%)	1,404 (18.26%)	1,467 (19.08%)
Testing Samples (Proportion)	1,514 (19,67%)	1,709 (22.2%)	1,573 (20.44%)	1,468 (19.07%)	1,433 (18.62%)

Table 4.6: Results of the information prediction problem, over 5 and 50 epochs. I include the best training and validation performances, alongside the test performance of the model achieving the best validation accuracy.

Classifier	*Training Accuracy*		*Validation Accuracy*		*Testing Accuracy*	
	5 epochs	**50 epochs**	**5 epochs**	**50 epochs**	**5 epochs**	**50 epochs**
Uniform Random	0.2000		0.2022		0.2035	
Weighted Random	0.2000		0.2000		0.2000	
Most Common Class	0.2004		0.2095		0.1967	
`SimCLR` Embedding + `MLP_C`	**0.8672**	**1.000**	**0.8486**	**0.8504**	**0.8433**	**0.8424**
`BYOL` Embedding + `MLP_C`	0.7656	0.9141	0.7602	0.7930	0.7502	0.7819

Looking at Table 4.6, running `MLP_C` for 5 epochs leads to consistent accuracy for both models across all datasets, indicating that the contrastive models generate representations which generalise well to unseen data (at least when encoding information amount).

Longer training leads to overfitting, implying that both contrastive models are adept at encoding information in a fine-grained manner. Nonetheless, `SimCLR` representations lead to the best performance across all datasets, so it might encode information more precisely, or dedicate more features to represent the amount of information in a patch.

Architecture choice is probably responsible for this performance gap. `SimCLR` uses the interplay between positive and negative pairs to generate representations, so effective encoding of information amount is a simple way of assessing rough similarity (for instance, it is easy to differentiate between a patch full of building and a patch with a single letter). This can lead to it learning more discriminative representations. Contrarily, `BYOL`'s loss relies on the similarity between the target network encoding and the online network's predictor encoding. Since the target network's weights are an exponential moving average of the online network's, the online network won't be pushed as hard to learn information amount, as then matching the target encoding becomes harder (as the target network is using "old" weights). This might lead to `BYOL` learning more semantic representations, which could explain the results in Table 4.6: `BYOL` prioritises "knowing" if in a patch there is a "road" or a "building", alongside its rough orientation and placement; factors such as shading or size might become secondary, so it becomes less precise when encoding the amount of information in a patch.

4.3.2 Invariance Under Transformations

In CL, image augmentations are typically used to generate positive pairs, but I used temporal differences. Thus, I wanted to see how augmentations affect the contrastive representations. I considered augmentations inspired by the `SimCLR` and `BYOL` papers: centre/random cropping, fixed/random rotation angle, gaussian blur, colour jitter, horizontal flip and grayscaling (see implementation in section C.6). Then, for positive pairs (P_i, Q_i), I applied each transformation to Q_i, and computed the similarity scores between P_i and each transformed Q_i (which I call the *transformed similarity score*).

Table 4.7: Original and standardised MSE between similarity scores before and after transformation. I have ordered the table in descending order of MSE.

Transformation	`BYOL` *MSE*		`SimCLR` *MSE*	
	Original	**Standardised**	**Original**	**Standardised**
Rotation (30°)	0.06816951	1.000000	0.3952508	1.000000
Horizontal Flip	0.06319004	0.9267467	0.3585143	0.9069046
Random Rotation (90°,180°,270°)	0.04029370	0.5899183	0.1678344	0.4236947
Random Crop (64×64)	0.022805834	0.3326539	0.1540349	0.3887248
Centre Crop (64×64)	0.02073835	0.3022392	0.14532146	0.3666436
Gaussian Blur	0.005725238	0.08138097	0.048866849	0.1222139
Colour Jittering	0.001208771	0.01493915	0.007873815	0.01833176
Grayscaling	0.0001932637	0.000000	0.0006399037	0.000000

To score the difference between transformed and untransformed similarity scores (similarity scores of P_i and Q_i without any transformation), I computed their Mean Square Error (MSE) (lower MSE indicates representations were less affected by the augmentation). The MSE exacerbates large differences, which should clarify which transformations affect the contrastive representations most. I standardised the MSEs (between 0 and 1) to make them more comparable between models.

The results from Table 4.7 show that rotations and random flips are the transformations which most notably alter the representations produced by both contrastive models. These seem to affect `BYOL` more significantly (higher standardised MSE), particularly with random rotations. This corresponds with what can be observed in Figure 4.1, where orientation is critical for querying the most similar patches (for instance, the most similar patches to a patch containing a road are patches containing roads which are positioned and oriented in the same way; see Figure D.2 and subsection D.2.1).

Conversely, colour transformations (gaussian blur, colour jittering, grayscaling) seem to have a negligible effect on the contrastive representations (particularly for `BYOL`). This also makes sense: ignoring colour and resolution differences between maps is critical to learn good contrastive representations.

Generally, the results in Table 4.7 showcase desirable properties for the representations. Colour invariance is important for finding similar patches in maps from different time periods, and sensitivity to orientation/location is imperative for map-related tasks (differences in these attributes greatly change the semantics of a patch).

However, cropping seems to substantially affect representations, which could indicate sensitivity to feature size (since patches are resized after cropping), or that the models aren't fully attending to local features. Encoding fine-grained local structure is critical for patch representation, as it provides a discriminatory nuance which can better align human and model judgement. Hence, it could have been useful to include cropping as an augmentation for this project. Alternatively, I could have used the global and local contrastive losses suggested by Chaitanya et al. [20], or do as Agastya et al. [26], and provide a large contextual patch to help directly learn local features.

4.4 Geographical Awareness

4.4.1 Geographically-Aware Representations

4.4.1.1 Motivation

I thought I'd be able to improve the contrastive representations by imbuing them with both visual and geospatial information. This was inspired by Ayush et al. [28], where they learnt contrastive representations with both a contrastive and classification objectives. They clustered images by longitude and latitude with `K-Means`, and used the representations to predict the cluster. However, I didn't think this would work for my project: their images ranged over the whole world, whilst our maps encompass a small, neatly subdivided rectangular region. Hence, clustering the patches' longitude and latitude wouldn't be too informative, as it wouldn't preserve local structure (for example, 2 very different areas, like city and grasslands, could be clustered together).

4.4.1.2 GeoSimCLR

I felt that for this project, directly imbuing geographical information within the contrastive representations was the way to go. I devised `GeoSimCLR`, a new architecture which learns latent representations using 2 separate contrastive objectives. I based myself on the `SimCLR` architecture, although it could be adapted for `BYOL`.

`GeoSimCLR` learns a latent geocontrastive representation $\underline{z} \in \mathbb{R}^d$ for an image which is composed of 2 distinct parts. The "upper-half" of $\underline{z}$ is a visual representation $\underline{z}_v \in \mathbb{R}^{d/2}$ encoding visual similarity (akin representations learnt by standard `SimCLR` models). The "lower-half" of $\underline{z}$ is a contextual representation $\underline{z}_c \in \mathbb{R}^{d/2}$ encoding contextual similarity, and should maximise the similarity of a patch with its directly adjacent neighbours. For instance, given 2 neighbouring patches p, r, $\underline{z}_c^p$ and $\underline{z}_c^r$ should be similar in (contextual) latent space. To do this, I use 3 patches: a reference patch p_1, a visual patch p_2 (a patch of the same region as p_1, but from a different map) and a contextual patch r (a patch directly adjacent to p_1, which is randomly sampled). Passing them through an encoder f generates representations $\underline{z}^{p_1}, \underline{z}^{p_2}, \underline{z}^r \in \mathbb{R}^d$. The visual ($\underline{z}_v^*$) and contextual ($\underline{z}_c^*$) representations get passed through different projectors g_v, g_c, to generate projections $\underline{q}_v^*, \underline{q}_c^*$. Then, a visual contrastive loss ℓ_v is computed between $\underline{z}_v^{p_1}$ and $\underline{z}_v^{p_2}$, and a contextual contrastive loss ℓ_c is computed between $\underline{z}_c^{p_1}$ and $\underline{z}_c^r$ to generate a contextual contrastive loss. The geocontrastive loss is a weighted sum of these 2 losses:

$$\ell = w_v \cdot \ell_v + w_c \cdot \ell_c, \quad w_v \in [0,1] \quad w_c = 1 - w_v$$

I chose $w_v = 0.7$, since I wanted to prioritise learning good visual representations, but optimising w_v, w_c to suit specific tasks could be further investigated.

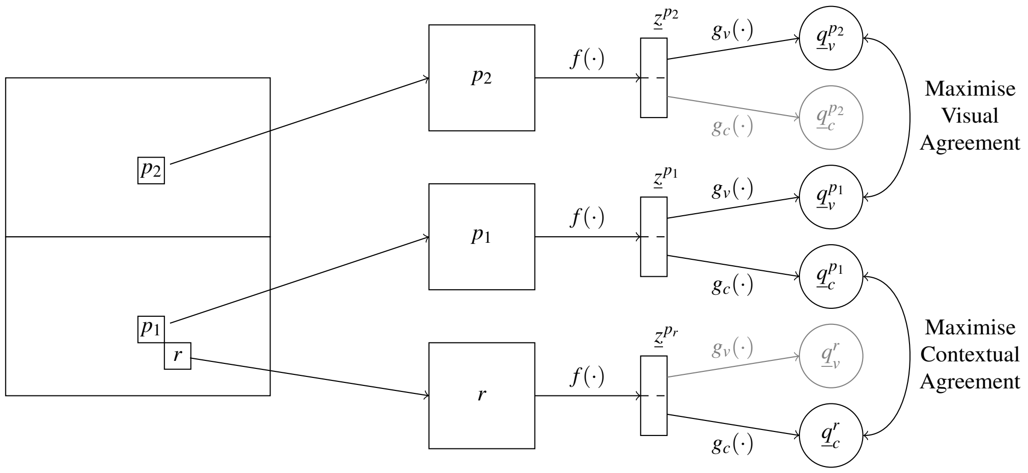

Figure 4.4: Sketch of how `GeoSimCLR` uses 2 separate contrastive losses to learn latent representations: one for visual similarity, and one for contextual similarity.

4.4.1.3 PPIT with **`GeoSimCLR`**

To train the `GeoSimCLR` model, I used a `CNN` encoder (as it gave the best results in the PPIT from subsection 4.2.2), and followed the procedure from subsection 4.1.2, although without early stopping. Since visual and contextual representations are smaller (256-dimensional), encoding useful information should be harder, so I wanted to allow more training time. Nonetheless, from epoch 13 onwards the best validation loss barely changed, so I think that training for all 25 epochs wasn't that necessary, particularly since a `CNN` might not benefit as much as a `ResNet` from longer training.

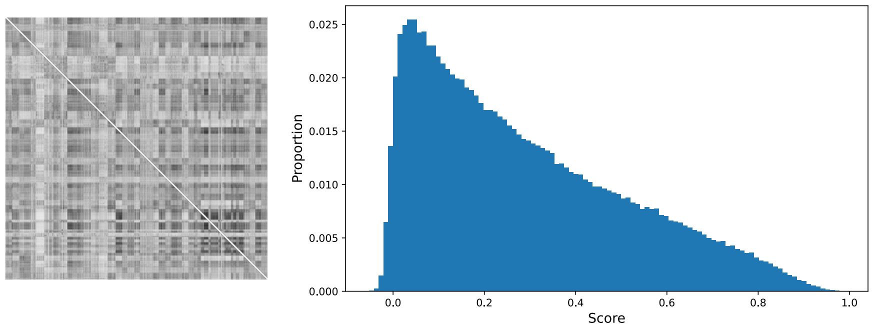

(a) Similarity score distribution for the `GeoSimCLR` model.

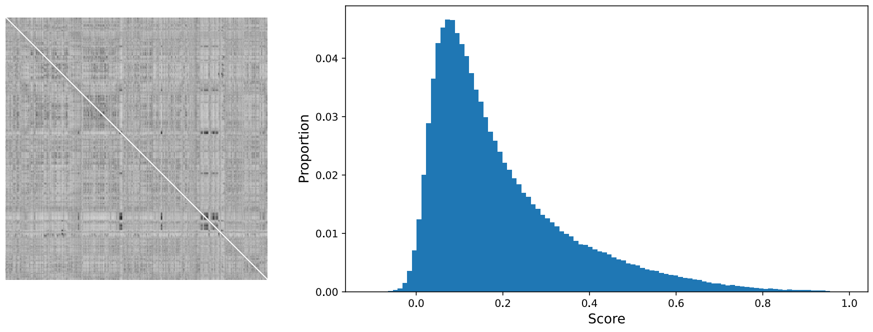

(b) Similarity score distribution for the visual representation from the `GeoSimCLR` model.

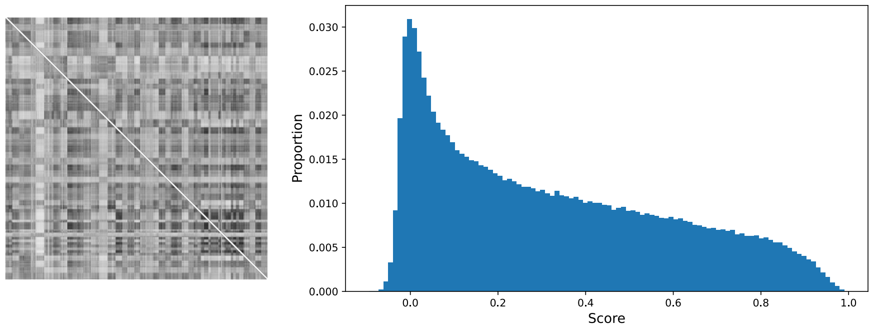

(c) Similarity score distribution for the contextual representation from the `GeoSimCLR` model.

Figure 4.5: The visual similarity score distribution is akin to that showcased in Figure 4.3a. The contextual similarity score distribution remains left-skewed due to the contrastive objective, but since different patches are likely to share a lot more contexts, contextual similarity is likely to be higher in general. Notice how the contextual representation heavily influences the geocontrastive representation.

I then evaluated the model with the best validation loss on the PPIT. Surprisingly, using the full geocontrastive representations lead to extremely poor results in the PPIT. These tasks weren't defined to evaluate contextual similarity, so perhaps including a contextual representation harmed the similarity scores. I was able to confirm this by visualising the similarity score matrix for the `GeoSimCLR` model, alongside the similarity score matrices for the visual and contextual representations (see Figure 4.5). Therefore, I also evaluated the visual representations on the PPIT.

Moreover, I defined a weighted geographical similarity matrix as a weighted sum of the visual and contextual similarity matrices. From Figure 4.5a, the geocontrastive similarity score matrix seems to be most similar to the contextual similarity score matrix in Figure 4.5c. With this weighted sum I hoped to push similarity scores in the direction of visual similarity, whilst still encoding some contextual information. For the following results, I used 0.9 as a weight for the visual similarity score matrix, and 0.1 as a weight for the contextual similarity score matrix (I also tried $0.7, 0.75, 0.8, 0.85, 0.95$, but I found that 0.9 resulted in a good balance between visual and contextual similarity).

Table 4.8: Results for the PPIT. I compare the 2 best contrastive models with `GeoSimCLR`.

Model	Top-1 Accuracy	Top-5 Accuracy	Top-10 Accuracy	Positive Pair Accuracy
Best `SimCLR`	**0.22654**	**0.76305**	**0.80272**	**0.74905**
Best `BYOL` ($\tau = 0.90$)	0.22256	0.74759	0.79679	0.73359
`GeoSimCLR`	0.01925	0.07059	0.09334	0.06529
Visual `GeoSimCLR`	0.21079	0.69965	0.76296	0.68085
Weighted `GeoSimCLR`	0.17151	0.57608	0.68284	0.54171

4.4.1.4 Future Improvements

Preliminarily, the results in Table 4.8 aren't spectacular: adding contextual information seems to hinder the model's positive pair identification capacity. Moreover, there is a significant accuracy difference when comparing `GeoSimCLR`'s visual representations with the representations from `SimCLR`. I believe that this is likely due to `SimCLR` learning larger representations (512-dimensional) than the visual representations learnt by `GeoSimCLR` (256-dimensional), which allows better encoding of key details. This could indicate that larger representations lead to better contrastive encodings. In retrospect, and keeping this in mind, I can think of a variety of improvements, which would allow `GeoSimCLR` to incorporate both visual and contextual information more effectively.

Firstly, the contrastive objective could be modified to ensure that visual and contextual representations are learnt more cohesively: since projection and contrastive loss utilise different parts of the representation, these don't work synergistically in representing similarity. Ideally, I'd like visually similar patches appearing in similar contexts to obtain the highest similarity scores, which isn't currently happening. To enforce this, instead of splitting the representation, I could pass the whole representation through 2 distinct projectors, and apply the visual and contextual contrastive losses to these 512-dimensional representations. The main drawback is that visual and contextual representations won't be distinguishable.

Secondly, using a `CNN` encoder for `GeoSimCLR` could be too ambitious, particularly when gauging contextual information, so the enhanced feature extraction capabilities of a `ResNet` could be more appropriate.

Thirdly, it seems that the contextual representation is getting too highly weighted, especially after normalising the geocontrastive represention to compute similarity scores, so perhaps I could reduce the number of features involved in encoding contextual information (i.e only use 10% of the features, instead of 50%).

Lastly, the data could be changed. Instead of randomly sampling contextual patches from different positions for each visual positive pair, I could use the same contextual patch position for visual patch pairs of the same region (for example, for a given region, always use the upper right neighbouring patch). This would reduce the variability of contextual patches to which the model is exposed to, which should hopefully improve the sharpness of the contextual representations. Alternatively, perhaps the data itself isn't too representative of context, so the contrastive representations are encoding other features unrelated to context. To fix this, perhaps a more selective contextual sample procedure could be used (for example, if a road is divided into 2 patches, make sure these patches appear as contextual pairs), or an alternative way of providing context could be used (for instance, use a 256×256 patch which contains the reference patch).

4.4.2 Clustering

The contrastive objective gives us representations which should be close in latent space, so it is natural to ask whether there is any structure to them within the space. To investigate this, I clustered the different contrastive representations, using 2 methods. The first one was `K-Means`, due to its simplicity. However, it requires that I define the number of clusters. Therefore, I also considered `HDBSCAN` [37] (Hierarchical Densitiy-Based Spatial Clustering of Applications with Noise): not only does it automatically find the number of clusters, it can also detect outliers, and has soft clustering capabilities. For `K-Means`, I employ the `scikit-learn` [38] implementation, whilst for `HDBSCAN`, I employ the implementation developed by McInnes, Healy, and Astels [37].

Since contrastive models use cosine similarity in latent space to define representation similarity, it is the most natural measure with which to cluster these representation. However, neither `K-Means` nor `HDBSCAN` have cosine distance as an available metric. Thus, for clustering, I normalised all the representations to unit vectors; then Euclidean distance becomes proportional to cosine distance. Indeed, if $\underline{x}, \underline{y}$ are unit vectors, the larger the cosine similarity, the smaller the Euclidean distance:

$$\begin{aligned}
||\underline{x}-\underline{y}||_2^2 &= (\underline{x}-\underline{y})^T(\underline{x}-\underline{y}) \\
&= \underline{x}^T\underline{x} - 2\underline{x}^T\underline{y} + \underline{y}^T\underline{y} \\
&= ||\underline{x}||_2^2 + ||\underline{y}||^2 - 2\cos(\theta)||\underline{x}||_2||\underline{y}||_2 \\
&= 2(1-\cos(\theta))
\end{aligned}$$

I also considered an alternative pipeline: first, reduce the dimensionality of the embeddings (I considered 2,3,5,10, 15 and 100 dimensions), and then cluster the resulting lower-dimensional embeddings with Euclidean distance. For dimensionality reduction, I considered 2 methods: Principal Component Analysis (`PCA`), since it is simple and fast (using the `scikit-learn` [38] implementation) and `UMAP` [39], since it is good at preserving local and global structure (using the implementation by McInnes, Healy, and Melville [39]).

4.4.2.1 Clustering Validation Data

I began by clustering the 5,538 unique patch representations from the validation data using `HDBSCAN` (manually specifying cluster number for `K-Means` meant that dissimilar patches were often clustered together). Since clustering all these 512-dimensional representations directly took too long, I applied dimensionality reduction. `UMAP` produced semantically consistent clusters (meaning that patches in a cluster are semantically similar) when using 10-100 features, although with less features the number of clusters and outliers decreased (see Table C.6 for details). `PCA` generated small clusters and deemed most representations as outliers, regardless of the number of features used. Thus, I used 15 features for dimensionality reduction, alongside `HDBSCAN` for clustering.

Generally, `BYOL`-derived clusters tended to be very semantically consistent, whilst `SimCLR`-based clusters often included anomalous patches (for instance, clusters which predominantly had patches with trees sometimes contained patches with buildings). Surprisingly, `GeoSimCLR` clusters mainly contained patches from a single map style, without much regard to visual content (I found a cluster containing patches with rail tracks, trees and buildings which seemed to come from the same map). This could indicate that contextual representations learnt by `GeoSimCLR` are encoding map style instead of context. Cluster examples available at subsection C.7.5.

`PCA` clusters were extremely semantically consistent for `BYOL` representations (I could immediately come up with a textual label to describe cluster content) and distinct. Conversely, different clusters generated with `UMAP` contained similar patches (although clusters remained semantically consistent). Nonetheless, they were impressively nuanced, particularly with `BYOL` and `SimCLR`. For instance, a variety of clusters contained rail tracks, differentiated by orientation and positioning (cluster 24 had horizontal rail tracks on the top of the patch, while cluster 57 had rail tracks at the bottom going diagonally from left to right). I also found clusters with natural elements (small or large number of trees, trees alongside roads, mountains, grasslands), city-based (building blocks, roads) and containing text.

Evaluating clustering systematically, particularly with unlabelled data, is a challenge. In this case, I have exploited the canonical similarity score of the contrastive representations to visualise how scores are distributed over clusters. In particular, for each cluster (excluding outliers), I computed the similarity score between each of its patches, grouped all these scores together, and plotted a histogram using 100 bins.

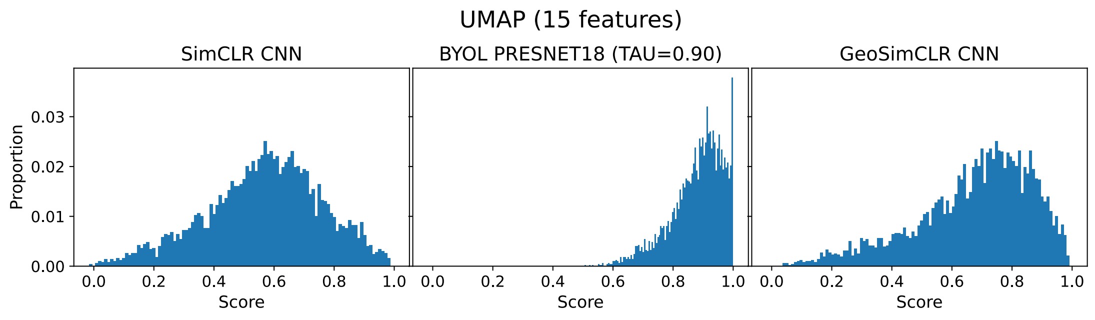

(a) `UMAP` with 15 features and `HDBSCAN` (excluding outliers).

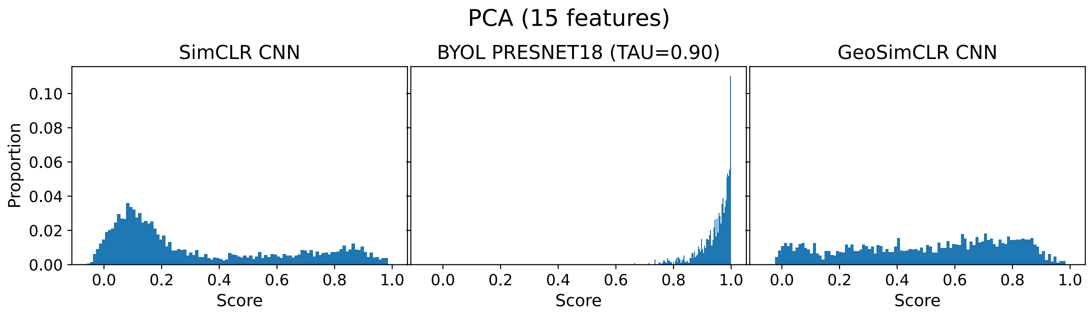

(b) PCA with 15 features and HDBSCAN (excluding outliers).

Figure 4.6: Similarity score distribution across all clusters after using UMAP/PCA and HDBSCAN. The y-axis corresponds to the proportion of similarity scores falling in a bin.

The distributions in Figure 4.6 are fairly different to those from Figure 4.3 and Figure 4.5. With UMAP, all distribution become markedly more right-skewed; with PCA this is only the case with BYOL. These distributions correspond with what I observed above, whereby BYOL seems to form highly similar clusters with both PCA and UMAP, whilst SimCLR clusters benefit from the complexity of UMAP. This could indicate that BYOL generates representations in a simpler or more structured manner, such that even a simple method like PCA is capable of reducing the dimensions whilst preserving similarity information.

4.4.2.2 Visualising Contextual Representations

Following from subsubsection 4.4.2.1, I wanted to see whether GeoSimCLR's contextual representations were encoding stylistic features instead of contextual features. If this were the case, then high similarity scores will be biased towards patch pairs from the same map style, which would hinder the PPIT of the geocontrastive representations, as observed in Table 4.8. To this end, I fetched all the patches corresponding to the same region from the training, validation and test datasets (which came from 3 or 4 distinct maps). I converted these into a geocontrastive representations, applied UMAP and PCA to convert the geocontrastive, visual and contextual representations into 2-dimensional vectors, which I finally clustered with HDBSCAN.

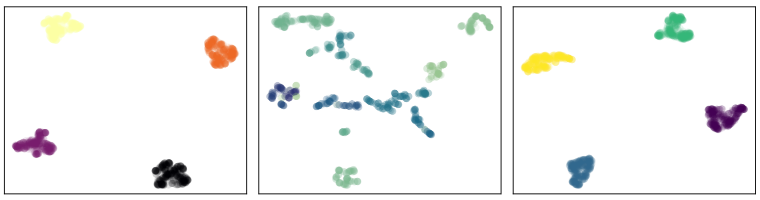

(a) Clusters for region 8, represented by 4 maps.

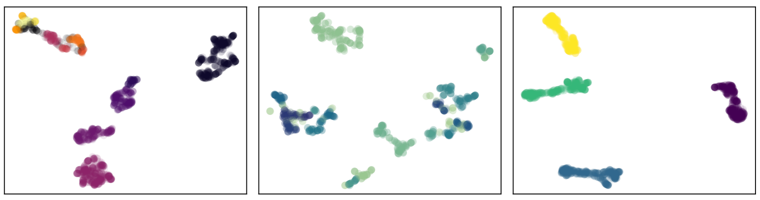

(b) Clusters for region 17, represented by 4 maps.

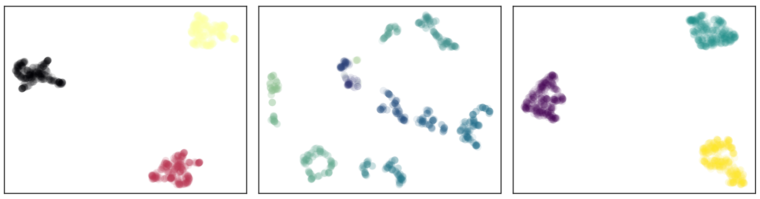

(c) Clusters for region 52, represented by 3 maps.

Figure 4.7: Depiction of contrastive representations in 2 dimensions for 3 different regions. The colours represent the cluster to which a representation is assigned. From left to right, the geocontrastive, visual and contextual representations.

The cluster depictions from Figure 4.7 were produced using `UMAP` + `HDBSCAN` (additional results in subsection C.7.7). I chose these 3 regions arbitrarily, but observed the same pattern throughout all other regions I tested: `UMAP` neatly separated contextual representations in embedding space according to the number of maps for a given region. Moreover, each cluster was composed predominantly by patches from a single map, with just 1 or 2 outliers. This strongly indicates that the contextual representations are capturing stylistic information from the maps, instead of contextual information.

Retrospectively, this makes sense, since it is likely that the contextual patches don't share many visual similarities with the reference patches; in order to make these 2 patches similar, `GeoSimCLR` might simply default to focusing on patch style, since things like map colour, line types, etc... will be shared between the reference and contextual patches. As can be seen in Figure 4.7 this can heavily affect the geocontrastive representations. For regions 8 and 52, despite the visual clustering showcasing clear visual differences, the geocontrastive representations get tightly clustered in similar fashion to the contextual representations.

Admittedly, one must be careful: conclusions about lower-dimensional representations might not apply in the original representation space. However, the consistency of the pattern across different regions, alongside the fact that even `PCA` can pick up on these distinct contextual clusters (see subsection C.7.7) provides good evidence that my conclusion is valid. Moreover, taking the geocontrastive representations for the different maps of a region, I computed their similarity score matrix, which revealed that contextual similarity is significantly higher amongst representations coming from the same map, whilst visual similarity remains relatively uniform (see Figure C.16).

4.4.2.3 Segmentation Through Clustering

Another way of illustrating structure in latent space is by clustering patches belonging to a single map. By colouring the patches according to cluster, and then reconstructing the map, good representations should reveal the semantic differences between different regions of a map. For this, we took all patches corresponding to a given map from training, validation and testing data. I clustered using `HDBSCAN` and `K-Means` (with $K = 4$). I only used `UMAP` with 15 features for dimensionality reduction. Since the number of patches was small, I also used `HDBSCAN` to cluster directly in latent space.

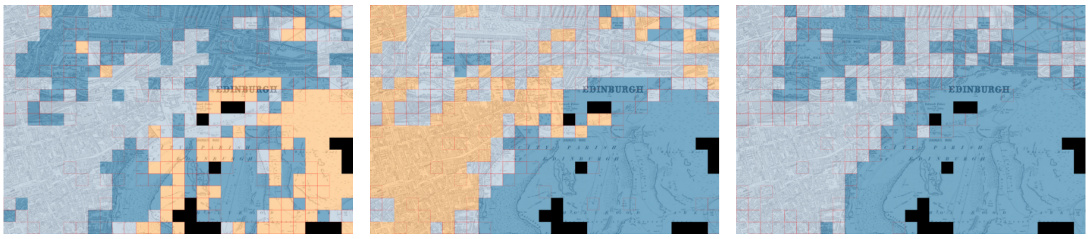

(a) Segmentation using HDBSCAN in latent space.

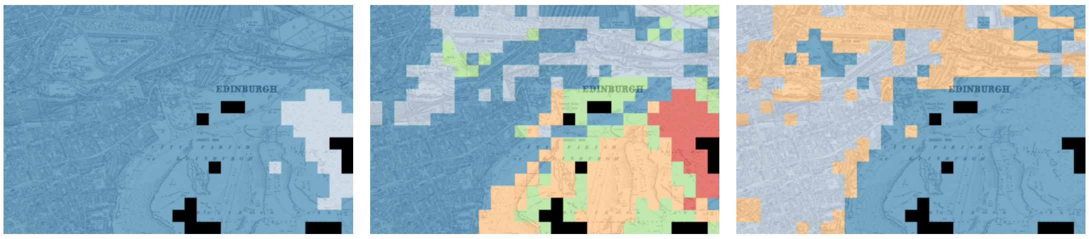

(b) Segmentation using UMAP (15 features) + HDBSCAN.

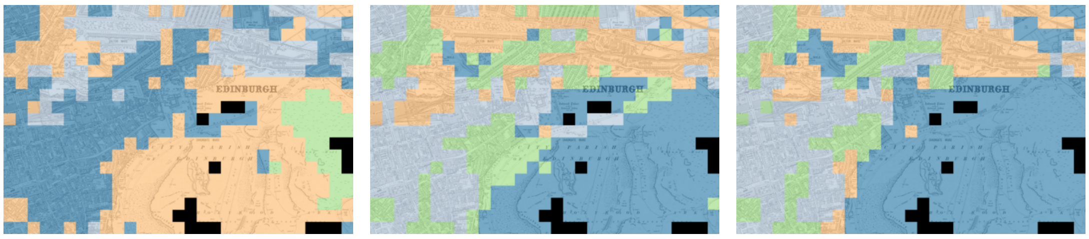

(c) Segmentation UMAP (15 features) + K-Means ($K = 4$).

Figure 4.8: Segmentations for map 82877412. Outliers for HDBSCAN were assigned a cluster by using soft clustering. These are denoted by a red box around the patch. From left to right, the segmentations use SimCLR, BYOL and GeoSimCLR representations. Segmentations for different maps of the same region available at subsection C.7.9.

From Figure 4.8, it seems that the most semantically significant segmentations are obtained by using HDBSCAN directly with the BYOL representations. The dark blue cluster corresponds to nature, the orange cluster to buildings and the light blue cluster corresponds to railtracks. The other segmentations are either too simple (like using UMAP + HDBSCAN with SimCLR representations, or HDBSCAN directly on GeoSimCLR representations), or put semantically different patches in the same cluster (for example, the green cluster for BYOL representations using UMAP + K-Means, which contains nature, buildings and railtracks).

Notice that in all SimCLR segmentations, there is a distinct region corresponding to grasslands which is always generated as a cluster (the green cluster when using UMAP + K-Means). However, this isn't found by any other method (only by BYOL with UMAP + HDBSCAN). This hints at the high discriminative capacity of SimCLR, since the grassland patches are particularly distinctive.

It seems that the best segmentation strategy with SimCLR is using UMAP + K-Means, as it generally identifies the distinct regions of the map well (although some buildings are put as part of the nature cluster, and a part of the railtracks are included within the buildings). For GeoSimCLR, UMAP + HDBSCAN seems to work best.

Chapter 5

Discussion and Conclusions

5.1 Main Conclusions

In conclusion, I belive that I have reasonably demonstrated the effectiveness of CL in encoding features in temporally-spaced historical maps. I have systematically compared how different hyperparameter settings influence the capacity of SimCLR and BYOL to learn useful representations, which allow them to recall true positive patch pairs. I have observed that SimCLR is generally better at correctly identifying true positive pairs, and that it learns in a more robust manner than BYOL, which given certain hyperparamter settings, can collapse its representations. Nonetheless, I have showcased how the positive pair finding capacity of the models can be useful when exploring similarities across different maps, and I propose a framework for using these learnt representations to align unseen maps.

I visualised the similarity score distributions for the 2 models, and observed a stark differences with regards to the range and shape of the distributions, likely due to the choice of encoder, alongside the use of negative pairs during training.

I was quite surprised that, according to the PPIT, the best SimCLR model for these tasks seemed to employ a simple CNN encoder. Moreover, I have observed that even if I train more complex, ResNet-based models for longer, the performance in these evaluation metrics isn't too significant. On the other hand, for BYOL using a ResNet-based model substantially improved performance in these tasks.

I also sought to better understand how these different models encode the features. Throughout the proposed tasks, I have observed a significant contrast in the sort of patches that the different models find similar. SimCLR seems to be a lot more discriminative, which allows it to more decisively gauge whether 2 patches are similar or dissimilar. On the other hand, BYOL seems to learn more semantically oriented representations, as it seems to be more capable at abstracting away broad features from the patches.

SimCLR representations seem to have encoded stylistic nuances present in the maps (which allow it to more readily discriminate when 2 patches are from the same year of production), whilst BYOL seems to be fairly invariant to these stylistic features.

Moreover, SimCLR is also better at encoding the degree of information present within patches than BYOL.

To further explore the factors influencing the learnt features, I applied transformations to the patches, from which I observed that the representations for both models are most sensitive to the orientation and location of patch attributes, whereas transformations which change the colour or blurriness of a patch have the least effect. I believe that these features are highly desirable for an application involving maps. However, I observed that the representations are also fairly influenced by cropping, which can indicate that the models are not gauging local features well, and are instead encoding feature combinations as a whole.

I developed a new contrastive framework, GeoSimCLR, with the hope of learning contrastive representations which encode both visual and contextual information. I hoped that these representations would be more useful for map-based applications, were understanding the surroundings of a given patch can be critical to finding patches which are similar, and appear in similar contexts. However, I found that this combination of visual and contextual information ultimately hurt the performance of the representations, particularly since the contextual features were being weighted too heavily.

To investigate the structure of the representations in latent space, I employed clustering. I observed that BYOL-based clusters were more semantically consistent, whereas SimCLR clusters tended to have more outliers, which didn't follow the general semantic meaning of the cluster. When clustering GeoSimCLR, I discovered that the learnt contextual representations seemed to primarily encode stylistic attributes. This meant that similarity scores were biased towards patches coming from the same map type. Nonetheless, I showed that by more heavily weighting the visual representations, I obtained similarity scores which better aligned with human judgement.

I also used clustering to semantically segment individual maps. Generally, segmentations weren't perfect, with different clusters overlapping. However, the clusters do seem to encode some broad-sense awareness of semantics, particularly when clustering BYOL representations directly in latent space.

5.2 Future Work

There are several areas of future work that could improve upon the results of this project. First, in terms of data processing, exploring the use of overlapping patches could provide the model with more information and feature combinations, leading to more robust representations. Secondly, extending the project to include a wider variety of maps with distinct styles, such as Bartholomew maps, would increase the usability of these contrastive models, particularly given how challenging aligning maps with such different styles is. Lastly, a more fine-grained hyperparameter tuning could be employed to shed light on why CNN encoders work best with SimCLR for this purpose, and why certain BYOL settings lead to representation collapse. One could also evaluate a ResNet-based SimCLR model on temporal/information awareness tasks, to see whether this improves the semantic awareness of the model, in contrast to when a CNN is used.

When evaluating the contrastive representations, I have avoided a direct comparison between the two models (which is critical given their distributional difference), which motivated the development of the PPIT showcased in subsection 4.2.2, a novel, unsupervised way of evaluating different contrastive models. Nonetheless, these tasks are just a proxy for selecting “good enough” models and, for example, don’t take into account the quality of negative pairs found by the contrastive models (for example, given a reference patch containing a building in a certain style/orientation, we should expect a better model to find negative pairs which share these features, but currently this information isn’t taken into account). The dowsntream classification tasks presented in subsection 4.3.1 provided a simple way of analysing the difference in representations learnt by the two models, but these could be further refined.

For example, through hand-labelling, an object classifier such as YOLO [40] can be trained, to detect features such as trees, buildings or text. A classifier can then be trained to determine which objects are present in a patch, based solely on the contrastive representation, which would provide more concrete evidence on how these models encode visual information. Furthermore, the contrastive representations could be used to generate a canonical map patch in a given style; this could reveal which features are encoded by contrastive representations, and would provide a framework for homogenising different maps of the same region (as they’d all be converted into the “same” map). I tried this using a UNet [41] to convert OS map representations into both OSM and OS style maps, and found that simple shapes (such as roads) could be successfully extracted from the representations (including a relatively correct orientation and positioning). However, the model struggled with more complex features (such as building shapes), so perhaps more complex systems (such as diffusion models [42]) could be used.

I was able to exploit the nature of our representations, in order to derive somewhat meaningful conclusions from the clustering results. However, given the large number of parameters that both UMAP and HDBSCAN allow, the results could be further refined to reveal more information. This would be particularly relevant when using clustering for map segmentation, whereby the segmentations weren’t always consistent, and they were only meaningful for maps with many different sets of features. Nonetheless, this could be an interesting route to further explore, particularly since segmenting these historical maps in a completely unsupervised manner can be quite useful (for example, exploring city development through time).

Bibliography

[1] Kasra Hosseini et al. *MapReader: A Computer Vision Pipeline for the Semantic Exploration of Maps at Scale*. 2021. DOI: 10.48550/ARXIV.2111.15592. URL: https://arxiv.org/abs/2111.15592.

[2] Kaiming He et al. "Deep Residual Learning for Image Recognition". In: *CoRR* abs/1512.03385 (2015). arXiv: 1512.03385. URL: http://arxiv.org/abs/1512.03385.

[3] Zekun Li. "Generating Historical Maps from Online Maps". In: *Proceedings of the 27th ACM SIGSPATIAL International Conference on Advances in Geographic Information Systems*. SIGSPATIAL '19. Chicago, IL, USA: Association for Computing Machinery, 2019, pp. 610–611. ISBN: 9781450369091. DOI: 10.1145/3347146.3363463. URL: https://doi.org/10.1145/3347146.3363463.

[4] Jun-Yan Zhu et al. *Unpaired Image-to-Image Translation using Cycle-Consistent Adversarial Networks*. 2017. DOI: 10.48550/ARXIV.1703.10593. URL: https://arxiv.org/abs/1703.10593.

[5] OpenStreetMap contributors. *Planet dump retrieved from https://planet.osm.org*. 2017. URL: https://www.openstreetmap.org.

[6] Zekun Li et al. "An Automatic Approach for Generating Rich, Linked Geo-Metadata from Historical Map Images". In: *Proceedings of the 26th ACM SIGKDD International Conference on Knowledge Discovery & Data Mining*. KDD '20. Virtual Event, CA, USA: Association for Computing Machinery, 2020, pp. 3290–3298. ISBN: 9781450379984. DOI: 10.1145/3394486.3403381. URL: https://doi.org/10.1145/3394486.3403381.

[7] Ashish Jaiswal et al. "A Survey on Contrastive Self-Supervised Learning". In: *Technologies* 9.1 (2021). ISSN: 2227-7080. DOI: 10.3390/technologies9010002. URL: https://www.mdpi.com/2227-7080/9/1/2.

[8] Lanling Xu et al. *Negative Sampling for Contrastive Representation Learning: A Review*. 2022. arXiv: 2206.00212 [cs.IR].

[9] S. Chopra, R. Hadsell, and Y. LeCun. "Learning a similarity metric discriminatively, with application to face verification". In: 1 (2005), 539–546 vol. 1. DOI: 10.1109/CVPR.2005.202.

[10] Florian Schroff, Dmitry Kalenichenko, and James Philbin. "FaceNet: A unified embedding for face recognition and clustering". In: (June 2015). DOI: 10.1109/cvpr.2015.7298682. URL: https://doi.org/10.1109%2Fcvpr.2015.7298682.

[11] Kihyuk Sohn. “Improved Deep Metric Learning with Multi-class N-pair Loss Objective”. In: 29 (2016). Ed. by D. Lee et al. URL: https://proceedings.neurips.cc/paper/2016/file/6b180037abbebea991d8b1232f8a8ca9-Paper.pdf.

[12] Aaron van den Oord, Yazhe Li, and Oriol Vinyals. *Representation Learning with Contrastive Predictive Coding*. 2018. DOI: 10.48550/ARXIV.1807.03748. URL: https://arxiv.org/abs/1807.03748.

[13] Ting Chen et al. “A Simple Framework for Contrastive Learning of Visual Representations”. In: (2020). DOI: 10.48550/ARXIV.2002.05709. URL: https://arxiv.org/abs/2002.05709.

[14] Kaiming He et al. *Momentum Contrast for Unsupervised Visual Representation Learning*. 2019. DOI: 10.48550/ARXIV.1911.05722. URL: https://arxiv.org/abs/1911.05722.

[15] Jean-Bastien Grill et al. *Bootstrap your own latent: A new approach to self-supervised Learning*. 2020. arXiv: 2006.07733 [cs.LG].

[16] Jia Deng et al. *ImageNet: A large-scale hierarchical image database*. 2009. DOI: 10.1109/CVPR.2009.5206848.

[17] Yuhao Zhang et al. *Contrastive Learning of Medical Visual Representations from Paired Images and Text*. 2020. DOI: 10.48550/ARXIV.2010.00747. URL: https://arxiv.org/abs/2010.00747.

[18] Yawen Wu et al. *Distributed Contrastive Learning for Medical Image Segmentation*. 2022. DOI: 10.48550/ARXIV.2208.03808. URL: https://arxiv.org/abs/2208.03808.

[19] Shekoofeh Azizi et al. *Big Self-Supervised Models Advance Medical Image Classification*. 2021. DOI: 10.48550/ARXIV.2101.05224. URL: https://arxiv.org/abs/2101.05224.

[20] Krishna Chaitanya et al. *Contrastive learning of global and local features for medical image segmentation with limited annotations*. 2020. DOI: 10.48550/ARXIV.2006.10511. URL: https://arxiv.org/abs/2006.10511.

[21] Xu Xie et al. “Contrastive Learning for Sequential Recommendation”. In: *2022 IEEE 38th International Conference on Data Engineering (ICDE)*. 2022, pp. 1259–1273. DOI: 10.1109/ICDE53745.2022.00099.

[22] Ishan Dave et al. “TCLR: Temporal contrastive learning for video representation”. In: *Computer Vision and Image Understanding* 219 (2022), p. 103406. ISSN: 1077-3142. DOI: https://doi.org/10.1016/j.cviu.2022.103406. URL: https://www.sciencedirect.com/science/article/pii/S1077314222000376.

[23] Patrick Helber et al. “Introducing Eurosat: A Novel Dataset and Deep Learning Benchmark for Land Use and Land Cover Classification”. In: (2018), pp. 204–207. DOI: 10.1109/IGARSS.2018.8519248.

[24] Yao-Yi Chiang et al. “Training Deep Learning Models for Geographic Feature Recognition from Historical Maps”. In: *Using Historical Maps in Scientific Studies: Applications, Challenges, and Best Practices*. Cham: Springer International Publishing, 2020, pp. 65–98. ISBN: 978-3-319-66908-3. DOI: 10.1007/978-3-319-66908-3_4. URL: https://doi.org/10.1007/978-3-319-66908-3_4.

[25] Keiron O’Shea and Ryan Nash. *An Introduction to Convolutional Neural Networks*. 2015. arXiv: 1511.08458 [cs.NE].

[26] Chitra Agastya et al. *Self-supervised Contrastive Learning for Irrigation Detection in Satellite Imagery*. 2021. DOI: 10.48550/ARXIV.2108.05484. URL: https://arxiv.org/abs/2108.05484.

[27] Gencer Sumbul et al. "Bigearthnet: A Large-Scale Benchmark Archive for Remote Sensing Image Understanding". In: *IGARSS 2019 - 2019 IEEE International Geoscience and Remote Sensing Symposium*. IEEE, July 2019. DOI: 10.1109/igarss.2019.8900532. URL: https://doi.org/10.1109%2Figarss.2019.8900532.

[28] Kumar Ayush et al. *Geography-Aware Self-Supervised Learning*. 2020. DOI: 10.48550/ARXIV.2011.09980. URL: 8.

[29] Gordon Christie et al. *Functional Map of the World*. 2017. DOI: 10.48550/ARXIV.1711.07846. URL: https://arxiv.org/abs/1711.07846.

[30] Kihyuk Sohn. *Improved Deep Metric Learning with Multi-class N-pair Loss Objective*. Ed. by D. Lee et al. 2016. URL: https://proceedings.neurips.cc/paper/2016/file/6b180037abbebea991d8b1232f8a8ca9-Paper.pdf.

[31] Adam Paszke et al. "PyTorch: An Imperative Style, High-Performance Deep Learning Library". In: *Advances in Neural Information Processing Systems 32*. Curran Associates, Inc., 2019, pp. 8024–8035. URL: http://papers.neurips.cc/paper/9015-pytorch-an-imperative-style-high-performance-deep-learning-library.pdf.

[32] National Library of Scotland. *Discover the World in Maps*. https://www.nls.uk/collections/maps/. URL: https://www.nls.uk/collections/maps/.

[33] Ordnance Survey. *Ordnance Survey: See a Better place*. https://www.nls.uk/collections/maps/. URL: https://www.ordnancesurvey.co.uk.

[34] G. Bradski. "The OpenCV Library". In: *Dr. Dobb's Journal of Software Tools* (2000). URL: https://opencv.org.

[35] Weiyuan Wu. *dovahcrow/patchify*. Mar. 2021. URL: https://github.com/dovahcrow/patchify.py.

[36] John Canny. "A computational approach to edge detection". In: *IEEE Transactions on pattern analysis and machine intelligence* 6 (1986), pp. 679–698.

[37] Leland McInnes, John Healy, and Steve Astels. "hdbscan: Hierarchical density based clustering". In: *The Journal of Open Source Software* 2.11 (2017), p. 205.

[38] F. Pedregosa et al. "Scikit-learn: Machine Learning in Python". In: *Journal of Machine Learning Research* 12 (2011), pp. 2825–2830.

[39] Leland McInnes, John Healy, and James Melville. *UMAP: Uniform Manifold Approximation and Projection for Dimension Reduction*. 2018. DOI: 10.48550/ARXIV.1802.03426. URL: https://arxiv.org/abs/1802.03426.

[40] Joseph Redmon et al. *You Only Look Once: Unified, Real-Time Object Detection*. 2016. arXiv: 1506.02640 [cs.CV].

[41] Olaf Ronneberger, Philipp Fischer, and Thomas Brox. *U-Net: Convolutional Networks for Biomedical Image Segmentation*. 2015. arXiv: 1505.04597 [cs.CV].

[42] Jonathan Ho, Ajay Jain, and Pieter Abbeel. *Denoising Diffusion Probabilistic Models*. 2020. arXiv: 2006.11239 [cs.LG].

[43] Sean Gillies et al. *Rasterio: geospatial raster I/O for Python programmers*. https://github.com/mapbox/rasterio. Mapbox, 2013. URL: https://github.com/mapbox/rasterio.

[44] Alan D. Snow et al. *pyproj4/pyproj: 3.0.1rc0*. https://github.com/pyproj4/pyproj. Version 3.0.1rc0. Mar. 2021. DOI: 10.5281/zenodo.4571637. URL: https://doi.org/10.5281/zenodo.4571637.

[45] Sean Gillies et al. *Shapely: manipulation and analysis of geometric objects*. toblerity.org, 2007. URL: https://github.com/shapely/shapely.

Appendix A

Additional Work

A.1 Aligning Maps of the Same Region from Georeference Information

A key aspect of this project is being able to automatically find whether 2 maps are meant to represent the same region, as without this, no alignment is possible for positive patch pairs. Thankfully, since I had the georeferenced maps, I could leverage the metadata of the maps to automatically group together maps which corresponded to the same area.

Our first approach to this was to employ the metadata inherent in the original (unprocessed) `TIFF` files. Amongst other things, this included the coordinate system for the map and a bounding box for the map in those coordinates. Using the package `rasterio` [43], the bounding box for the map could be extracted. Using `pyproj` [44], I then converted the bounding box into longitudes and latitudes (the NLS used the British National Grid system for encode coordinates), since these are easier to work with and understand. I thought that using these coordinates, I could then group together the maps which shared the same bounding box. However, upon discovering that no groups were found, I decided to plot the bounding boxes using `geojson.io`:

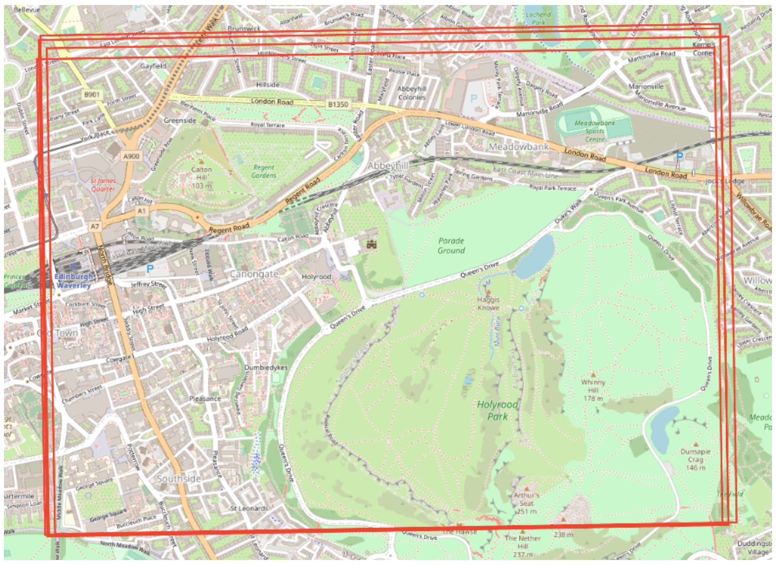

Figure A.1: Bounding boxes for 4 maps of the same region. Image generated using geojson.io (see B.1.2).

As one can see, the rotation observed in the maps seemed to affect the bounding boxes stored as metadata. To mitigate this, I could have tried rotating the bounding boxes by the angle used to rectify the original maps. However, this posed unnecessary complications, and wasn't likely to work: longitudes and latitudes correspond to coordinates on a spherical surface, so applying an affine transformation wouldn't lead to a perfect bounding box alignment. Instead, I chose to use the `shapely` [45] package, which allowed us to convert the bounding boxes into shapes. Critically, this package allows me to compute the intersection area between 2 shapes. I used this intersection area as a signal to determine if 2 maps represented the same region: for any 2 maps, I can compute the intersection area between their bounding boxes; if this area corresponds to a high proportion of the area of each of the bounding boxes, then the 2 maps are likely to represent the same region. Using a threshold of 0.8 for the intersection area proportion, I was able to quickly and efficiently group maps together.

Once I had access to the metadata from Table B.1, I was able to confirm that this method found the exact same region alignments, which means tha tthis method could be used in situations where such metadata might not be available.

A.2 Aligning Maps at the Patch Level

The last step in handling the maps was to, given 2 maps of the same region, be able to generate pairs of patches which are aligned: that is, finding sets of patches which correspond to the same area. Initially, I worked under the assumption that this would be an additional pre-processing step, since the maps were of different shapes, and I were told that during scanning, slight warping could have been introduced into the maps. Our alignment algorithm was tested on the 4 OS maps corresponding to the region portrayed in Figure 3.1. I felt that this was a fairly representative map, since it contained a variety of interesting features, both from the city (buildings, roads, rail tracks) and from the countryside (mountains, lakes, grasslands). For these tests, the 4 OS maps were split into 2,301 64×64 patches, after applying the bilinear interpolator with kernel 4. Because of this, I already had a "rough" alignment.

Once I had a rough alignment, our alignment algorithm worked as follows. Say I have 2 maps: a reference map, and a query map. Our objective is that, for each $i \in [1, 2301]$, I can shift each patch q_i in the query map, such that it has the best possible alignment with its corresponding patch r_i in the reference map.

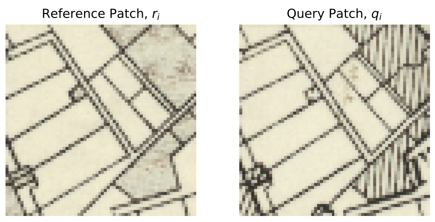

Figure A.2: I aim to, given this rough alignment of r_i, q_i, find the best possible way of shifting q_i, such that it is as aligned with r_i as possible.

To define the best possible alignment, I considered a maximum number of vertical and horizontal shifts, v_{shift}, h_{shift} (for our experiments, I used $v_{shift} = h_{shift} = 7$). I then padded the query and reference patches, using white pixels. Finally, I applied a binary, adaptive threshold to q_i, r_i (which converts each pixel into either black or white), and then iterated over all possible combinations $(\Delta y, \Delta x) \in [-v_{shift}, v_{shift}] \times [-h_{shift}, h_{shift}]$. For each $(\Delta y, \Delta x)$, I shifted q_i vertically by Δy pixels, and horizontally by Δx pixels (call the result q_i^{shift}), and then computed a pixel-wise XOR of q_i^{shift} with r_i. Summing this then tells us the number of pixels in common between q_i^{shift} and r_i, which I use as our alignment measure: the higher this value, the stronger the alignment.

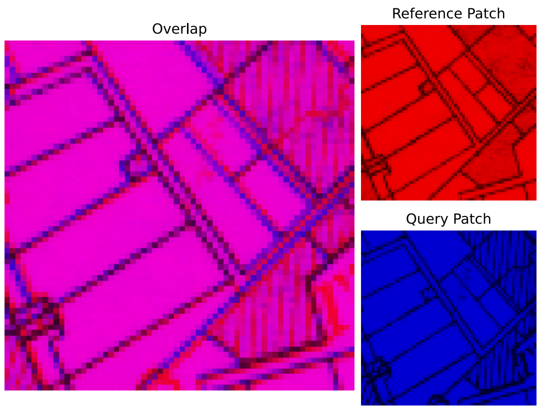

Figure A.3: One way of visualising the misalignment between 2 patches is by using the red channel of the reference, and the blue channel of the query. I can construct then overlap them as a single image. Regions which appear red/blue in the overlapped image correspond to misalignments. As can be seen, these 2 patches barely misalign. In fact, our algorithm assigns optimal alignment by using $\Delta y = -1$ and $\Delta x = 0$ (I just need to shift the query patch one pixel down).

I can then apply this procedure over each roughly aligned patch between 2 maps (taking care to instead of including the padding in q_i^{shift}, to crop out the corresponding map region). I can then visualise the misalignment between 2 maps, by counting the number of times a given shift had to be used to obtain the best possible alignment:

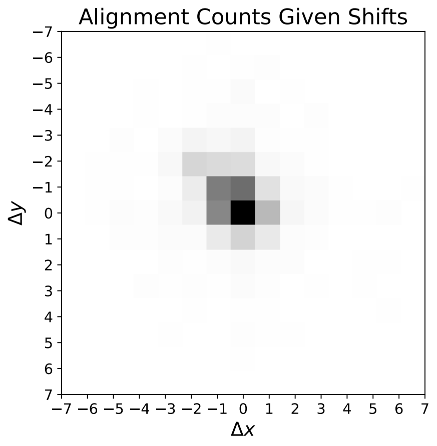

Figure A.4: Heatmap showing the number of times a given alignment shift $(\Delta y, \Delta x)$ was used in our alignment algorithm, over all patches in 2 maps. The darker a region, the more times a given shift was used. I can see that by far, most patches required no shift at all, with the great majority of patches requiring at most 2 pixel shifts vertically and/or horizontally.

Based on Figure A.2, it seemed reasonable to not use the alignment algorithm: most patches were reasonably aligned, and the minor misalignments found shouldn't impact our contrastive models in any significant way (after all, CL involves applying transformations to positive pairs, in order to learn more robust representations, so I were getting these transformations directly from the data). Just in case, I decided to explore which patches required large shifts in order to align them. I found that (broadly) these were encompassed in 3 categories: largely empty patches (patches have some noise, so darker regions will appear in different places for different empty patches), patches containing words (since words tended to vary in positioning and size across the maps) and patches containing symbols (since both symbol style and placement varied across maps). Moreover, this method has a clear flaw, in that it relies on some degree of stylistic similarity between the patches. Because of this, it wouldn't be reliable if I wanted to align a Bartholomew and OS patch, for instance. Moreover, computing so many alignments over all the maps in our data would be extremely costly. Hence, I thought that it wouldn't be reasonable to continue pursuing the automatic alignment route, since the rough alignments obtained by just applying `patchify` without overlapping patches were good enough.

A.3 Aligning OS Maps with Bartholomew Maps

One of the capabilities of `rasterio` is that it can be used to recover the pixel corresponding to a given geographical coordinate from `GeoTIFFs`. Because of this, I wanted to see whether it would be possible to extract the region of a Bartholomew map corresponding to the region of some other OS map. Before, with the faulty metadata inherent in the original `TIFF` files, this would have been pointless. However, now that I had the metadata table, this was a bit more feasible. Naturally, the alignment wouldn't be perfect, since the Bartholomew metadata is also faulty.

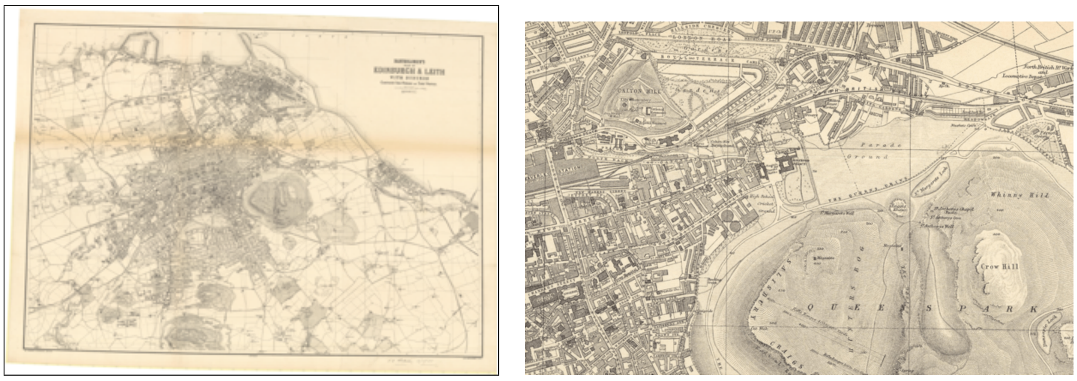

Figure A.5: To the left, a Bartholomew map before being pre-processed. After pre-processing, I crop out a region corresponding to the OS map showcased in Figure 3.1. The result is shown to the right. Notice, comparing this with Figure 3.1, they seem very similar, but the cropped out Bartholomew map is slightly larger. This is due to the fact that the Bartholomew map had to be rotated and cropped. But without this, the cutoff would have been rotated, and so, the alignment would be even worse.

Overall, this supports my decision to not work with Bartholomew maps. Firstly, they have a high variability, even amongst themselves (compare Figure 3.1 with Figure A.5). Secondly, as can be seen from Figure A.5, the borders of Bartholomew maps don't form a boundary with the padding. As such, our current pre-processing method doesn't work too well with Bartholomew maps, and a new technique would need to be developed these borders. However, this is highly non-trivial, since the different Bartholomew maps are inconsistent in their bordering (sometimes theres one border, other times there are multiple parallel border lines). Thirdly, aligning them correctly with OS maps, in an automatic and efficient manner would require a lot more effort and ingenuity. One way of doing this could be identifying common landmarks between the two, but again, this would be an arduous task which could constitute a project all by itself.

A.4 Modifying Representations Through Learning Task

Initially, I tried to enforce geographical awareness by defining a classification task: given some patch *p*, and another patch *r* which appears in its context (that is, one of the 8 patches which will be immediately adjacent to *p*), can I predict the position of *r*, just from their contrastive representations?

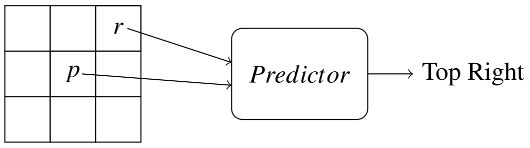

To do this, I learnt 2 simple feedforward models. The first one encoded the latent representations for *p* and *r*, which were then concatenated, and passed to thesecond feedforward layer, which used a softmax activation to predict one of 8 classes (top left, top, top right, left, right, bottom left, bottom or bottom right). However, I didn't obtain great results (around 60% validation and test accuracy), even after 100 epochs of training. Moreover, after passing the contrastive embeddings through the network, the resulting representations didn't preserve the similarity features which made our original representations desirable (for instance, a given patch still obtained a high similarity score with a corresponding positive pair, but its similarity score with other completely different patches also increased).

Appendix B

Maps and Metadata

B.1 GeoJSONs

B.1.1 GeoJSON Containing Full Map Region

```
{
  "type": "FeatureCollection",
  "features": [
    {
      "type": "Feature",
      "geometry": {
        "type": "Polygon",
        "coordinates": [
          [
            [-3.38374788940603,
              55.8715983250667
            ],
            [
              -3.07422210721001,
              55.8715983250667
            ],
            [
              -3.07422210721001,
              56.0020051346329
            ],
            [
              -3.38374788940603,
              56.0020051346329
            ],
            [
              -3.38374788940603,
              55.8715983250667
            ]
          ]
        ]
      },
      "properties": {
        "stroke": "#ff0000",
        "fill" : "none",
        "fill-opacity" : 0
      }
    }
  ]
}
```

B.1.2 GeoJSON of Overlapping Bounding Boxes

```
{
  "type": "FeatureCollection",
  "features": [
    {
      "type": "Feature",
      "geometry": {
        "type": "GeometryCollection",
        "geometries": [
          {
            "type": "Polygon",
            "coordinates": [
              [
                [
                  -3.192112616595414,
                  55.9423625178286
                ],
                [
                  -3.149118538110902,
                  55.94277108265303
                ],
                [
                  -3.149638014166486,
                  55.96030038664902
                ],
                [
                  -3.192651513330189,
                  55.95989155384999
                ],
                [
                  -3.192112616595414,
                  55.9423625178286
                ]
              ]
            ]
          },
          {
            "type": "Polygon",
            "coordinates": [
              [
                [
                  -3.1916248563612144,
                  55.94244979270547
                ],
                [
                  -3.1486045560362697,
                  55.94285843127807
                ],
                [
                  -3.149112581883714,
                  55.960009178369596
                ],
                [
                  -3.1921518949151615,
                  55.959600277564434
                ],
                [
                  -3.1916248563612144,
                  55.94244979270547
                ]
              ]
            ]
          },
          {
            "type": "Polygon",
            "coordinates": [
              [
                [
                  -3.1922529047804167,
                  55.942420425296774
                ],
                [
                  -3.1494971017459723,
                  55.942826815554305
                ],
                [
                  -3.1499948839664507,
                  55.95961890427993
                ],
                [
                  -3.192769187420956,
                  55.959212258688744
                ],
                [
                  -3.1922529047804167,
                  55.942420425296774
                ]
              ]
            ]
          },
          {
            "type": "Polygon",
            "coordinates": [
              [
                [
                  -3.1920101891085304,
                  55.942429550011795
                ],
                [
                  -3.149129078602052,
                  55.942837024945554
                ],
                [
                  -3.149651211538686,
                  55.96045572776686
                ],
                [
                  -3.1925517905857155,
                  55.96004798420948
                ],
                [
                  -3.1920101891085304,
                  55.942429550011795
                ]
              ]
            ]
          }
        ]
      },
      "properties": {
        "stroke": "#ff0000",
        "fill" : "none",
        "fill-opacity" : 0
      }
    }
  ]
}
```

B.2 Code for Rotating and Cropping the Badly Scanned Maps

This code assumes that the image is horizontal, and that the padding is white. This function was developed by adapting:

- How to rotate skewed fingerprint image to vertical upright position [closed]
- How to remove whitespace from an image in OpenCV?

```python
import numpy as np
import cv2 as cv

def rotate_crop_map(map_img):
    gray = cv.cvtColor(map_img, cv.COLOR_RGB2GRAY)
    gray = 255 - gray
    thresh = cv.threshold(gray, 0, 255, cv.THRESH_BINARY + cv.THRESH_OTSU)
        [1]

    # Compute rotated bounding box
    coords = np.column_stack(np.where(thresh > 0))
    center_rect, dims, angle = cv.minAreaRect(coords)

    if angle < -45:
        angle = -angle
    else:
        angle = 90-angle
    print(angle)

    # Rotate image to deskew
    (h, w) = map_img.shape[:2]
    center = (w // 2, h // 2)
    M = cv.getRotationMatrix2D(center, angle, 1.0)
    rotated = cv.warpAffine(map_img, M, (w, h), flags=cv.INTER_CUBIC,
        borderMode=cv.BORDER_REPLICATE)

    gray = cv.cvtColor(rotated, cv.COLOR_BGR2GRAY)
    gray = 255*(gray < 128).astype(np.uint8) # To invert the text to white
    coords = cv.findNonZero(gray) # Find all non-zero points (text)
    x, y, w, h = cv.boundingRect(coords) # Find minimum spanning bounding
        box
    rect = rotated[y:y+h, x:x+w]
    rect = cv.cvtColor(rect, cv.COLOR_BGR2RGB)

    return rect
```

B.3 Metadata Table Columns

Table B.1: Description of the metadata table provided by the NLS. The original table has more columns, but they contained redundant information (i.e same information as other columns). I thus only list the key columns of the metadata table.

Column Name	**Type of Data**
`WKT`	Bounding boxes in Well-Known Text format. Coordinates are stored as longitudes and latitudes.
`SERIES`	The type of map. For example: `Scotland - 25 Inch 2nd and Later Editions`.
`COUNTY`	The country represented in the map. All these maps corresponded to Edinburghshire.
`SHEET_NO`	The sheet number for the map. This helps identify the geographical area covered by the map. These are of the form `007_05`, and there were 57 such unique numbers.
`EDITION`	The edition of the map. All the maps were a second, third, fourth or fifth edition.
`IMAGEURL`	A URL to visualise the map in the NLS website. For instance: https://maps.nls.uk/view/82877892.
`YEAR`	The year in which the map was published. As discussed, these range from 1894 to 1947.

B.4 Code for Removing Uninformative Patches

The method for removing patches with uninformative features was part of the `CLPatchDataset` class, which is the class I used to store the patch dataset for the contrastive algorithms.

```
import numpy as np
import cv2 as cv
from torch.utils.data import Dataset

class CLPatchDataset(Dataset):

    ...

    @staticmethod
    def count_black_pixels(edges):
        black_pixel_idx = np.where(edges == 255)
        return len(black_pixel_idx[0])
```

```
@staticmethod
def get_edges(patch):
    gray = cv.cvtColor(np.array(patch), cv.COLOR_RGB2GRAY)
    gray = cv.GaussianBlur(gray, (3, 3), 0)
    return cv.Canny(gray, 50, 150)

@staticmethod
def is_empty_patch(patch):
    edges = CLPatchDataset.get_edges(patch)
    patch_width = patch.shape[0]

    n_black_pixels = CLPatchDataset.count_black_pixels(edges)

    min_black_pixels = int(0.01 * patch_width * patch_width)
    edge_pixel_range = int(0.1 * patch_width)
    max_edge_pixels = int(0.5 * n_black_pixels)

    if n_black_pixels <= min_black_pixels:
        return True
    else:
        for row in range(edge_pixel_range):
            if CLPatchDataset.count_black_pixels(edges[row, :]) >=
                max_edge_pixels \
                    or CLPatchDataset.count_black_pixels(edges[len(edges
                        ) - 1 - row, :]) >= max_edge_pixels \
                    or CLPatchDataset.count_black_pixels(edges[:, row])
                        >= max_edge_pixels \
                    or CLPatchDataset.count_black_pixels(edges[:, len(
                        edges) - 1 - row]) >= max_edge_pixels:
                return True

    return False
```

Appendix C

Experimental Results

C.1 Estimate for Runtime

We used the set of hypterparameter choices which we used for running our experiments:

- encoder $\in \{$`ResNet18, ResNet34`$\}$
- pretrain $\in \{True, False\}$
- $\tau \in \{0.80, 0.90, 0.95, 0.99\}$
- $\eta \in \{1 \times 10^{-3}, 1 \times 10^{-2}\}$
- batch size $\in \{32, 64\}$
- patch size $\in \{128, 224\}$

Based on preliminary experiments, we obtained a lenient estimate of 12 hours to run 5 epochs (including evaluating the model 100 times per epoch on the validation set), this would amount to around 64 days of training, for *each* of the contrastive models. Typically, `BYOL` took much longer to train than `SimCLR`, and the estimate of around 12 hours is the approximate runtime we observed for `SimCLR` experiments.

C.2 All Experiments Run

Note, for the experiments using 224×224 patches, our dataset changed. In particular, I obtained 24,093 training positive pairs, 2,938 validation positive pairs and 2,886 testing positive pairs. Notice, due to the patch size, certain maps weren't included in this dataset, since upon splitting them into corresponding patches, some regions contained maps with a different number of patches. Said regions weren't included in the final dataset.

Table C.1: Set of all experiments run.

Architecture	**Encoder**	**Pretrained**	τ	**Learning Rate**	**Patch Size**	**Batch Size**
`BYOL`	`ResNet18`	✓	0.99	1×10^{-3}	128×128	64
`BYOL`	`ResNet18`	✓	0.99	1×10^{-2}	128×128	64
`BYOL`	`ResNet18`	✓	0.99	1×10^{-3}	128×128	32
`BYOL`	`ResNet34`	✓	0.99	1×10^{-3}	128×128	64
`BYOL`	`ResNet18`	✗	0.99	1×10^{-3}	128×128	64
`BYOL`	`ResNet18`	✓	0.99	1×10^{-3}	224×224	64
`BYOL`	`CNN`	✗	0.99	1×10^{-3}	128×128	64
`BYOL`	`ResNet18`	✓	0.95	1×10^{-3}	128×128	64
`BYOL`	`ResNet18`	✓	0.90	1×10^{-3}	128×128	64
`BYOL`	`ResNet18`	✓	0.80	1×10^{-3}	128×128	64
`SimCLR`	`ResNet18`	✓	0.99	1×10^{-3}	128×128	64
`SimCLR`	`ResNet18`	✓	0.99	1×10^{-2}	128×128	64
`SimCLR`	`ResNet18`	✓	0.99	1×10^{-3}	128×128	32
`SimCLR`	`ResNet34`	✓	0.99	1×10^{-3}	128×128	64
`SimCLR`	`ResNet18`	✗	0.99	1×10^{-3}	128×128	64
`SimCLR`	`ResNet18`	✓	0.99	1×10^{-3}	224×224	64
`SimCLR`	`CNN`	✗	0.99	1×10^{-3}	128×128	64
`SimCLR`	`ResNet18`	✓	0.95	1×10^{-3}	128×128	64
`SimCLR`	`ResNet18`	✓	0.90	1×10^{-3}	128×128	64
`SimCLR`	`ResNet18`	✓	0.80	1×10^{-3}	128×128	64

C.3 Losses for Experiments

C.3.1 `BYOL`

Table C.2: `BYOL` training and validation loss during experimental runs.

Model	**Total Training Time**	**Full Epochs Completed**	**Best Training Loss**	**Best Validation Loss**
`BYOL` (Base)	23.055	5	0.042	0.227
`BYOL` ($\tau = 0.95$)	26.673	5	0.039	0.209
`BYOL` ($\tau = 0.90$)	18.157	4	0.056	0.206
`BYOL` ($\tau = 0.80$)	18.473	4	0.057	0.214
`BYOL` (Not Pretrained)	23.061	5	0.059	0.252
`BYOL` (`ResNet34`)	22.479	3	0.084	0.237
`BYOL` (`CNN`)	8.169	5	0.070	0.287
`BYOL` (Patch Size 224)	**7.409**	5	0.034	0.240
`BYOL` (Batch Size 32)	36.925	8	**0.001**	**0.028**
`BYOL` ($\eta = 1 \times 10^{-2}$)	9.325	**2**	0.079	0.154

C.3.2 `SimCLR`

Table C.3: `SimCLR` training and validation loss during experimental runs. Notice, we expect a lower loss for models using $\tau < 0.99$, since a smaller τ will lead to a smaller loss, everything else equal.

Model	**Total Training Time (Hours)**	**Full Epochs Completed**	**Best Training Loss**	**Best Validation Loss**
`SimCLR` (Base)	14.910	5	3.871	4.143
`SimCLR` ($\tau = 0.95$)	15.012	5	3.828	4.115
`SimCLR` ($\tau = 0.90$)	13.382	5	3.776	4.081
`SimCLR` ($\tau = 0.80$)	13.237	5	3.647	3.995
`SimCLR` (Not Pretrained)	14.509	5	3.877	4.150
`SimCLR` (`ResNet34`)	12.938	**3**	3.882	4.148
`SimCLR` (`CNN`)	5.260	5	3.877	4.159
`SimCLR` (Patch Size 224)	**4.776**	5	**3.066**	4.089
`SimCLR` (Batch Size 32)	13.873	5	3.164	**3.541**
`SimCLR` ($\eta = 1 \times 10^{-2}$)	13.489	5	3.884	4.139

C.4 Results for Experiments Run Longer

C.4.1 Training Results

Table C.4: `SimCLR` training and validation loss during experimental runs, when run for 15 epochs without early stopping.

Model	**Total Training Time (Hours)**	**Full Epochs Completed**	**Best Training Loss**	**Best Validation Loss**
`SimCLR` ($\tau = 0.80$)	39.97	15	**3.617**	**3.974**
`SimCLR` (Not Pretrained)	**40.42**	15	3.855	4.135

C.4.2 PPIT Results

Table C.5: Comparing the best `SimCLR` model from the original runs with the second best models after 15 epochs of training (instead of early stopping).

	Model	**Top-1 Accuracy**	**Top-5 Accuracy**	**Top-10 Accuracy**	**Positive Pair Accuracy**
Early Stopping	`SimCLR` ($\tau = 0.80$)	0.22547	0.75158	0.80010	0.73515
	`SimCLR` (Not Pretrained)	0.22615	0.75790	0.79922	0.74210
	`SimCLR` (`CNN`)	0.22654	**0.76305**	**0.80272**	**0.74905**
15 Epochs	`SimCLR` ($\tau = 0.80$)	0.22372	0.75372	0.79951	0.73787
	`SimCLR` (Not Pretrained)	**0.22761**	0.75897	0.80165	0.74336

C.5 Deriving Automatic Thresholds for Information Awareness

```python
import numpy as np

def get_class_thresholds(pixel_counts):
    thresholds = []
    prev_min = 0

    for partition in pixel_counts:
        thresh = np.max(partition)

        if thresh > prev_min:
            thresholds.append(thresh)
        else:
            thresholds.append(np.min(partition[partition > thresh]))
    return thresholds

# pixel_counts is a list
# pixel_counts[i] contains the number of edge pixels
# in the ith patch from a dataset

# split pixel_counts after sorting
split_pixel_counts = np.array_split(np.sort(pixel_counts), n_classes)

# get the thresholds for the different classes
class_thresholds = get_class_thresholds(split_pixel_counts)

# generate the class labels for the task
# digitize: "Return the indices of the bins
# to which each value in input array belongs."
# the input array is pixel_counts, whilst the bins are class_thresholds
labels = np.digitize(pixel_counts, class_thresholds, right=True)
```

C.6 Transformations Applied

C.6.1 Rotation (30°)

The use of a 30°rotation angle was arbitrary, and was simply chosen since we thought it would significanlty distort the meaning of a patch.

```python
import torchvision.transforms as T

CROP_WIDTH = 64
IMG_WIDTH = 128

ROTATION_30_TRANSFORM = T.RandomRotation(
                            degrees = [ROTATION_ANGLE, ROTATION_ANGLE],
                                fill = 1)
```

C.6.2 Horizontal Flip

```
import torchvision.transforms as T

H_FLIP_PROBABILITY = 1

HORIZONTAL_FLIP_TRANSFORM = T.RandomHorizontalFlip(p = H_FLIP_PROBABILITY)
```

C.6.3 Random Rotation (90°, 180°, 270°)

The set of rotation angles were selected in agreement with what was used in the original `SimCLR` paper.

```
import torchvision.transforms as T
import numpy as np

ROTATION_RANGE = np.arange(90,360 + 90,90)

def ROTATION_RANDOM_TRANSFORM(img):
    angle = np.random.choice(ROTATION_RANGE)
    return T.RandomRotation(degrees = [angle, angle], fill = 1)(img)
```

C.6.4 Random Crop (64×64)

We chose a random crop of size 64×64, whilst in the original papers, they apply a random crop size (ranging from 0.08 and 1.00 in terms of proportion).

```
import torchvision.transforms as T

CROP_WIDTH = 64
IMG_WIDTH = 128

CROP_RESIZE_CENTRE_TRANSFORM = T.Compose([
                                    T.RandomCrop(CROP_WIDTH),
                                    T.Resize(IMG_WIDTH)
                                ])
```

C.6.5 Centre Crop (64×64)

```
import torchvision.transforms as T

CROP_WIDTH = 64
IMG_WIDTH = 128

CROP_RESIZE_CENTRE_TRANSFORM = T.Compose([
                                    T.CenterCrop(CROP_WIDTH),
                                      T.Resize(IMG_WIDTH)
                                  ])
```

C.6.6 Gaussian Blur

In the SimCLR paper, they randomly sample $\sigma \in [0.1, 2.0]$, and the kernel size is set to 10% of the image width/height. In our case, we picked a fixed $\sigma = 1$; since we had 128×128 patches, we used a kernel sie of 13×13.

```
import torchvision.transforms as T

BLUR_KERNEL_SIZE = 13
BLUR_SIGMA = 1

GAUSSIAN_BLUR_TRANSFORM = T.GaussianBlur(
                                kernel_size = BLUR_KERNEL_SIZE,
                                sigma = BLUR_SIGMA)
```

C.6.7 Colour Jittering

The colour jittering implementation is in accordance with the SimCLR, where they define a jitter strength. The choice of 0.5 as a jitter strength was arbitrary.

```
import torchvision.transforms as T

JITTER_STRENGTH = 0.5

COLOUR_JITTER_TRANSFORM = T.ColorJitter(0.8 * JITTER_STRENGTH,
                                    0.8 * JITTER_STRENGTH,
                                    0.8 * JITTER_STRENGTH,
                                    0.2 * JITTER_STRENGTH)
```

C.6.8 Grayscaling

```
import torchvision.transforms as T

GRAYSCALE_PROBABILITY = 1

GRAYSCALE_TRANSFORM = T.RandomGrayscale(p = GRAYSCALE_PROBABILITY)
```

C.7 Clustering Results

C.7.1 Settings for UMAP

```
from umap import UMAP

UMAP(verbose = True,
    n_jobs = -1,
    metric = "cosine",
    n_neighbors = 23,
    n_components = 100 #2,3,5,10,15,
    densmap = False,
    random_state = 23,
    negative_sample_rate = 10,
    low_memory = False,
    min_dist = 0)
```

C.7.2 Settings for HDBSCAN

```
from hdbscan import HDBSCAN

HDBSCAN(min_cluster_size = 23,
       min_samples = 13,
       metric = "minkowski",
       core_dist_n_jobs = -1,
       prediction_data = True,
       cluster_selection_epsilon = 0,
       cluster_selection_method = "eom",
       p = 2)
```

C.7.3 Clustering on Validation Data

Table C.6: Number of clusters and percentage of outliers for different dimensionality reduction techniques and contrastive models.

Dimensionality Reduction	**Features**	**Model**	**Clusters**	**Outliers**	**Percentage of Outliers**
`UMAP`	15	Best `SimCLR`	40	516	9.32%
`UMAP`	15	Best `BYOL`	52	497	8.97%
`UMAP`	15	`GeoSimCLR`	45	701	12.66%
`UMAP`	100	Best `SimCLR`	48	693	12.51%
`UMAP`	100	Best `BYOL`	62	732	13.22%
`UMAP`	100	`GeoSimCLR`	46	756	13.65%
`PCA`	15	Best `SimCLR`	5	2,596	46.88%
`PCA`	15	Best `BYOL`	17	4,190	75.66%
`PCA`	15	`GeoSimCLR`	7	3,194	57.67%
`PCA`	100	Best `SimCLR`	5	2,889	52.17%
`PCA`	100	Best `BYOL`	19	4,324	78.01%
`PCA`	100	`GeoSimCLR`	5	2,453	44.29%

C.7.4 Cluster Similarities Using 100 Features

		Cluster Similarity			**Model Similarity Percentile**		
Dimension Reducer	**Model**	**Mean**	**Median**	**Outlier**	**95th**	**99th**	**99.9th**
`UMAP` 100	Best `SimCLR`	0.63649	0.62903	0.24381	0.50193	0.69975	0.90003
`PCA` 100		0.67573	0.66517	0.23644			
`UMAP` 100	Best `BYOL`	0.90576	0.91141	0.70625	0.87729	0.95171	0.99755
`PCA` 100		0.94897	0.96135	0.66050			
`UMAP` 100	`GeoSimCLR`	0.71886	0.69242	0.35816	0.72689	0.85462	0.93467
`PCA` 100		0.60515	0.62288	0.26928			

C.7.5 Cluster Examples

C.7.5.1 BYOL Clusters

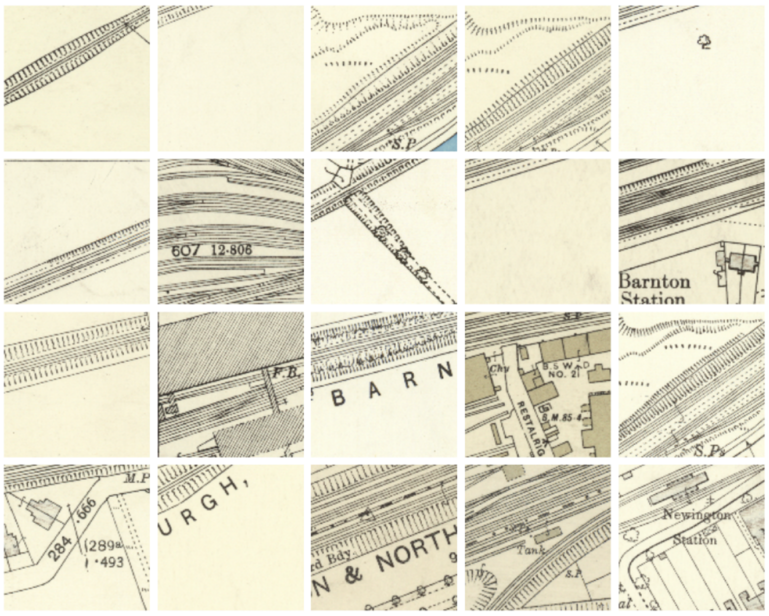

Figure C.1: UMAP (15 features) on BYOL representations.

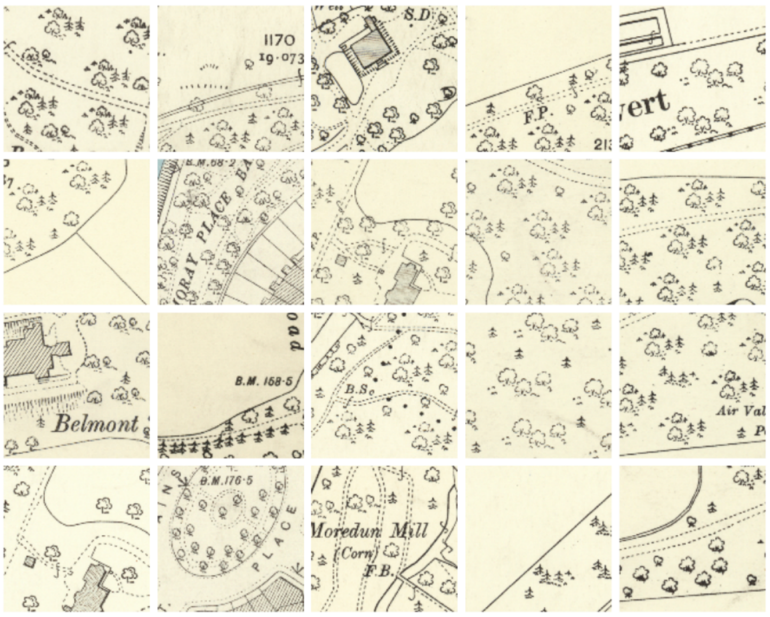

Figure C.2: UMAP (15 features) on BYOL representations.

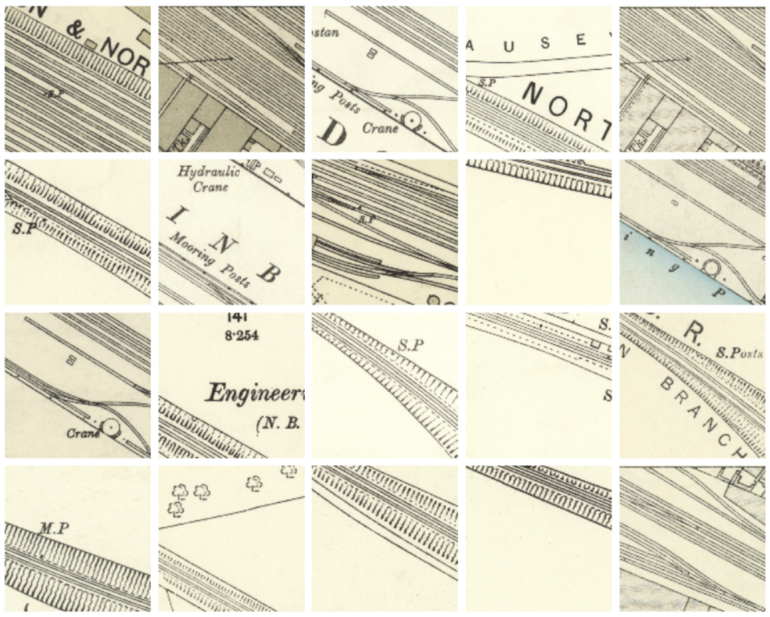

Figure C.3: `PCA` (15 features) on `BYOL` representations.

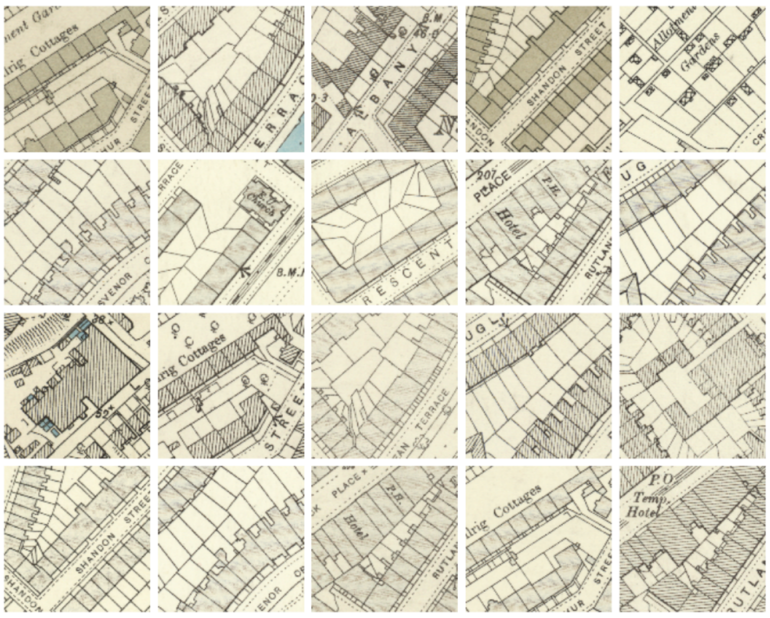

Figure C.4: `PCA` (15 features) on `BYOL` representations.

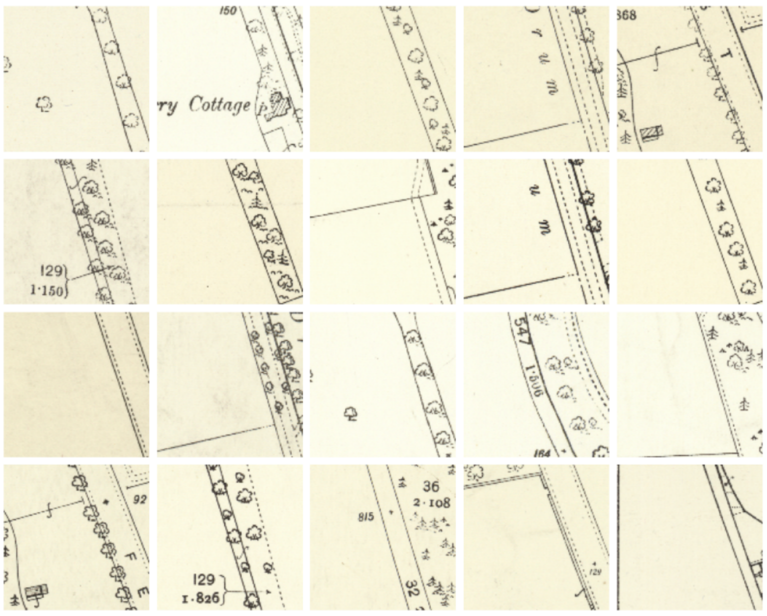

Figure C.5: `PCA` (15 features) on `BYOL` representations.

C.7.5.2 `SimCLR` Clusters

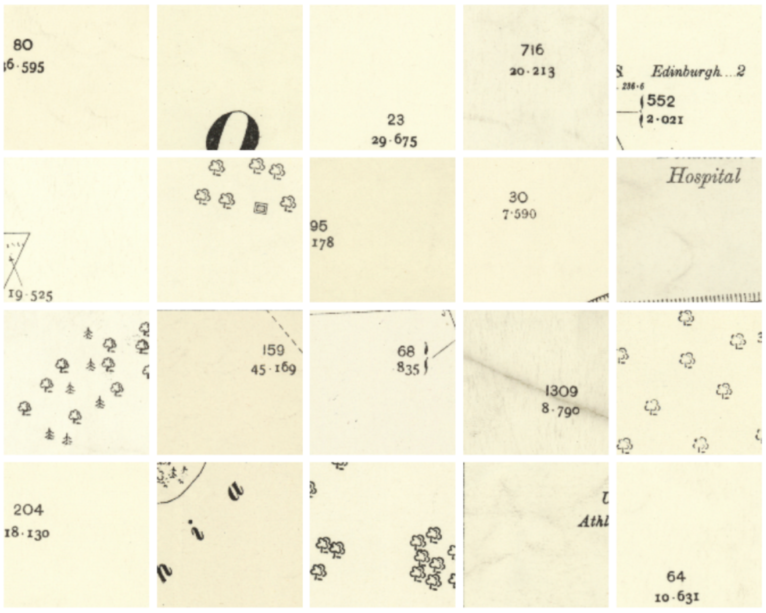

Figure C.6: `UMAP` (15 features) on `SimCLR` representations.

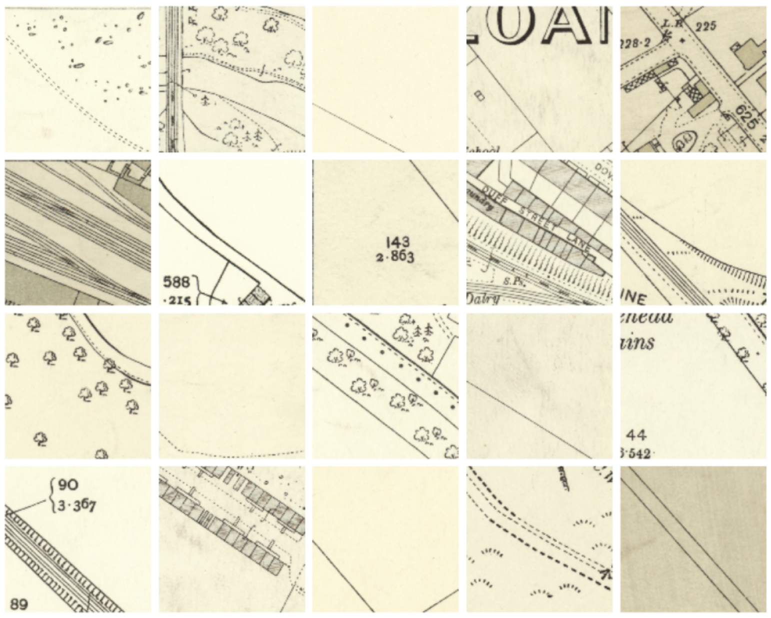

Figure C.7: `UMAP` (15 features) on `SimCLR` representations.

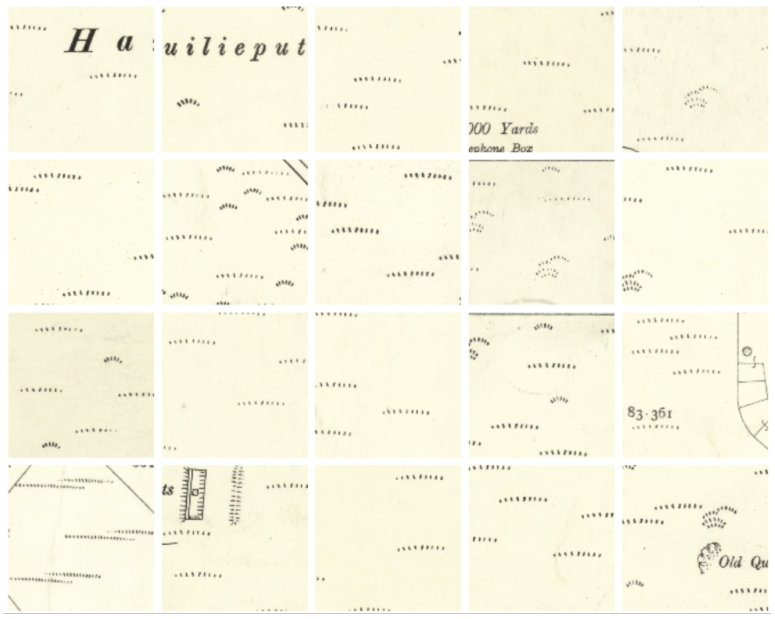

Figure C.8: `PCA` (15 features) on `SimCLR` representations.

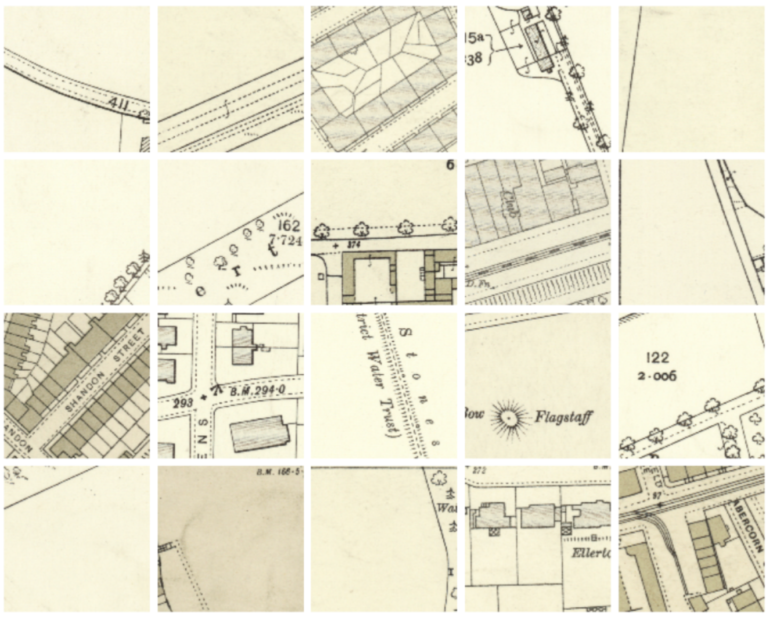

Figure C.9: PCA (15 features) on SimCLR representations.

C.7.5.3 GeoSimCLR Clusters

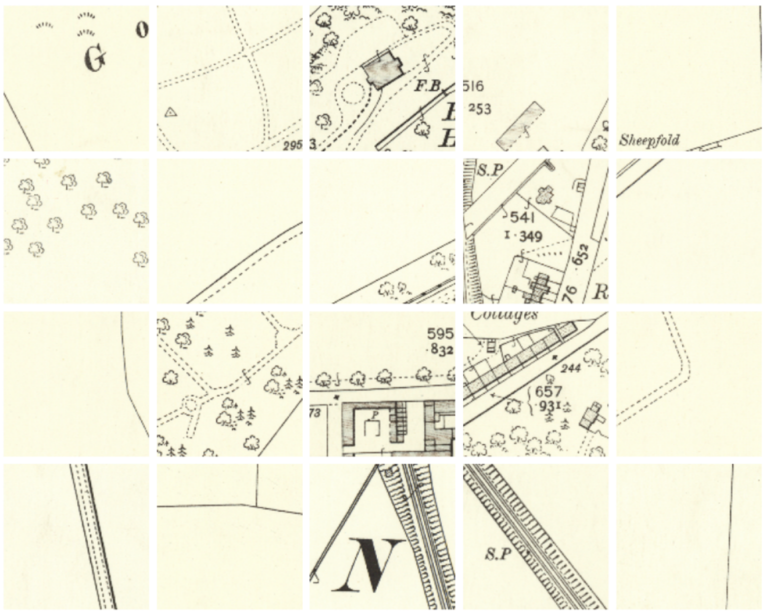

Figure C.10: UMAP (15 features) on GeoSimCLR representations.

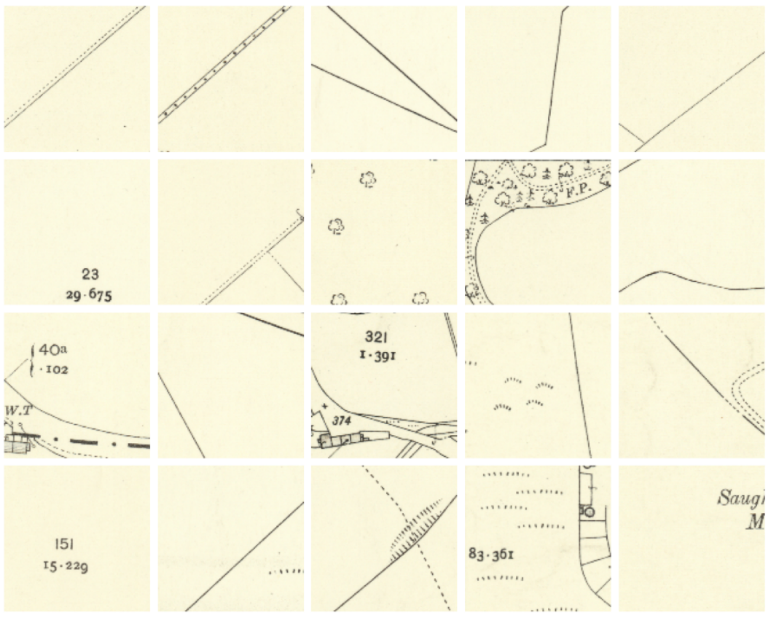

Figure C.11: `UMAP` (15 features) on `GeoSimCLR` representations.

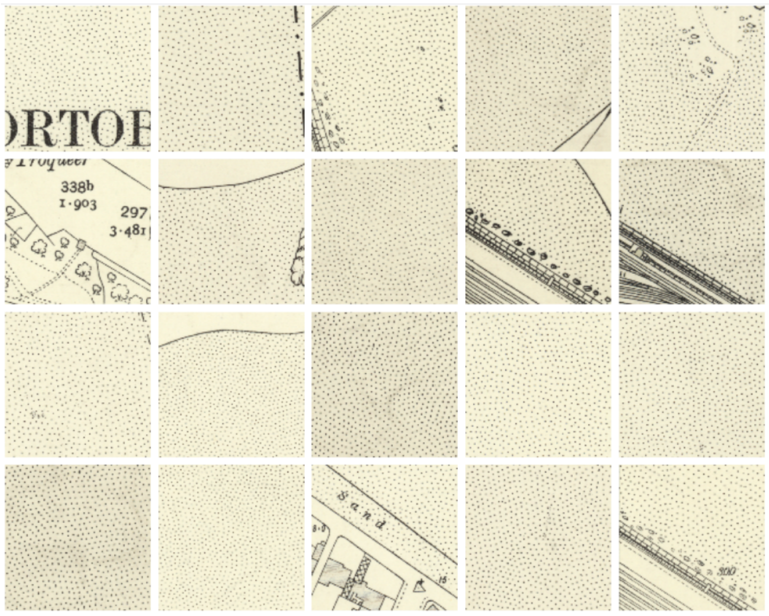

Figure C.12: `UMAP` (15 features) on `GeoSimCLR` representations.

C.7.6 Score Distributions for All Clusters

C.7.6.1 Cluster Similarity Statistics

To do this, for each cluster, I compute the average similarity amongst patches in the cluster, and then consider the average and median of these values across all clusters. This then gives us a numerical measure of how good the clusters are at encompassing similar patches. To see whether the similarity is due to the aptness of the clusters, I have compared these similarities with simple baselines, such as an *n*th percentile similarity score for a given contrastive method, or the similarity score for the outlier cluster. In particular, for each model, I can compute the set of all unique similarity scores between each patch $P_i \in P, Q_j \in Q$; using these I can then easily compute nth percentiles. I chose the 95th, 99th and 99.9th percentiles, since I found that all of our data fit in between these bins. I have also visualised the distribution of scores within a cluster, and compare these with the distributions showcased in Figure 4.3.

Table C.7: Cluster similarity results, after reducing contrastive representations to 15 dimensions, and clustering with `HDBSCAN`.

Dim. Reducer	**Model**	*Cluster Similarity*			*Model Similarity Percentile*		
		Mean	**Median**	**Outlier**	**95th**	**99th**	**99.9th**
`UMAP` 15	Best `SimCLR`	0.63246	0.64370	0.28298	0.50193	0.69975	0.90003
`PCA` 15		0.62638	0.73072	0.24650			
`UMAP` 15	Best `BYOL`	0.89492	0.90474	0.69894	0.87729	0.95171	0.99755
`PCA` 15		0.94131	0.95836	0.66047			
`UMAP` 15	`GeoSimCLR`	0.72217	0.71604	0.35030	0.72689	0.85462	0.93467
`PCA` 15		0.64038	0.67589	0.27531			

The above results show that the clusters are, in general, encompassing the notion of similar patches (at least from the point of view of the contrastive model), with the mean cluster similarity always falling well above the 95th percentile of similarity scores, and the median cluster similarity sometimes going above the 99th percentile.

C.7.6.2 Cluster Distributions (100 features)

We can compute the similarity score for each cluster, for each model. We then plot these scores as a histogram, where the y-axis corresponds to the proportion (that is, what proportion of all similarity scores does a bin correspond to), whilst the x-axis corresponds to the similarity scores of the cluster.

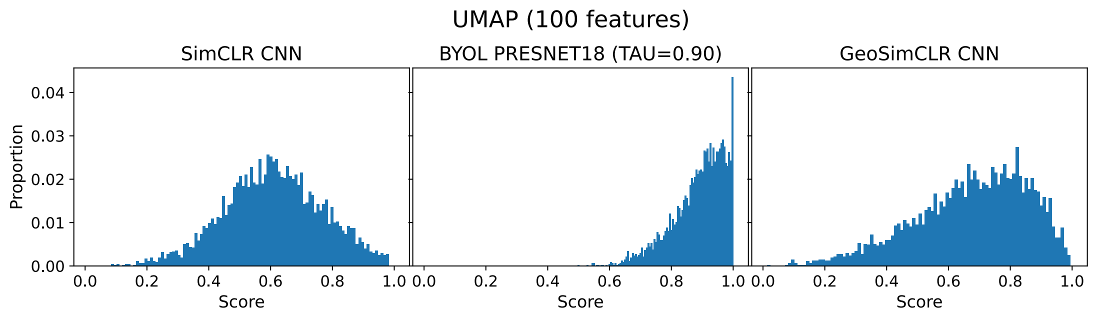

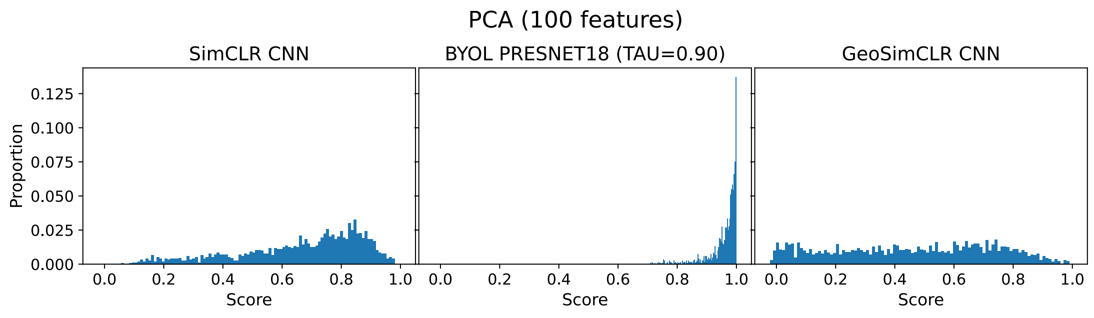

C.7.7 Clusters for Regions from GeoSimCLR Representations

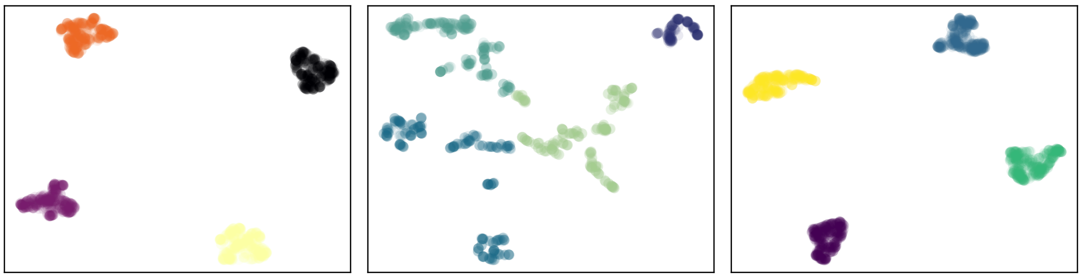

(a) Clusters for region 8, using UMAP and K-Means with $K = 4$.

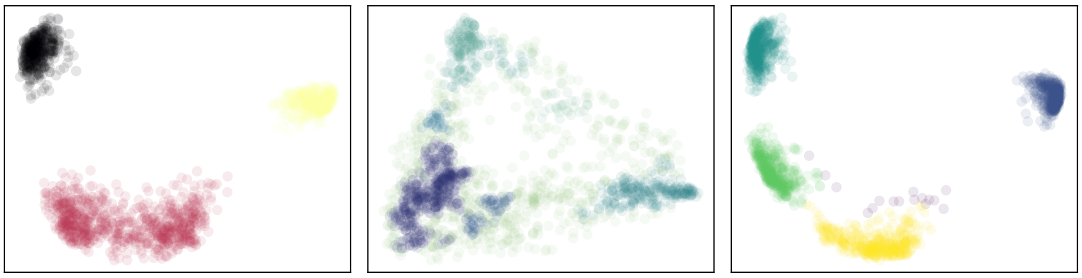

(b) Clusters for region 8, using PCA and HDBSCAN.

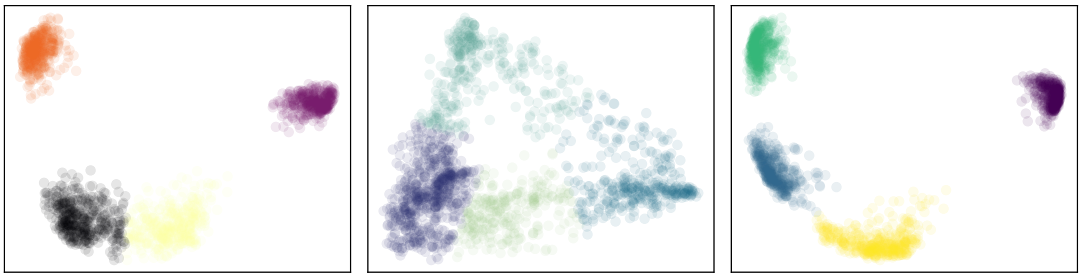

(c) Clusters for region 8, using PCA and K-Means with $K = 4$.

Figure C.13: Clusters for region 8, using different dimensionality reduction and clustering techniques. From left to right, I cluster the full geo-contrastive representation, the visual representation and the contextual representation.

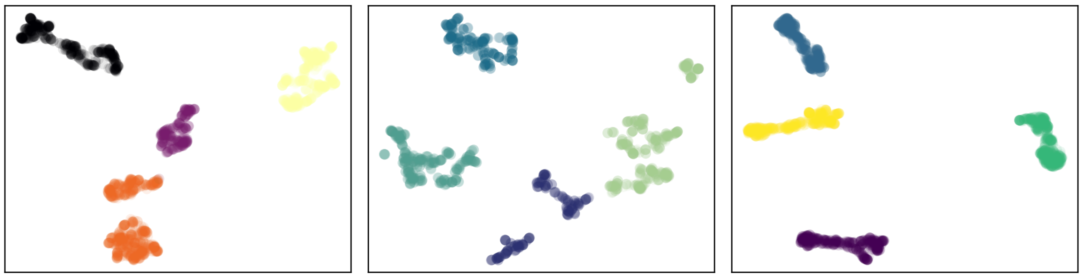

(a) Clusters for region 17, using `UMAP` and `K-Means` with $K = 4$.

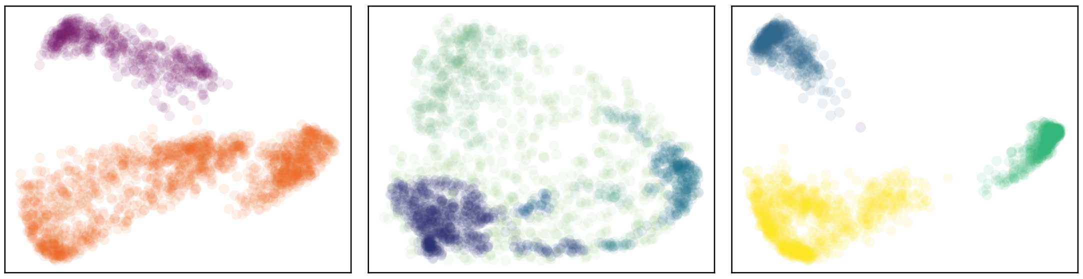

(b) Clusters for region 17, using `PCA` and `HDBSCAN`.

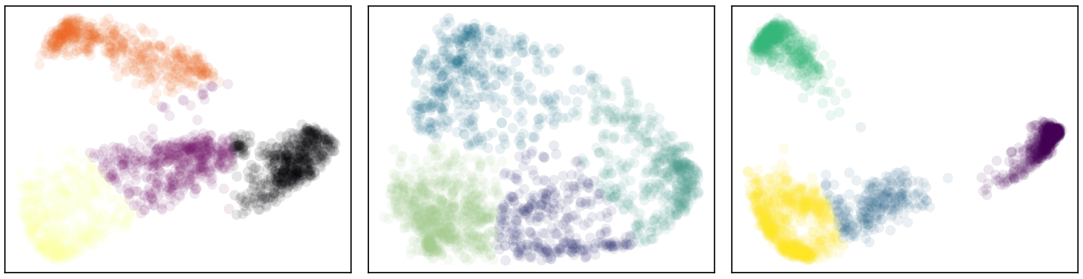

(c) Clusters for region 17, using `PCA` and `K-Means` with $K = 4$.

Figure C.14: Clusters for region 17, using different dimensionality reduction and clustering techniques. From left to right, I cluster the full geo-contrastive representation, the visual representation and the contextual representation.

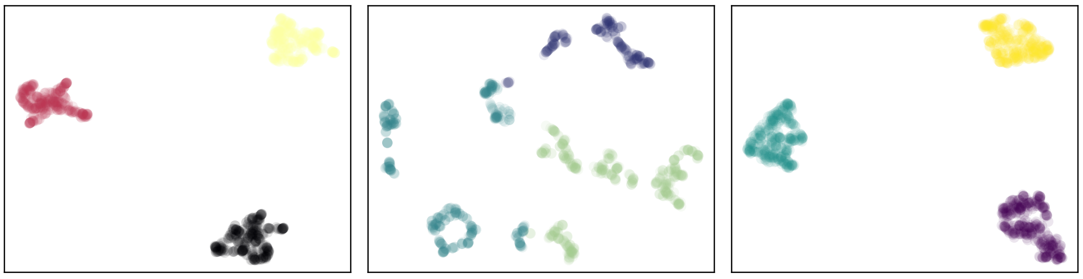

(a) Clusters for region 52, using `UMAP` and `K-Means` with $K = 3$.

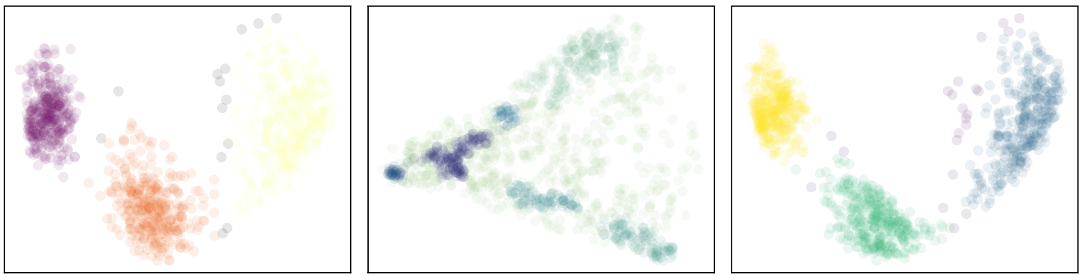

(b) Clusters for region 52, using `PCA` and `HDBSCAN`.

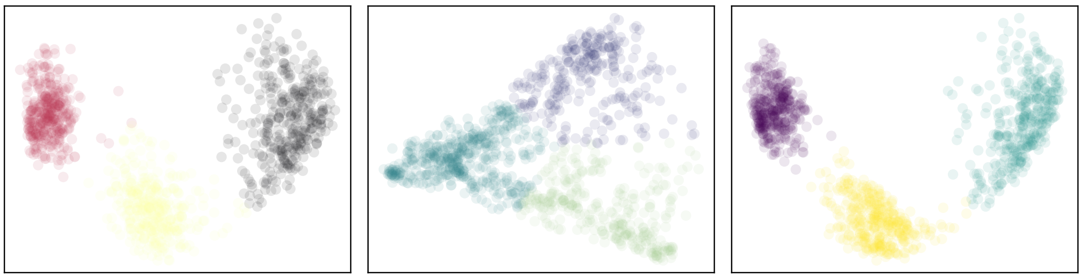

(c) Clusters for region 52, using `PCA` and `K-Means` with $K = 3$.

Figure C.15: Clusters for region 52, using different dimensionality reduction and clustering techniques. From left to right, I cluster the full geo-contrastive representation, the visual representation and the contextual representation.

C.7.8 Similarity Score Matrices for Region Patches from `GeoSimCLR` Representations

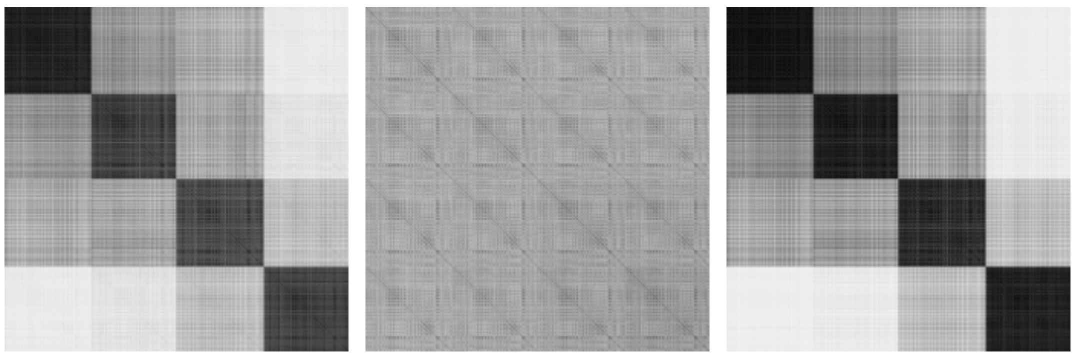

(a) Similarity scores for patches in region 8.

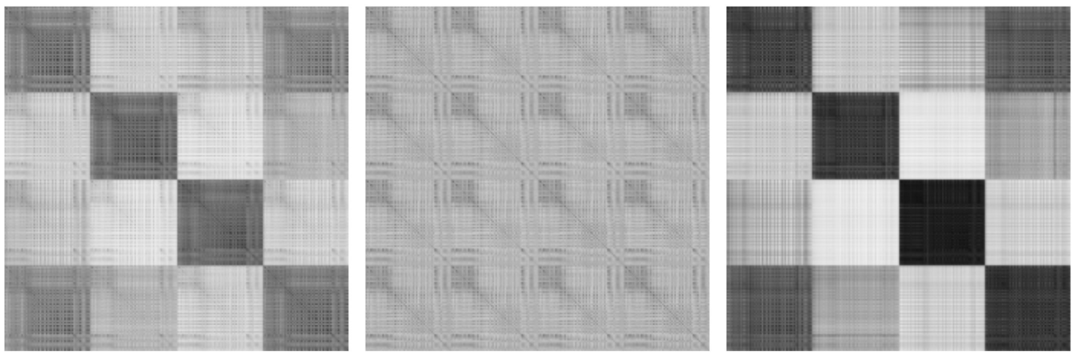

(b) Similarity scores for patches in region 17.

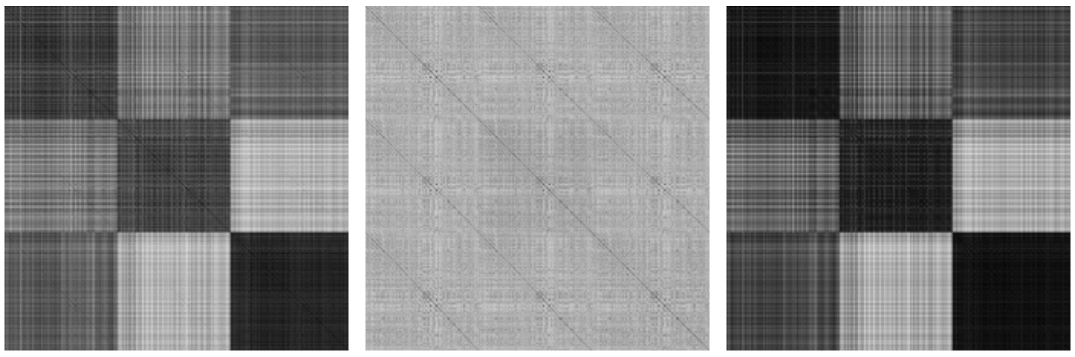

(c) Similarity scores for patches in region 52.

Figure C.16: Similarity score matrices for different regions (using the same patches as positive pairs of each other). From left to right, I use the full geo-contrastive representation, the visual representation and the contextual representation.

C.7.9 Map Segmentation Through Clustering

C.7.9.1 HDBSCAN

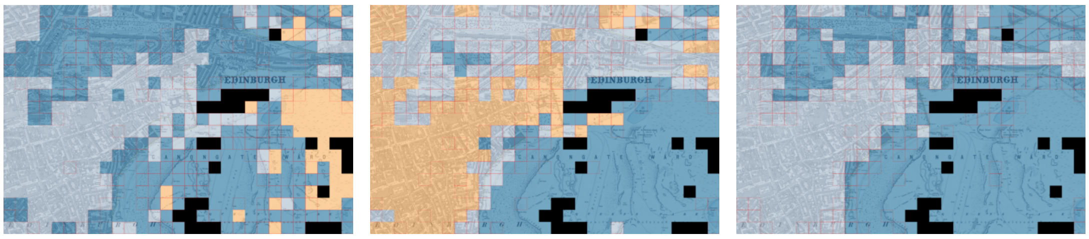

(a) Segmentation for `82877409.tiff`.

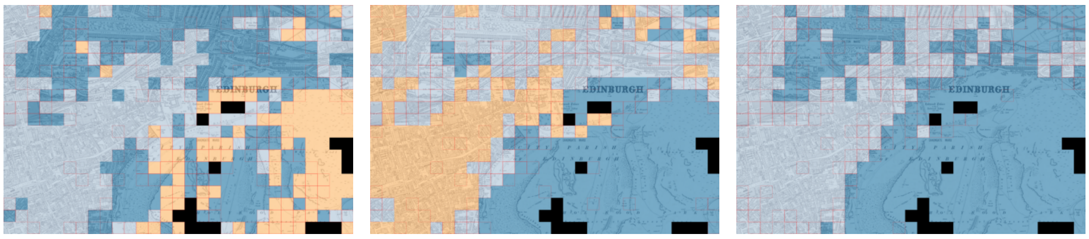

(b) Segmentation for `82877412.tiff`.

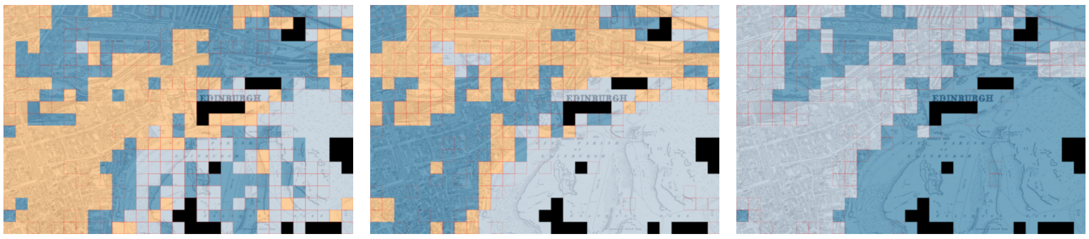

(c) Segmentation for `82877415.tiff`.

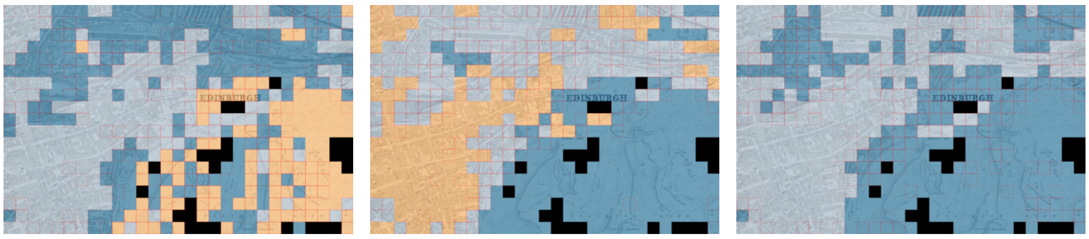

(d) Segmentation for `82877418.tiff`.

Figure C.17: Maps were segmented by using `HDBSCAN` directly on the contrastive representations. From left to right, the representations used were the best `SimCLR`, the best `BYOL` and `GeoSimCLR`.

C.7.9.2 UMAP + HDBSCAN

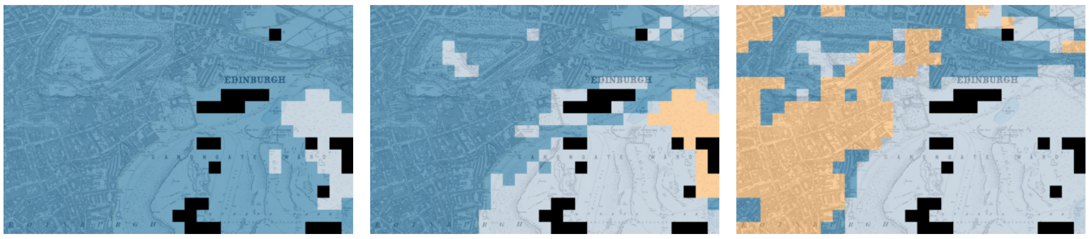

(a) Segmentation for `82877409.tiff`.

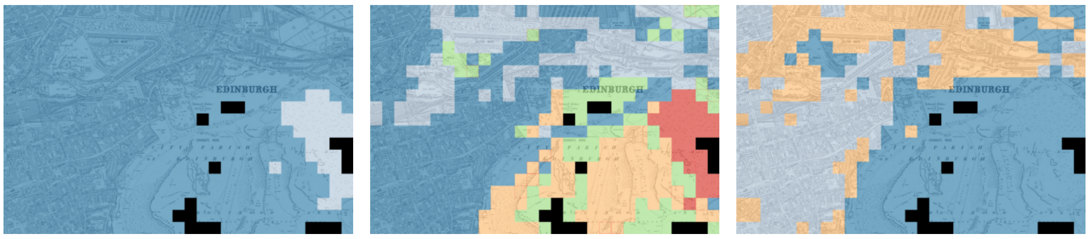

(b) Segmentation for `82877412.tiff`.

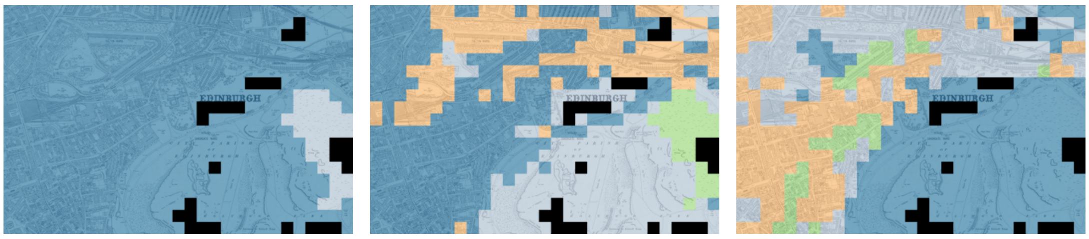

(c) Segmentation for `82877415.tiff`.

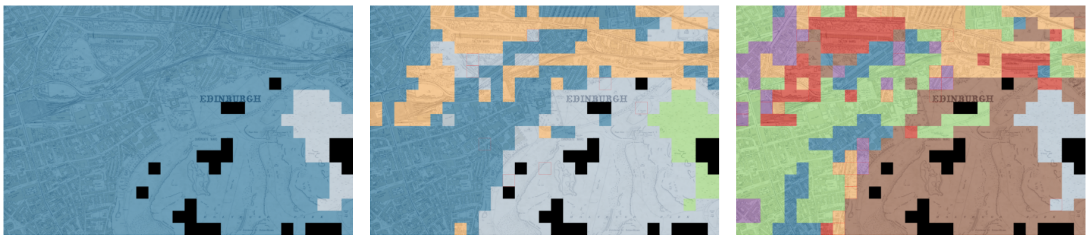

(d) Segmentation for `82877418.tiff`.

Figure C.18: Maps were segmented by using `UMAP` for dimensionality reduction of the contrastive representations, followed by `HDBSCAN` for clustering. From left to right, the representations used were the best `SimCLR`, the best `BYOL` and `GeoSimCLR`.

C.7.9.3 UMAP + KMeans

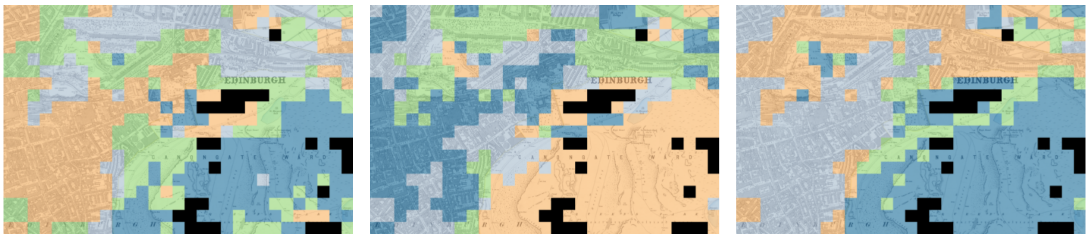

(a) Segmentation for `82877409.tiff`.

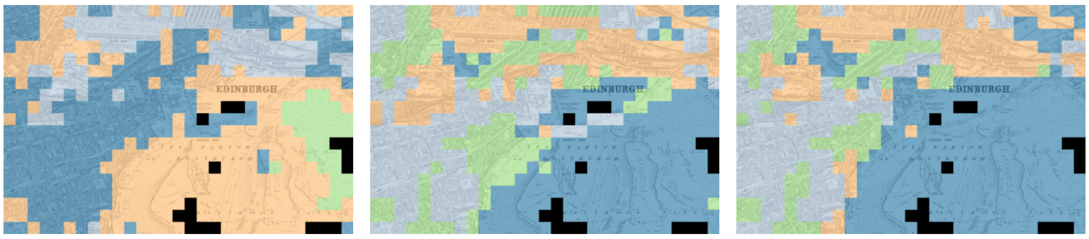

(b) Segmentation for `82877412.tiff`.

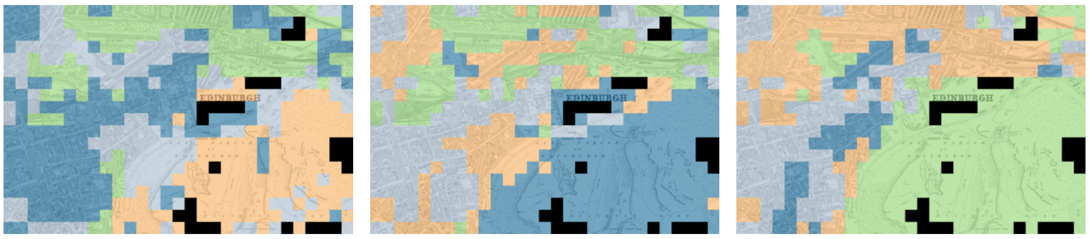

(c) Segmentation for `82877415.tiff`.

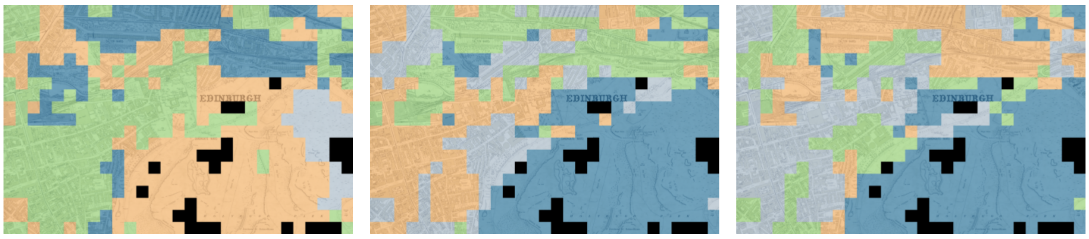

(d) Segmentation for `82877418.tiff`.

Figure C.19: Maps were segmented by using `UMAP` for dimensionality reduction of the contrastive representations, followed by `KMeans` for clustering, with $K = 4$. From left to right, the representations used were the best `SimCLR`, the best `BYOL` and `GeoSimCLR`.

Appendix D

Understanding Similarity Distributions

D.1 Similarity Score Distributions

D.1.1 BYOL

D.1.1.1 BYOL (Base)

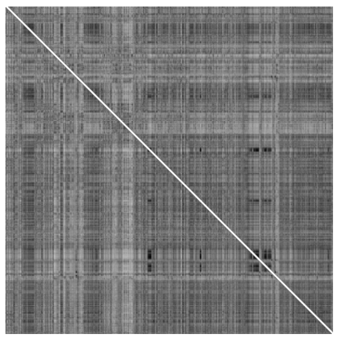

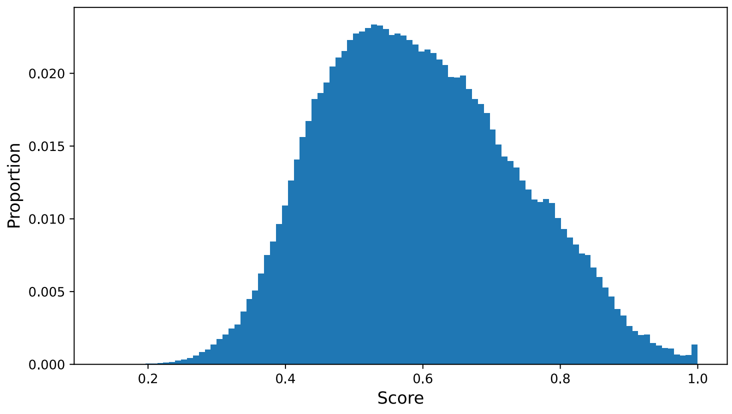

D.1.1.2 BYOL ($\tau = 0.95$)

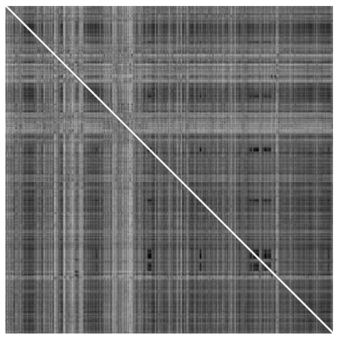

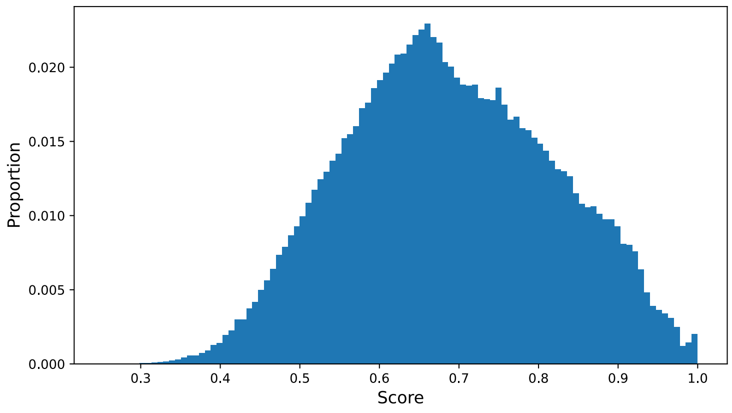

D.1.1.3 `BYOL` ($\tau = 0.80$)

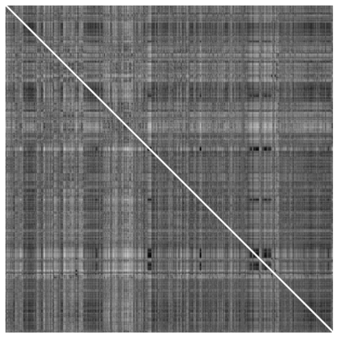

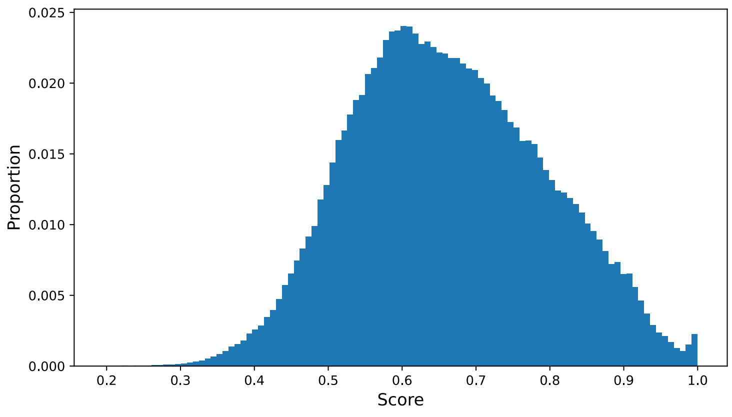

D.1.1.4 `BYOL` (Not Pretrained)

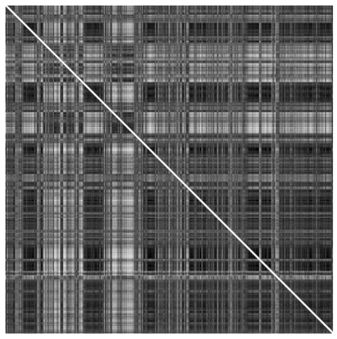

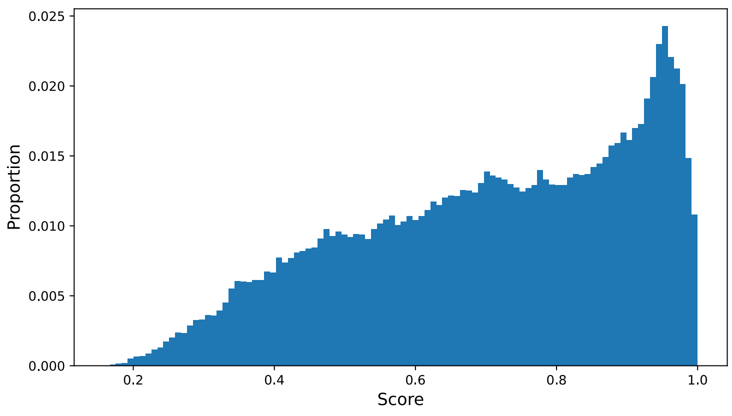

D.1.1.5 `BYOL` (`ResNet34`)

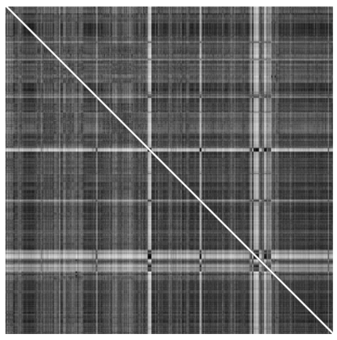

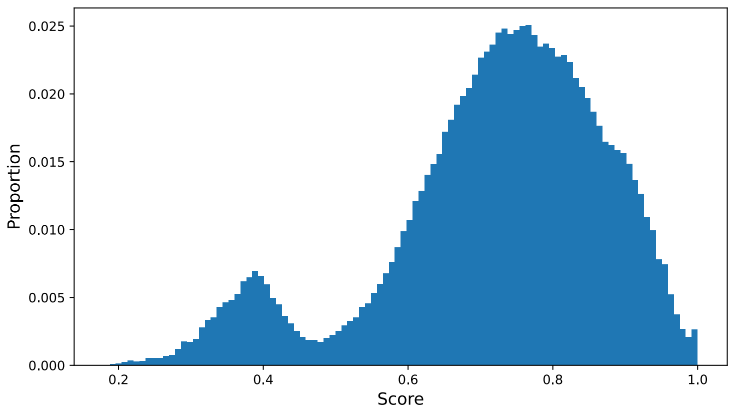

D.1.1.6 `BYOL` (`CNN`)

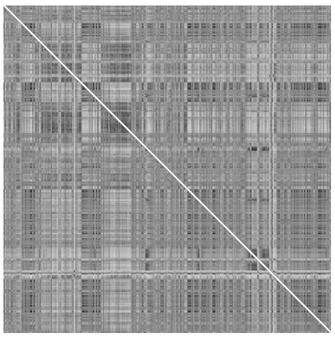

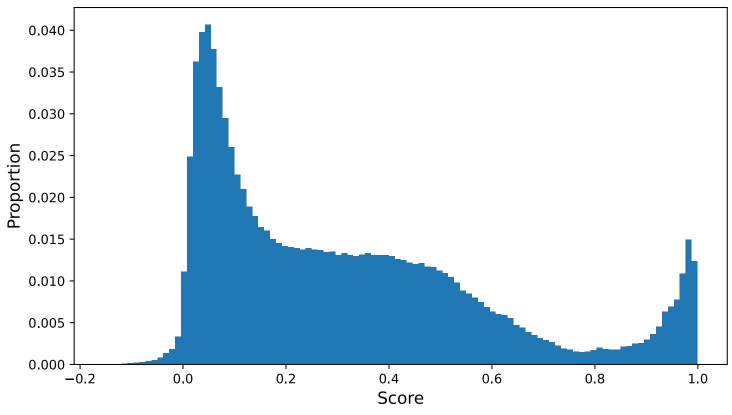

D.1.1.7 `BYOL` (Patch Size 224)

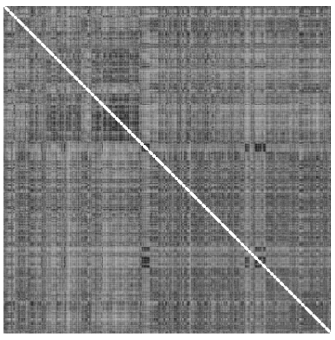

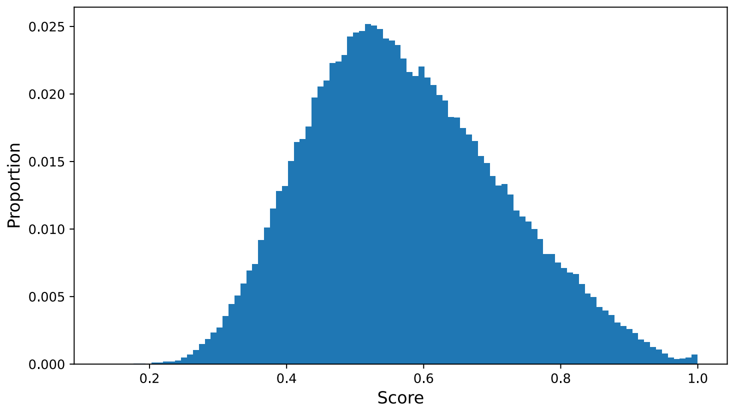

D.1.1.8 `BYOL` (Batch Size 32)

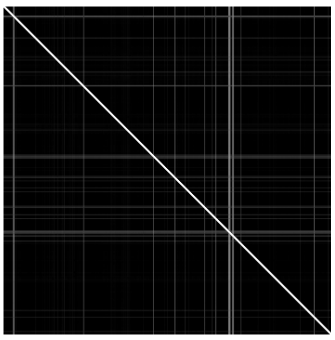

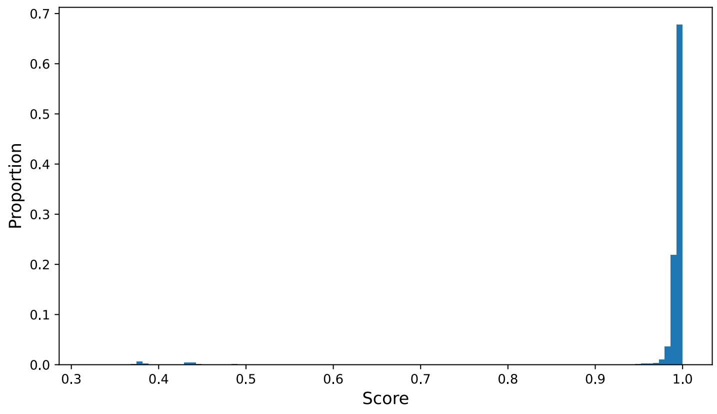

D.1.1.9 `BYOL` ($\eta = 1 \times 10^{-2}$)

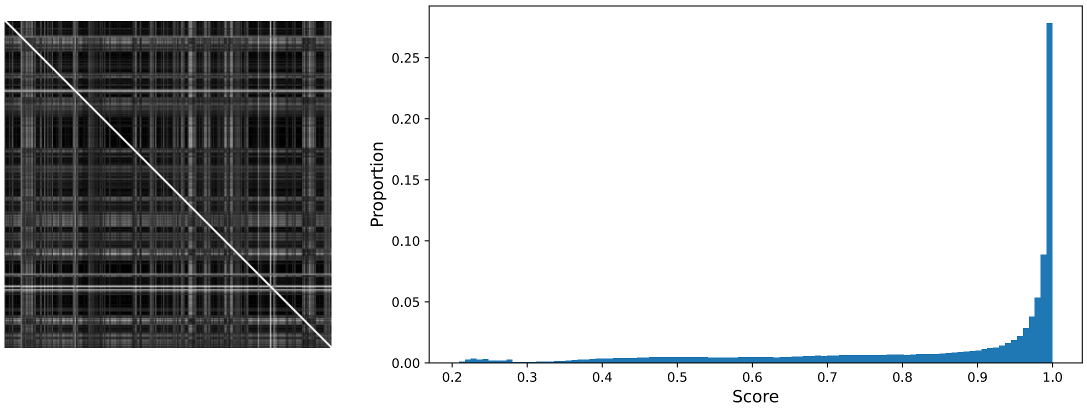

D.1.2 `SimCLR`

D.1.2.1 `SimCLR` (Base)

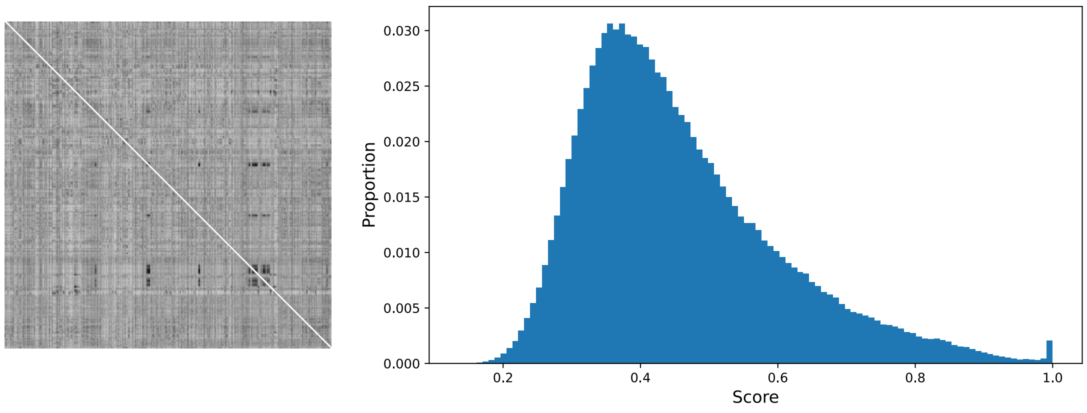

D.1.2.2 `SimCLR` ($\tau = 0.95$)

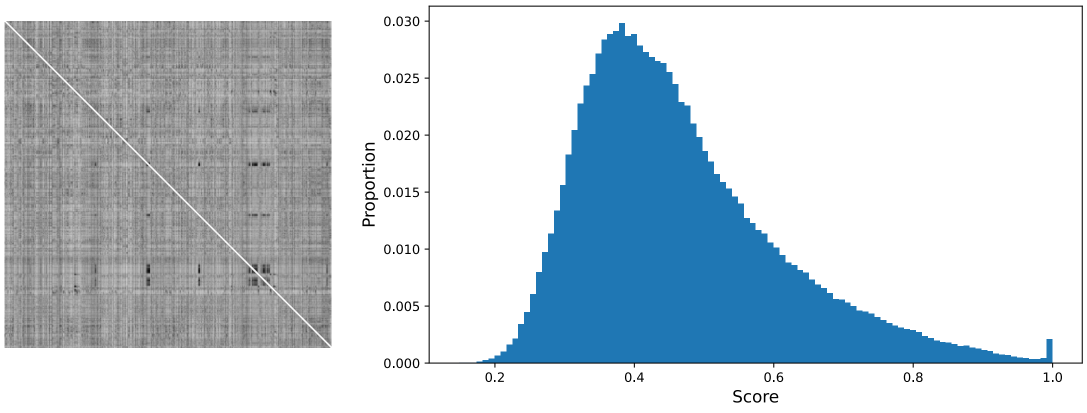

D.1.2.3 `SimCLR` ($\tau = 0.90$)

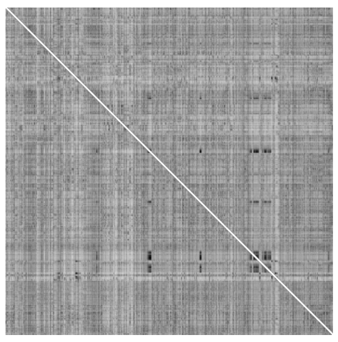

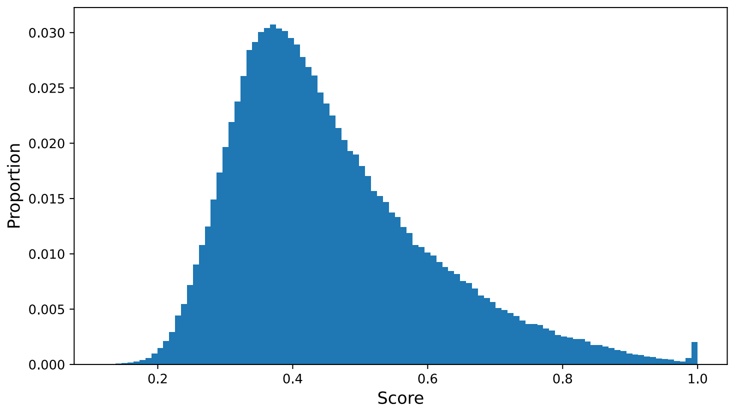

D.1.2.4 `SimCLR` ($\tau = 0.80$)

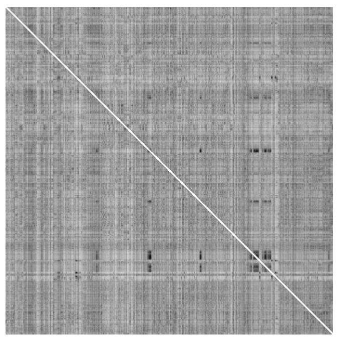

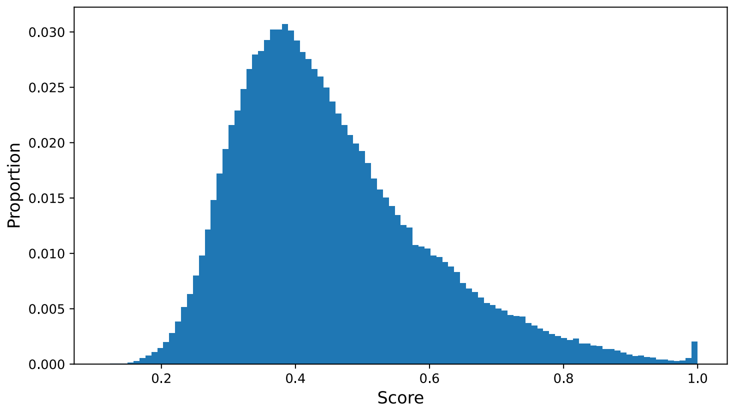

D.1.2.5 `SimCLR` (Not Pretrained)

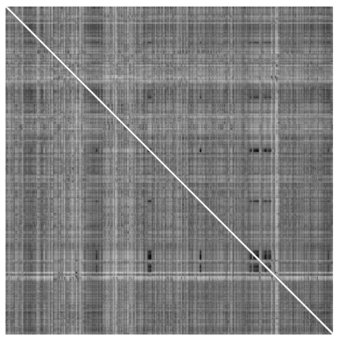

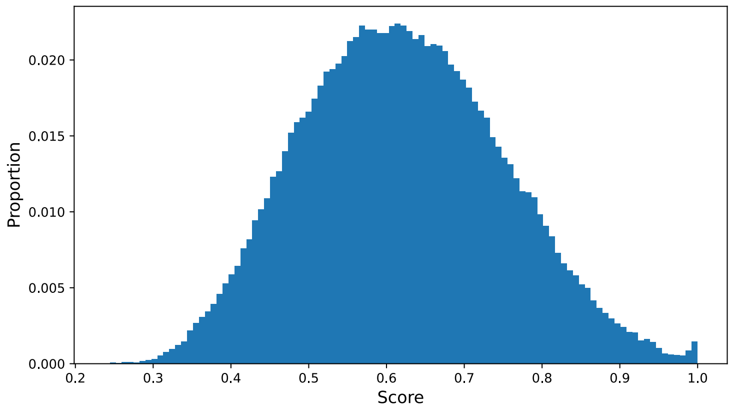

D.1.2.6 `SimCLR` (`ResNet34`)

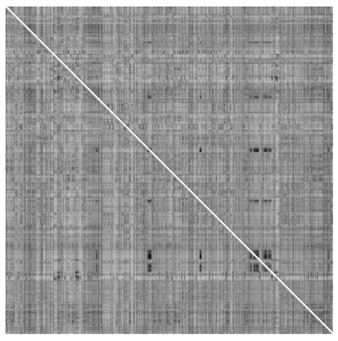

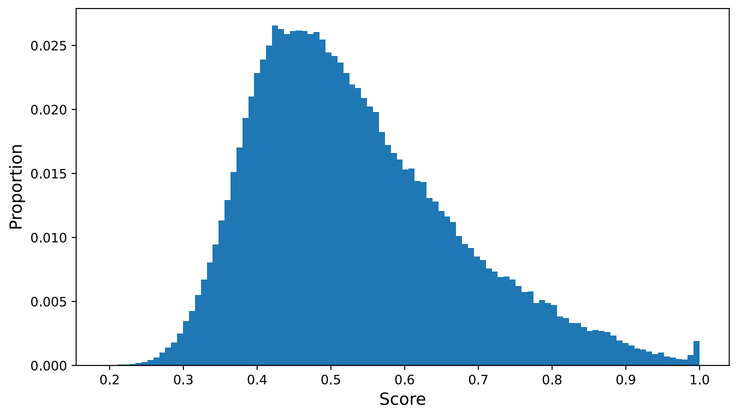

D.1.2.7 `SimCLR` (Patch Size 224)

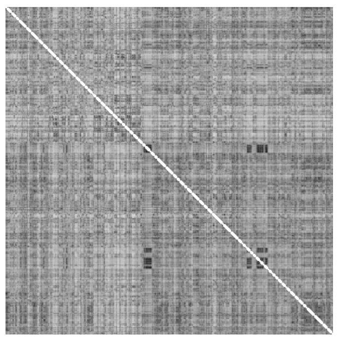

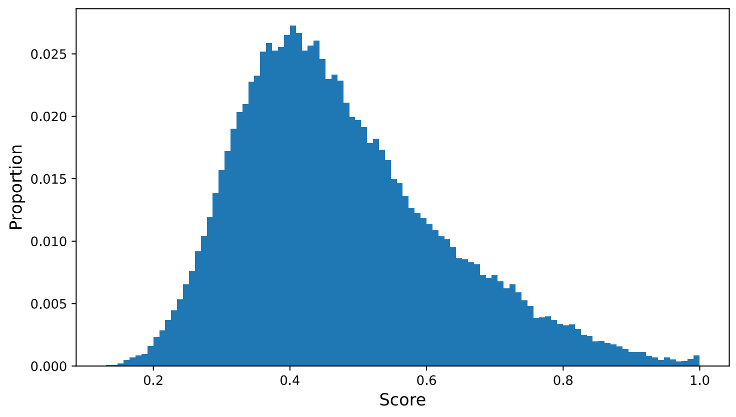

D.1.2.8 `SimCLR` (Batch Size 32)

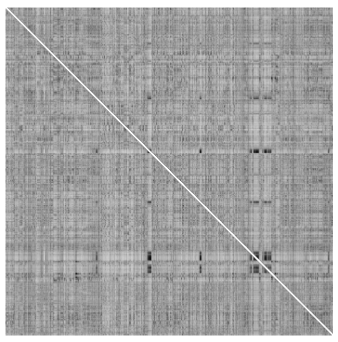

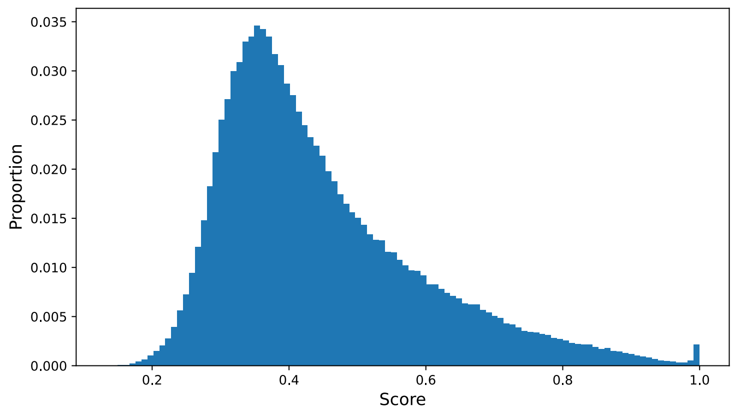

D.1.2.9 `SimCLR` ($\eta = 1 \times 10^{-2}$)

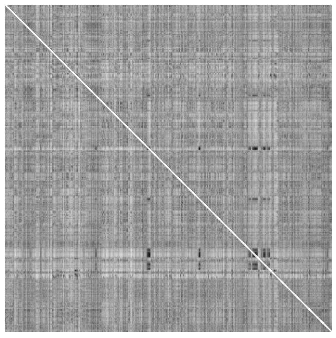
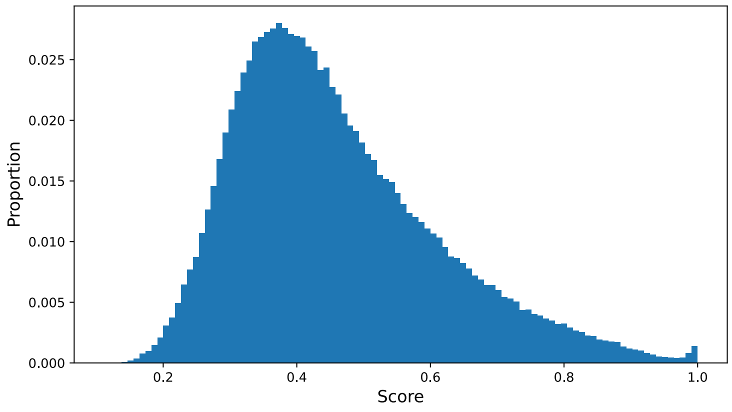

D.1.3 Weighted `GeoSimCLR`

D.1.3.1 Visual Weight = 0.7

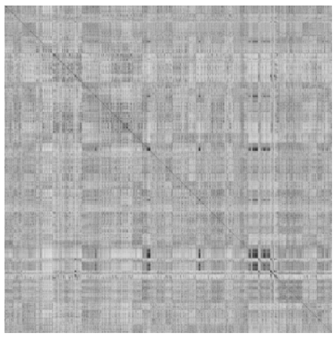
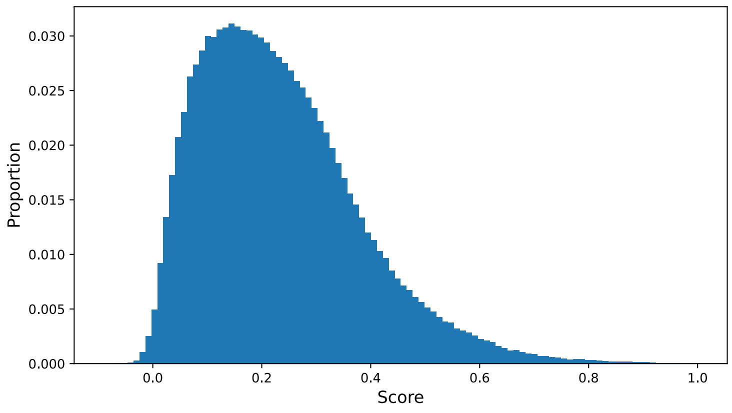

D.1.3.2 Visual Weight = 0.9

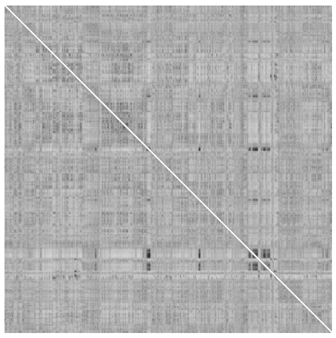
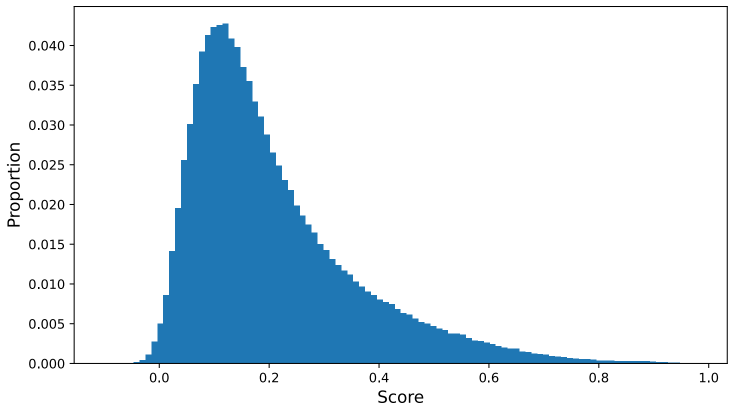

D.2 Most Similar Patches

D.2.1 `SimCLR` and `BYOL`

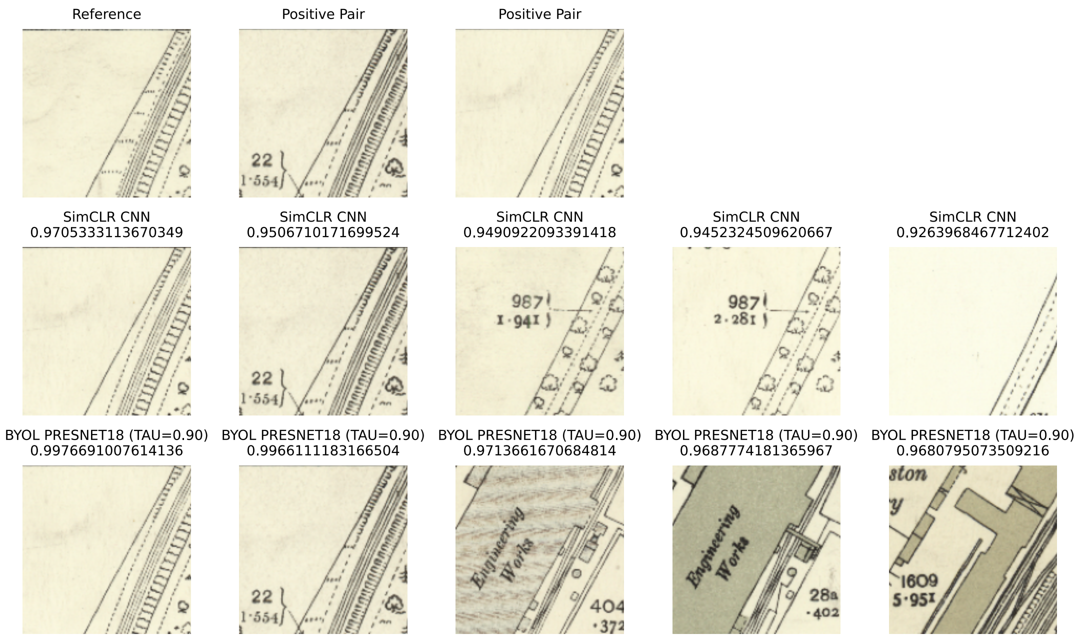

Figure D.1: Both `SimCLR` and `BYOL` easily find the correct positive pairs. Notice how the patch that they find most similar is a lot more stylistically similar to the reference patch. This is particularly noticeable with the `SimCLR` model, where the differenc ein similarity score between the first and second most similar patches is quite substantial. This example also showcases the differences in the representations learnt by both models. `SimCLR` is a lot more accurate in the sense that it finds road-like structures, in a correct location and orientation within the patch. On the other hand, `BYOL` finds patches which contain rail-like structures. Also, notice how both models find positive pairs

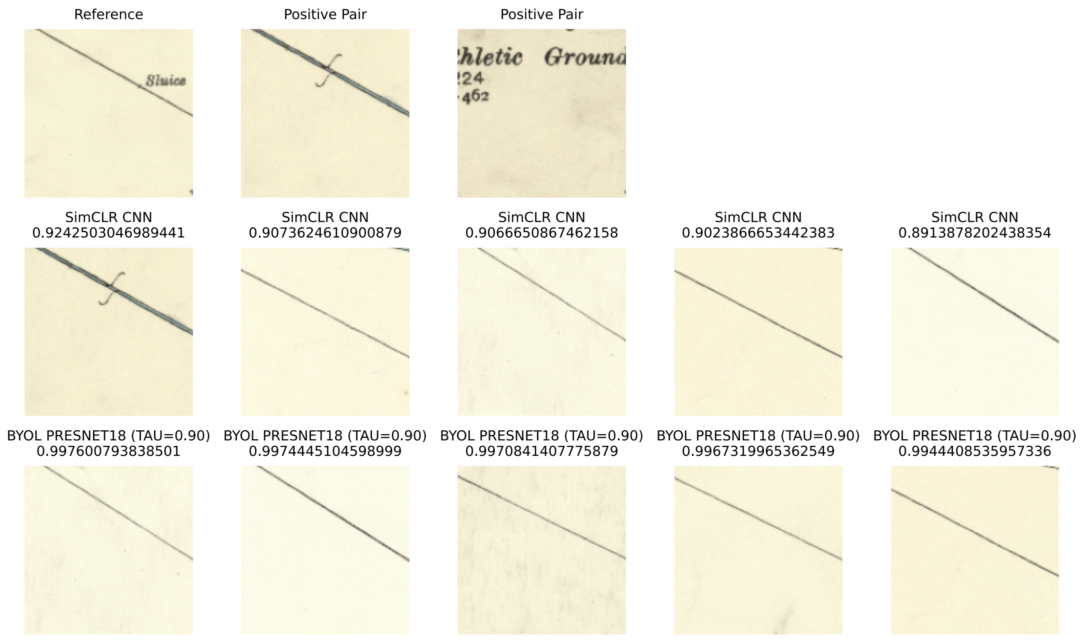
Reference
Positive Pair
Positive Pair
Sluice
hletic Ground
24
462
SimCLR CNN 0.9242503046989441
SimCLR CNN 0.9073624610900879
SimCLR CNN 0.9066650867462158
SimCLR CNN 0.9023866653442383
SimCLR CNN 0.8913878202438354
BYOL PRESNET18 (TAU=0.90) 0.997600793838501
BYOL PRESNET18 (TAU=0.90) 0.9974445104598999
BYOL PRESNET18 (TAU=0.90) 0.9970841407775879
BYOL PRESNET18 (TAU=0.90) 0.9967319965362549
BYOL PRESNET18 (TAU=0.90) 0.9944408535957336

Figure D.2: This example showcases how our positive pair creation process could be refined, since the second positive pair seems to have very little to do with the reference patch (this doesn't mean they don't represent the same region, this is likely due to the year differences). Nonetheless, both `SimCLR` and `BYOL` are capable of identifying suitable positive pairs. `SimCLR` is capable of correctly identifying the first positive pair, and with much higher similarity score than the other most similar patches, which all score very similarly. On the other, the more semantic representativity of `BYOL` means that it just finds patches containing a line with the correct positioning and orientation, and all such lines obtain a nearly identical similarity score.

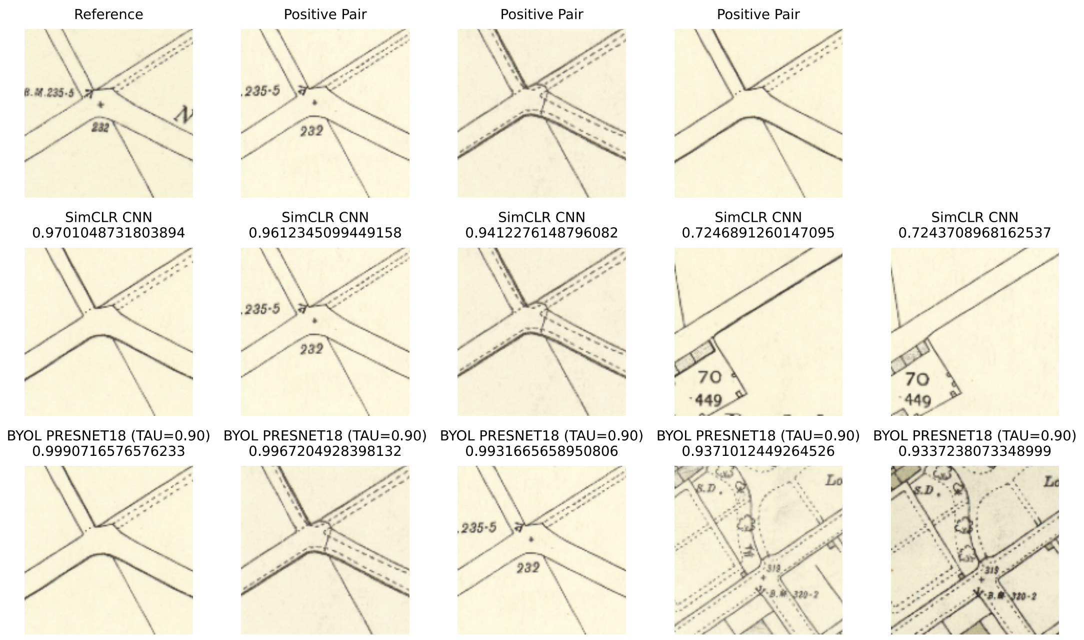
Reference
Positive Pair
Positive Pair
Positive Pair
SimCLR CNN 0.9701048731803894
SimCLR CNN 0.9612345099449158
SimCLR CNN 0.9412276148796082
SimCLR CNN 0.7246891260147095
SimCLR CNN 0.7243708968162537
BYOL PRESNET18 (TAU=0.90) 0.9990716576576233
BYOL PRESNET18 (TAU=0.90) 0.9967204928398132
BYOL PRESNET18 (TAU=0.90) 0.9931665658950806
BYOL PRESNET18 (TAU=0.90) 0.9371012449264526
BYOL PRESNET18 (TAU=0.90) 0.9337238073348999

Figure D.3: Again, both models correctly identify the true positive pairs correctly, and there is a drastic decrease in similarity score for the remaining patches. Again, `SimCLR` finds patches which aren't too related to the reference (except perhaps for the locationa nd direction of a main road). On the other hand, `BYOL` seems to have been able to identify the notion of a cross roads, alongside the dotted line patterns which are present in the positive pairs.

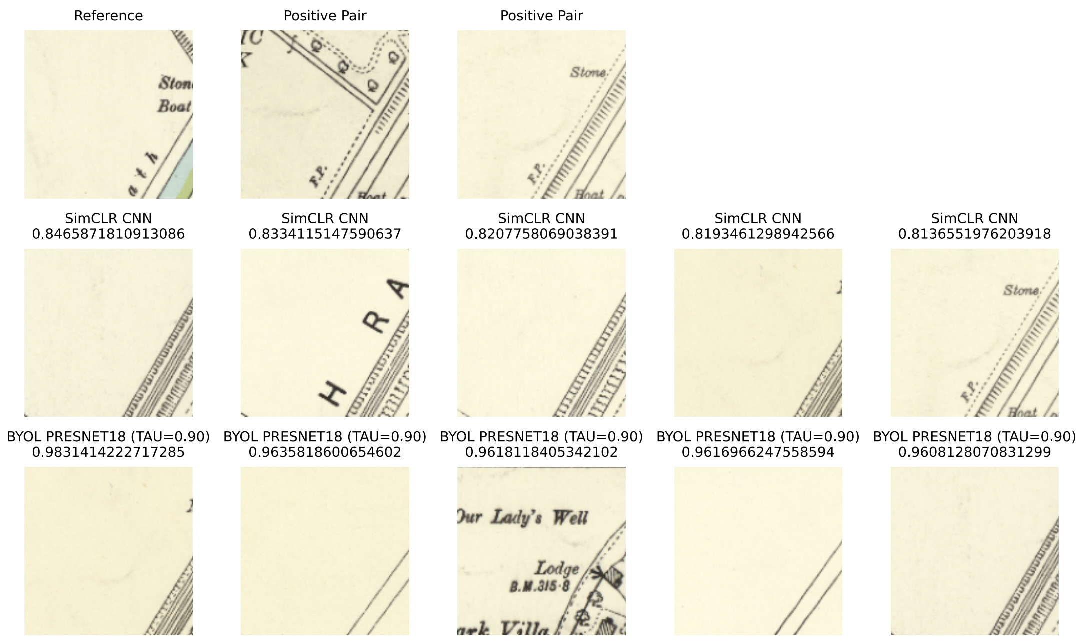
Reference
Positive Pair
Positive Pair
SimCLR CNN 0.8465871810913086
SimCLR CNN 0.8334115147590637
SimCLR CNN 0.8207758069038391
SimCLR CNN 0.8193461298942566
SimCLR CNN 0.8136551976203918
BYOL PRESNET18 (TAU=0.90) 0.9831414222717285
BYOL PRESNET18 (TAU=0.90) 0.9635818600654602
BYOL PRESNET18 (TAU=0.90) 0.9618118405342102
BYOL PRESNET18 (TAU=0.90) 0.9616966247558594
BYOL PRESNET18 (TAU=0.90) 0.9608128070831299
Ston
Boat
Stone
F.P.
Boat
Our Lady's Well
Lodge
B.M.315·8

Figure D.4: This exemplifies the impressive ability that these models have of understanding the information contained within the patches. Given that these are validation patches, the model has never seen any such patches. I f I look at the reference and the positive pairs, I struggled to see how these could constitute positive pairs, particularly given the reference. The only thing that they seem to have in common is a stripe pattern, alongside a general direction. Both models seems to be able to pick up on this, particularly `SimCLR`, which impressively is capable of finding a correct positive pair. `BYOL` seems to struggle a lot more with this task, as it seems to identify a mixture of rail tracks and plain roads, both features present within the reference patch.

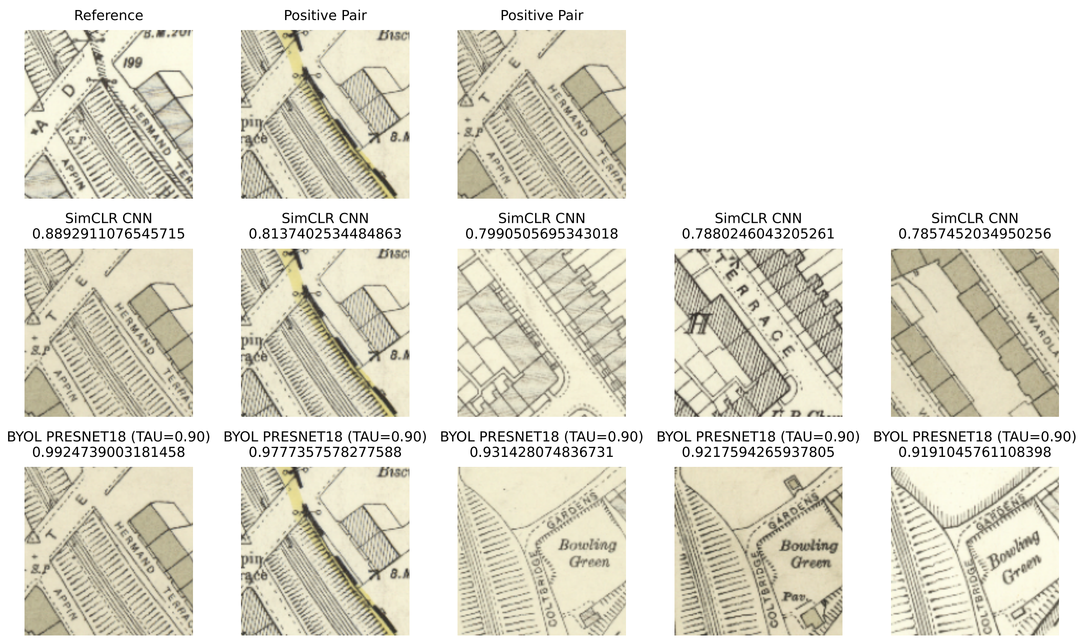
Reference
Positive Pair
Positive Pair
SimCLR CNN 0.8892911076545715
SimCLR CNN 0.8137402534484863
SimCLR CNN 0.7990505695343018
SimCLR CNN 0.7880246043205261
SimCLR CNN 0.7857452034950256
BYOL PRESNET18 (TAU=0.90) 0.9924739003181458
BYOL PRESNET18 (TAU=0.90) 0.9777357578277588
BYOL PRESNET18 (TAU=0.90) 0.931428074836731
BYOL PRESNET18 (TAU=0.90) 0.9217594265937805
BYOL PRESNET18 (TAU=0.90) 0.9191045761108398

Figure D.5: In this example, it is quite noticeable the effect that the band of black and yellow has on decreasing the similarity score for the positive patch pairs. Moreover, it is qutie significant to see how beyond the positive pairs, `SimCLR` seems to ignore the presence of the rail track, instead focusing on the presence of buildings with a road in between. On the other hand, `BYOL` does pick up on both the railtracks, but also the presence of lateral roads at either side of the tracks.

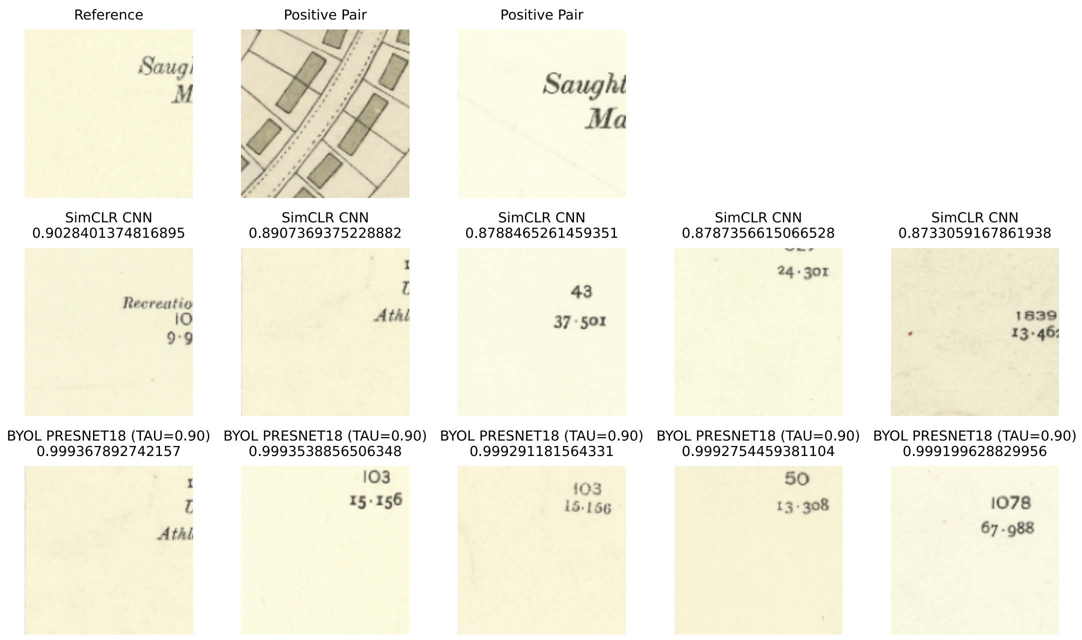
Reference
Positive Pair
Positive Pair
SimCLR CNN 0.9028401374816895
SimCLR CNN 0.8907369375228882
SimCLR CNN 0.8788465261459351
SimCLR CNN 0.8787356615066528
SimCLR CNN 0.8733059167861938
BYOL PRESNET18 (TAU=0.90) 0.999367892742157
BYOL PRESNET18 (TAU=0.90) 0.9993538856506348
BYOL PRESNET18 (TAU=0.90) 0.999291181564331
BYOL PRESNET18 (TAU=0.90) 0.9992754459381104
BYOL PRESNET18 (TAU=0.90) 0.999199628829956

Figure D.6: These examples showcases 2 key aspects. Firstly, the positional awareness of the representations: both models understand that the text is situated in the upper right corner of the patch. Secondly, `BYOL` is a lot more optimistic, assigning a similarity score above 0.999 for all patches, whilst `SimCLR` seems to be a lot more conservative, perhaps in understanding the difference between numbers and text.

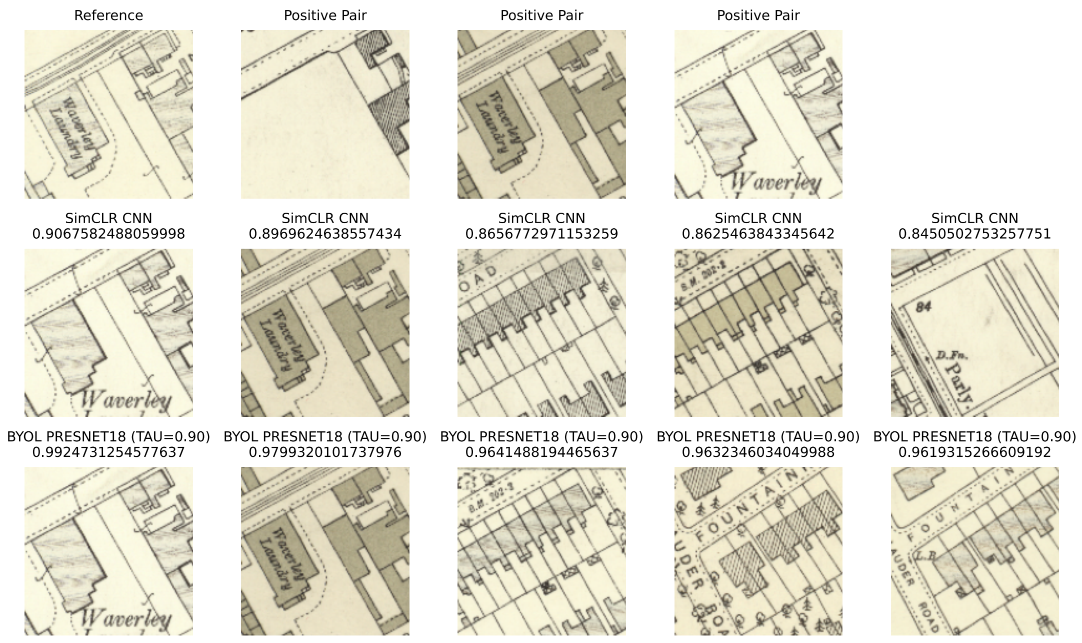
Reference
Positive Pair
Positive Pair
Positive Pair
SimCLR CNN 0.9067582488059998
SimCLR CNN 0.8969624638557434
SimCLR CNN 0.8656772971153259
SimCLR CNN 0.8625463843345642
SimCLR CNN 0.8450502753257751
BYOL PRESNET18 (TAU=0.90) 0.9924731254577637
BYOL PRESNET18 (TAU=0.90) 0.9799320101737976
BYOL PRESNET18 (TAU=0.90) 0.9641488194465637
BYOL PRESNET18 (TAU=0.90) 0.9632346034049988
BYOL PRESNET18 (TAU=0.90) 0.9619315266609192

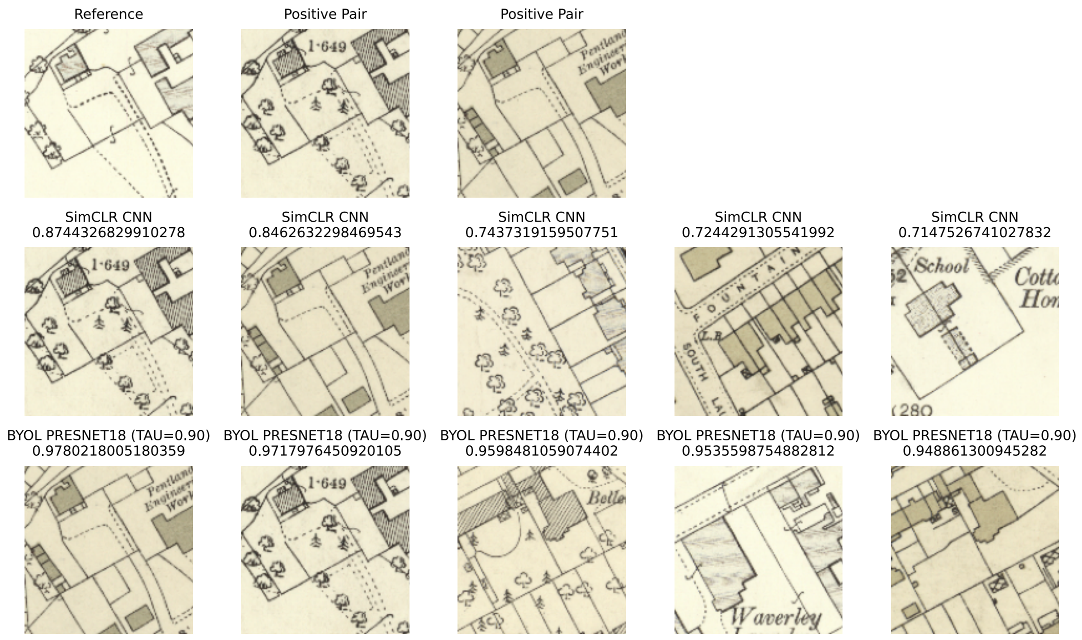
Reference
Positive Pair
Positive Pair
SimCLR CNN 0.8744326829910278
SimCLR CNN 0.8462632298469543
SimCLR CNN 0.7437319159507751
SimCLR CNN 0.7244291305541992
SimCLR CNN 0.7147526741027832
BYOL PRESNET18 (TAU=0.90) 0.9780218005180359
BYOL PRESNET18 (TAU=0.90) 0.9717976450920105
BYOL PRESNET18 (TAU=0.90) 0.9598481059074402
BYOL PRESNET18 (TAU=0.90) 0.9535598754882812
BYOL PRESNET18 (TAU=0.90) 0.948861300945282

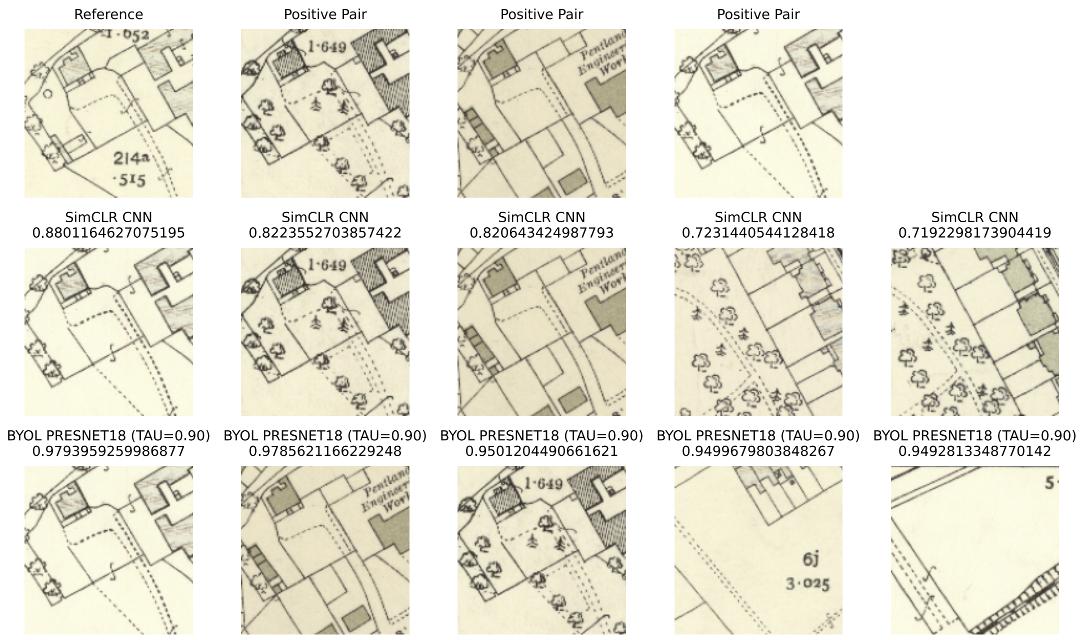
Reference
Positive Pair
Positive Pair
Positive Pair
SimCLR CNN 0.8801164627075195
SimCLR CNN 0.8223552703857422
SimCLR CNN 0.820643424987793
SimCLR CNN 0.7231440544128418
SimCLR CNN 0.7192298173904419
BYOL PRESNET18 (TAU=0.90) 0.9793959259986877
BYOL PRESNET18 (TAU=0.90) 0.9785621166229248
BYOL PRESNET18 (TAU=0.90) 0.9501204490661621
BYOL PRESNET18 (TAU=0.90) 0.9499679803848267
BYOL PRESNET18 (TAU=0.90) 0.9492813348770142

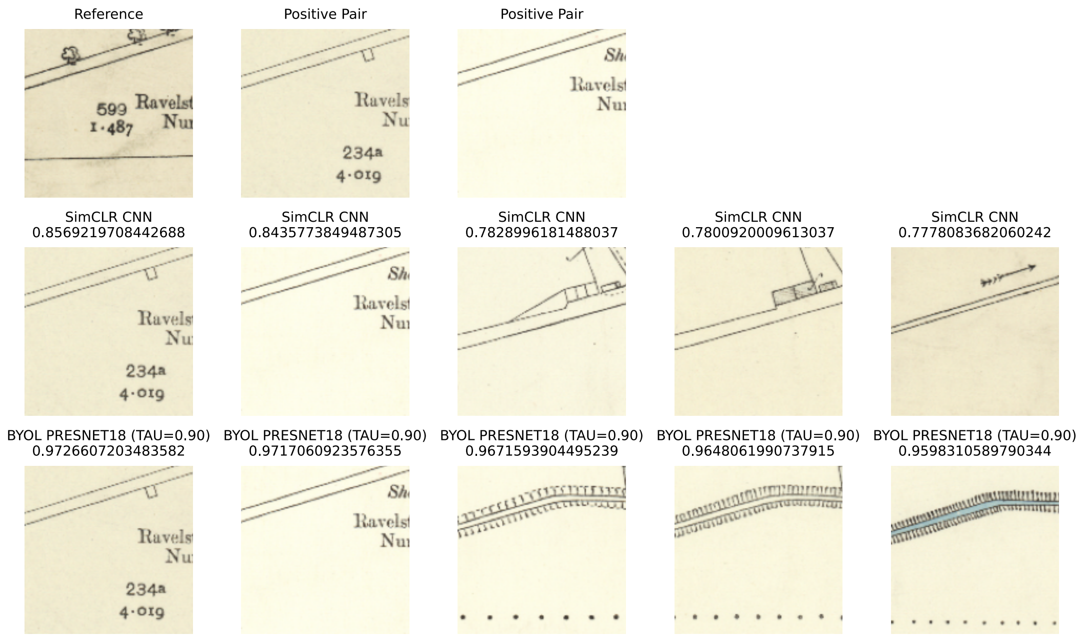
Reference
Positive Pair
Positive Pair
SimCLR CNN 0.8569219708442688
SimCLR CNN 0.8435773849487305
SimCLR CNN 0.7828996181488037
SimCLR CNN 0.7800920009613037
SimCLR CNN 0.7778083682060242
BYOL PRESNET18 (TAU=0.90) 0.9726607203483582
BYOL PRESNET18 (TAU=0.90) 0.9717060923576355
BYOL PRESNET18 (TAU=0.90) 0.9671593904495239
BYOL PRESNET18 (TAU=0.90) 0.9648061990737915
BYOL PRESNET18 (TAU=0.90) 0.9598310589790344

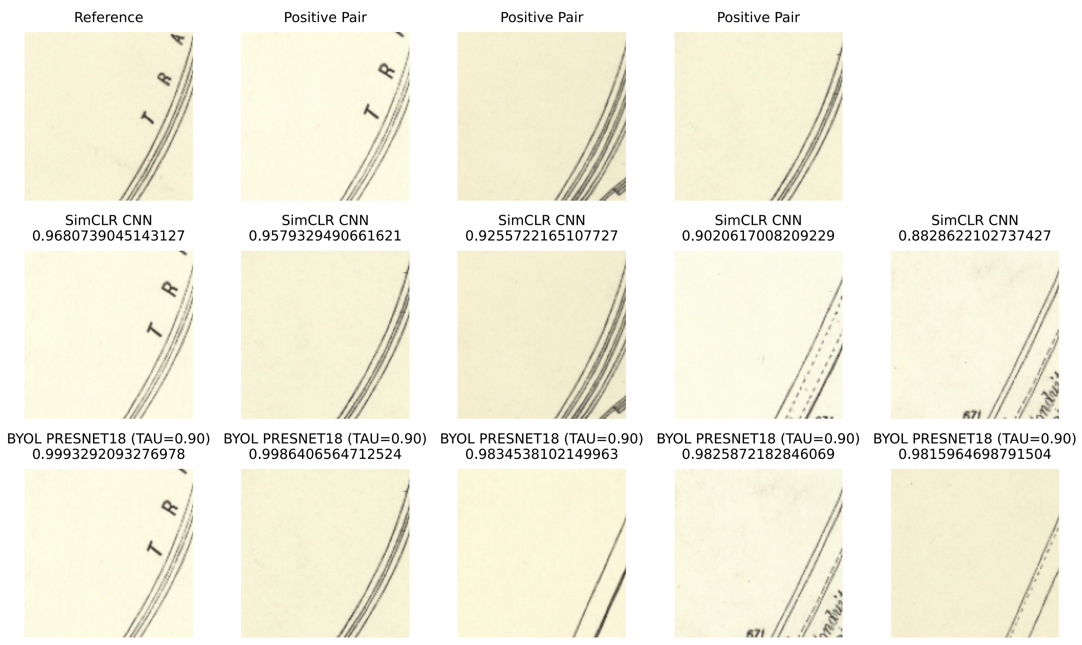
Reference
Positive Pair
Positive Pair
Positive Pair
SimCLR CNN 0.9680739045143127
SimCLR CNN 0.9579329490661621
SimCLR CNN 0.9255722165107727
SimCLR CNN 0.9020617008209229
SimCLR CNN 0.8828622102737427
BYOL PRESNET18 (TAU=0.90) 0.9993292093276978
BYOL PRESNET18 (TAU=0.90) 0.9986406564712524
BYOL PRESNET18 (TAU=0.90) 0.9834538102149963
BYOL PRESNET18 (TAU=0.90) 0.9825872182846069
BYOL PRESNET18 (TAU=0.90) 0.9815964698791504

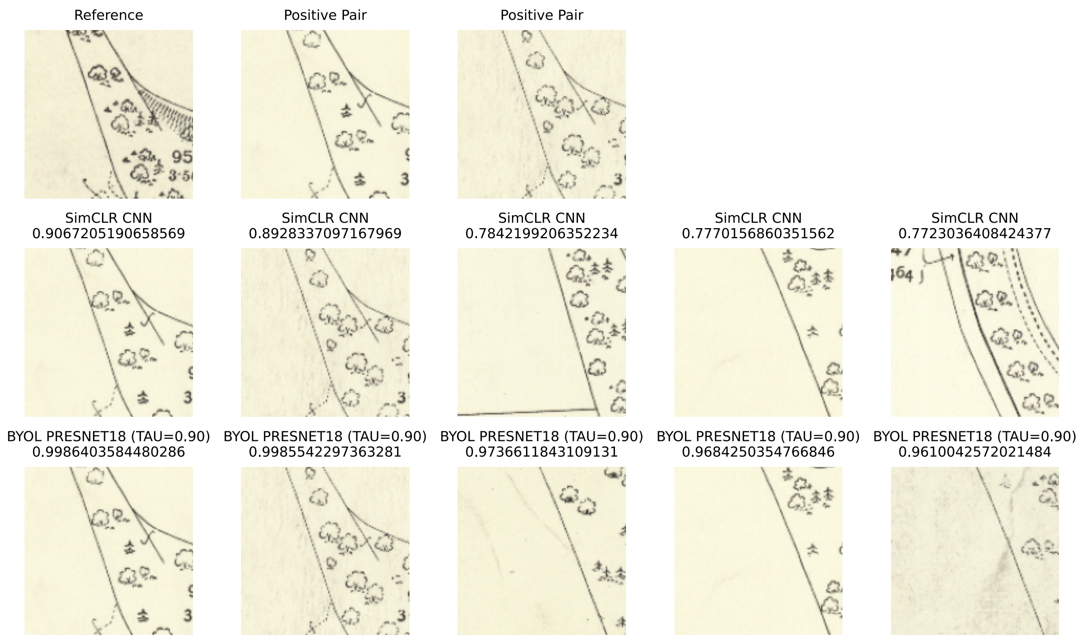
Reference
Positive Pair
Positive Pair
SimCLR CNN 0.9067205190658569
SimCLR CNN 0.8928337097167969
SimCLR CNN 0.7842199206352234
SimCLR CNN 0.7770156860351562
SimCLR CNN 0.7723036408424377
BYOL PRESNET18 (TAU=0.90) 0.9986403584480286
BYOL PRESNET18 (TAU=0.90) 0.9985542297363281
BYOL PRESNET18 (TAU=0.90) 0.9736611843109131
BYOL PRESNET18 (TAU=0.90) 0.9684250354766846
BYOL PRESNET18 (TAU=0.90) 0.9610042572021484

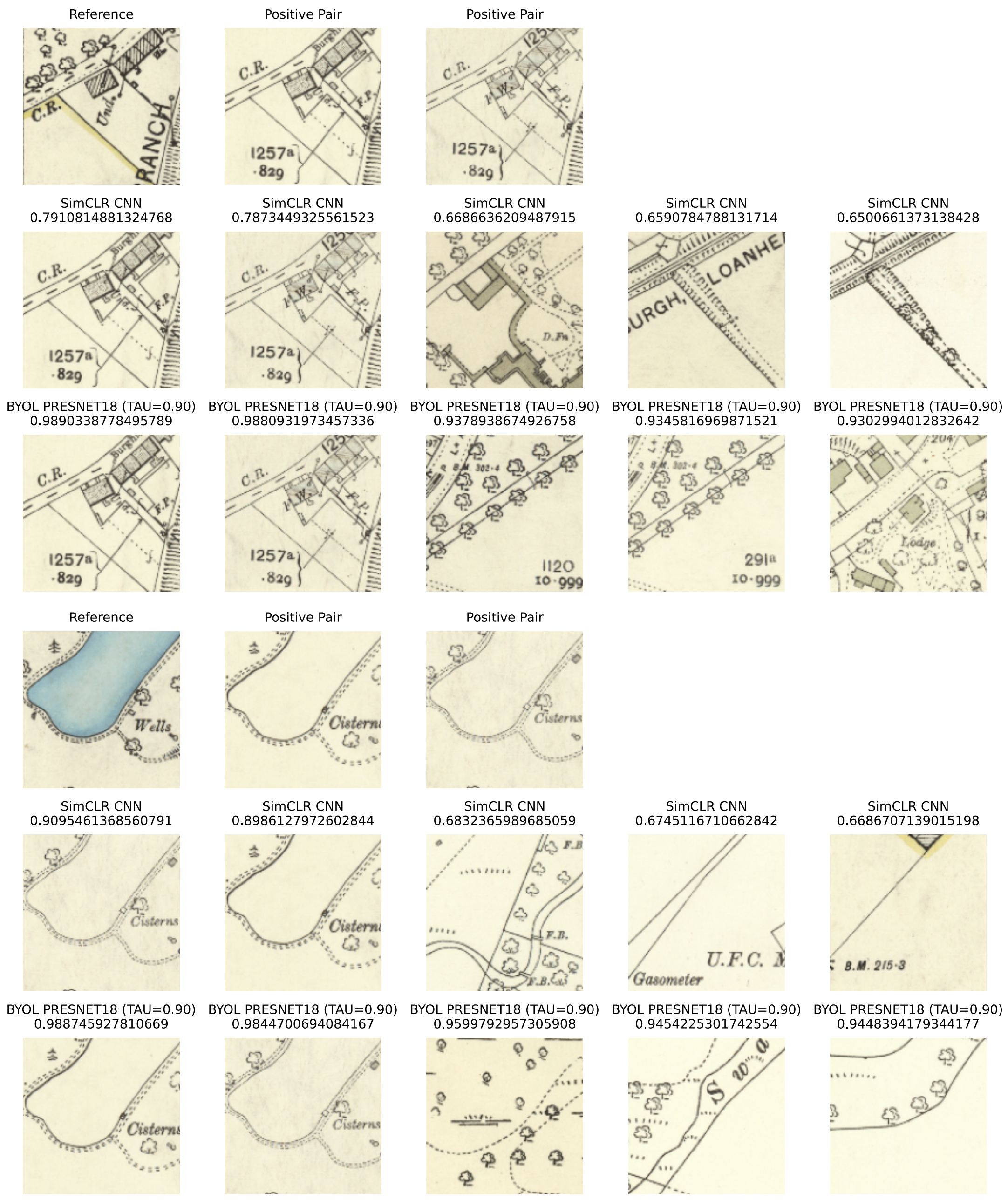
Reference
Positive Pair
Positive Pair
SimCLR CNN 0.7910814881324768
SimCLR CNN 0.7873449325561523
SimCLR CNN 0.6686636209487915
SimCLR CNN 0.6590784788131714
SimCLR CNN 0.6500661373138428
BYOL PRESNET18 (TAU=0.90) 0.9890338778495789
BYOL PRESNET18 (TAU=0.90) 0.9880931973457336
BYOL PRESNET18 (TAU=0.90) 0.9378938674926758
BYOL PRESNET18 (TAU=0.90) 0.9345816969871521
BYOL PRESNET18 (TAU=0.90) 0.9302994012832642
Reference
Positive Pair
Positive Pair
SimCLR CNN 0.9095461368560791
SimCLR CNN 0.8986127972602844
SimCLR CNN 0.6832365989685059
SimCLR CNN 0.6745116710662842
SimCLR CNN 0.6686707139015198
BYOL PRESNET18 (TAU=0.90) 0.988745927810669
BYOL PRESNET18 (TAU=0.90) 0.9844700694084167
BYOL PRESNET18 (TAU=0.90) 0.9599792957305908
BYOL PRESNET18 (TAU=0.90) 0.9454225301742554
BYOL PRESNET18 (TAU=0.90) 0.9448394179344177

Figure D.7: Given the specificity and uniqueness of the reference patch, we'd expect taht the true positive pairs should be fairly easy to find. What is most interesting is that for both models, the third most similar patch conserves information and shape relative to the reference (the fact that there are trees, and the general shapes that appear in the patches are fairly similar). However, the fourther and fifth most similar patches seem to be fairly unrelated, particularly for `SiMCLR` (with `BYOL` at least there is a notion of trees around black lines).

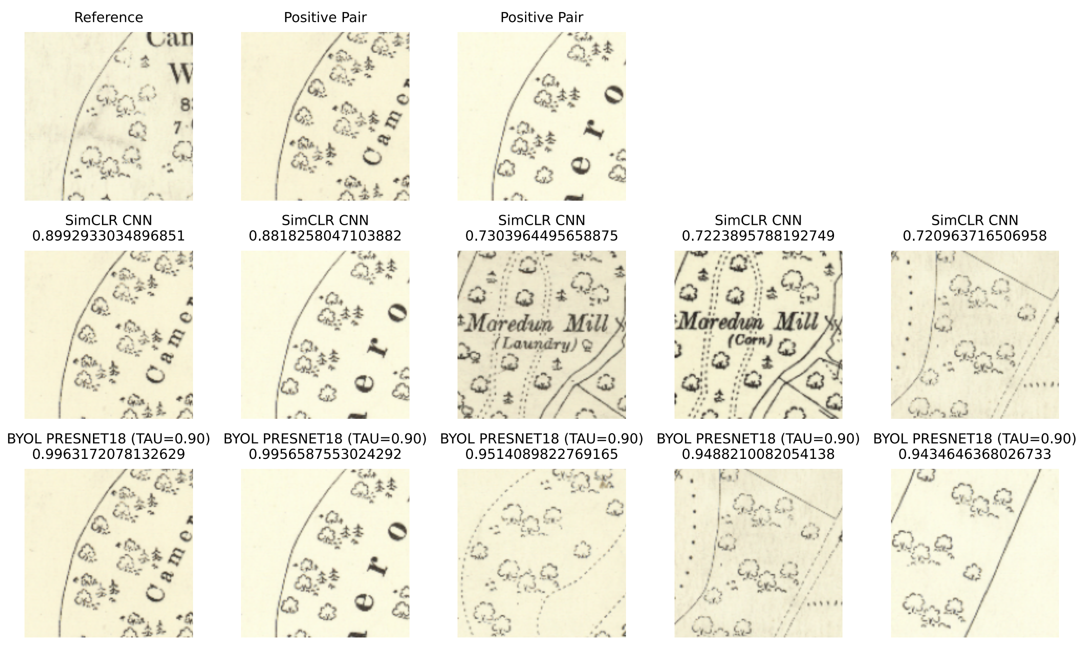
Reference
Positive Pair
Positive Pair
SimCLR CNN 0.8992933034896851
SimCLR CNN 0.8818258047103882
SimCLR CNN 0.7303964495658875
SimCLR CNN 0.7223895788192749
SimCLR CNN 0.720963716506958
BYOL PRESNET18 (TAU=0.90) 0.9963172078132629
BYOL PRESNET18 (TAU=0.90) 0.9956587553024292
BYOL PRESNET18 (TAU=0.90) 0.9514089822769165
BYOL PRESNET18 (TAU=0.90) 0.9488210082054138
BYOL PRESNET18 (TAU=0.90) 0.9434646368026733

Figure D.8: Here I showcase how `BYOL` seems to better understand the combination of features present within the reference (empty space + sparse trees in an enclosure). Once again, both models find the correct positive paris, and there is a marked difference between these and the other patches found.

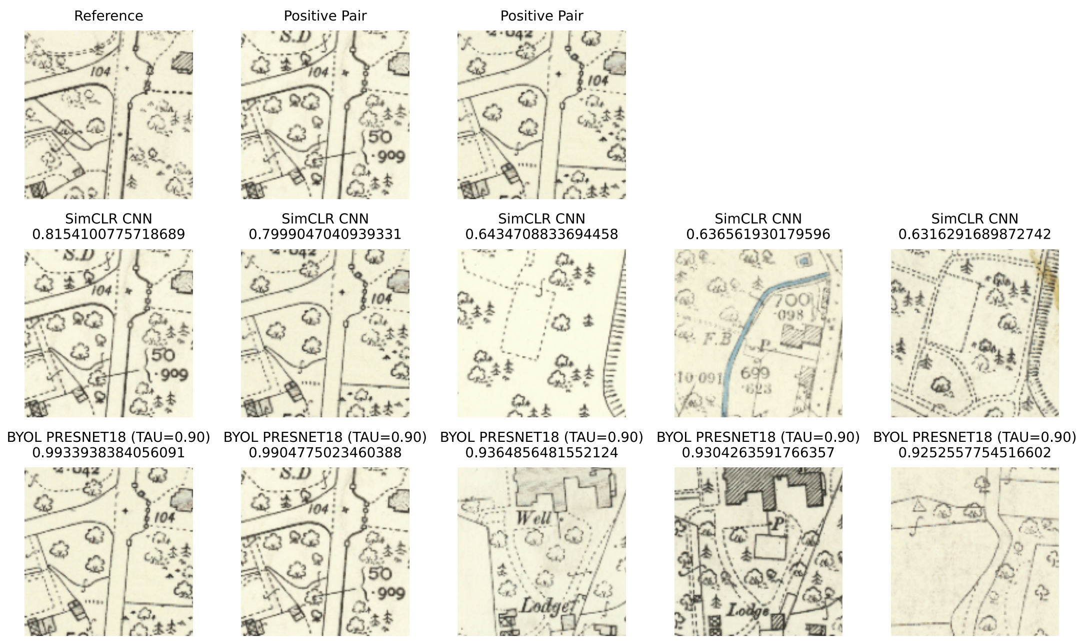
Reference
Positive Pair
Positive Pair
SimCLR CNN 0.8154100775718689
SimCLR CNN 0.7999047040939331
SimCLR CNN 0.6434708833694458
SimCLR CNN 0.636561930179596
SimCLR CNN 0.6316291689872742
BYOL PRESNET18 (TAU=0.90) 0.9933938384056091
BYOL PRESNET18 (TAU=0.90) 0.9904775023460388
BYOL PRESNET18 (TAU=0.90) 0.9364856481552124
BYOL PRESNET18 (TAU=0.90) 0.9304263591766357
BYOL PRESNET18 (TAU=0.90) 0.9252557754516602

D.2.2 `GeoSimCLR`

D.2.2.1 Weight = 0.7

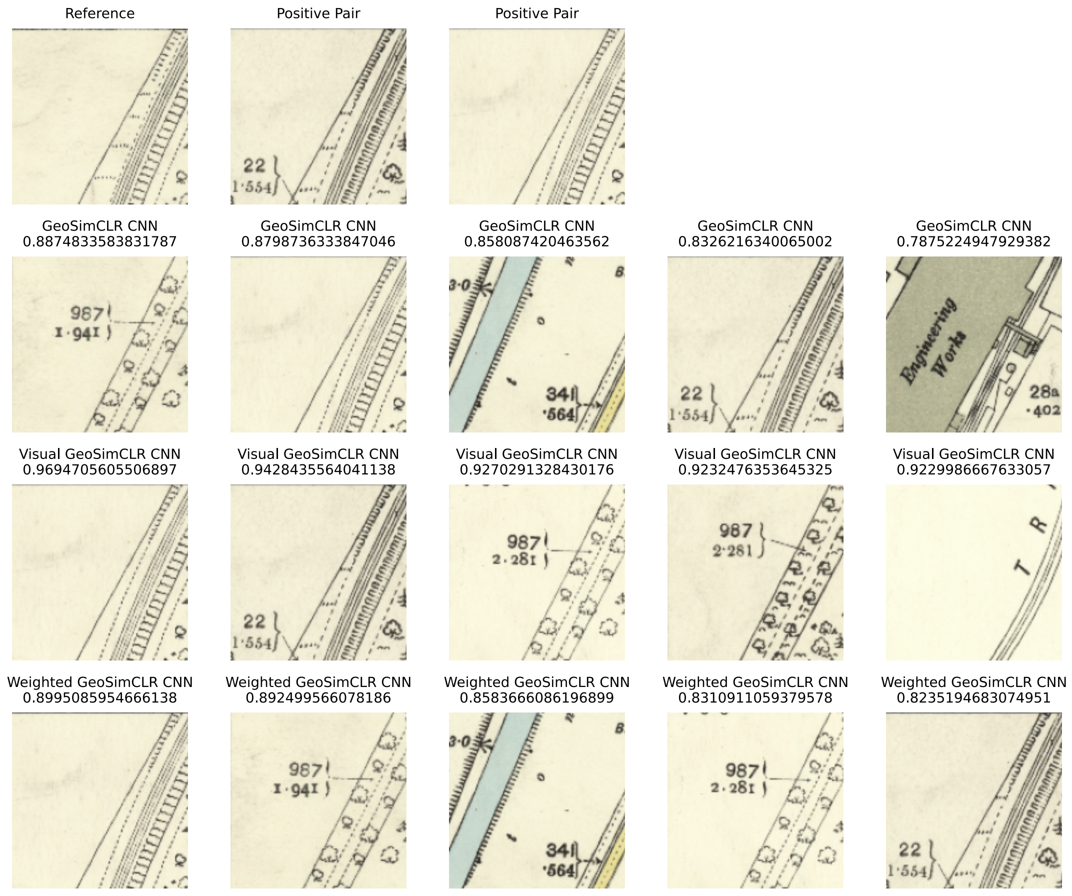
Reference
Positive Pair
Positive Pair
GeoSimCLR CNN 0.8874833583831787
GeoSimCLR CNN 0.8798736333847046
GeoSimCLR CNN 0.858087420463562
GeoSimCLR CNN 0.8326216340065002
GeoSimCLR CNN 0.7875224947929382
Visual GeoSimCLR CNN 0.9694705605506897
Visual GeoSimCLR CNN 0.9428435564041138
Visual GeoSimCLR CNN 0.9270291328430176
Visual GeoSimCLR CNN 0.9232476353645325
Visual GeoSimCLR CNN 0.9229986667633057
Weighted GeoSimCLR CNN 0.8995085954666138
Weighted GeoSimCLR CNN 0.892499566078186
Weighted GeoSimCLR CNN 0.8583666086196899
Weighted GeoSimCLR CNN 0.8310911059379578
Weighted GeoSimCLR CNN 0.8235194683074951

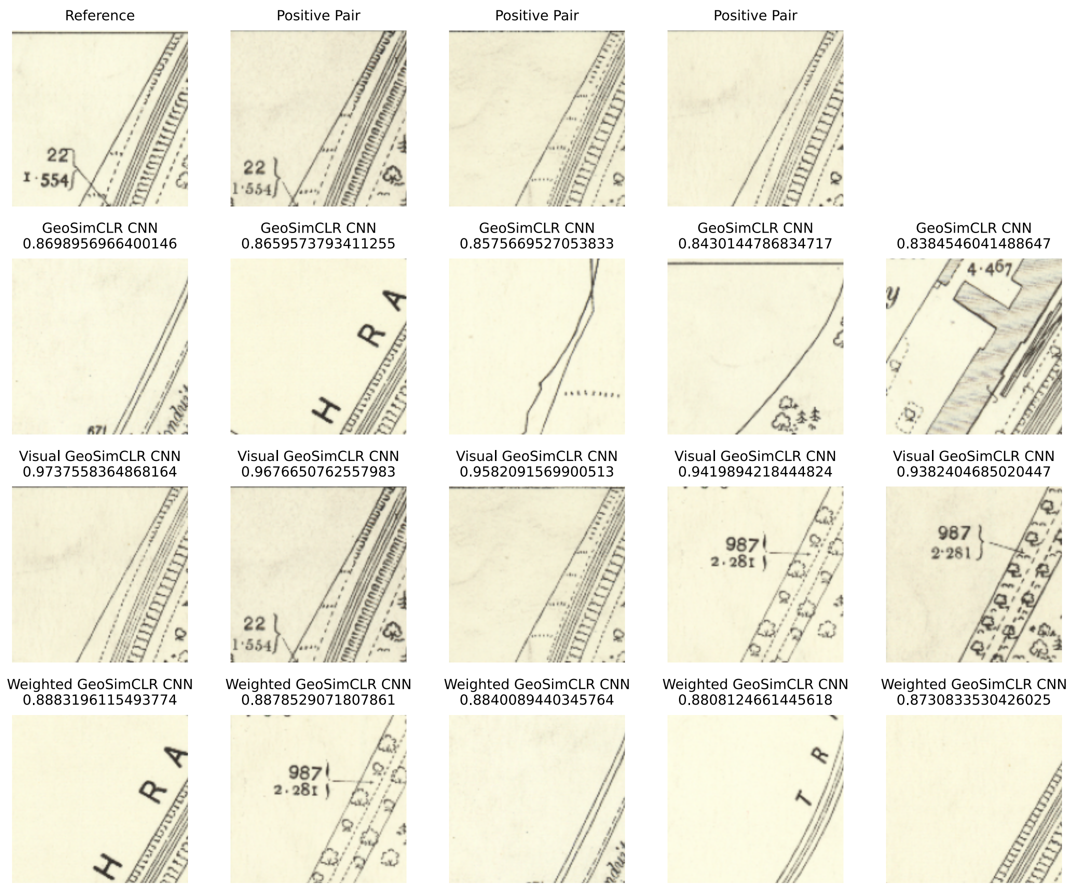
Reference
Positive Pair
Positive Pair
Positive Pair
GeoSimCLR CNN 0.8698956966400146
GeoSimCLR CNN 0.8659573793411255
GeoSimCLR CNN 0.8575669527053833
GeoSimCLR CNN 0.8430144786834717
GeoSimCLR CNN 0.8384546041488647
Visual GeoSimCLR CNN 0.9737558364868164
Visual GeoSimCLR CNN 0.9676650762557983
Visual GeoSimCLR CNN 0.9582091569900513
Visual GeoSimCLR CNN 0.9419894218444824
Visual GeoSimCLR CNN 0.9382404685020447
Weighted GeoSimCLR CNN 0.8883196115493774
Weighted GeoSimCLR CNN 0.8878529071807861
Weighted GeoSimCLR CNN 0.8840089440345764
Weighted GeoSimCLR CNN 0.8808124661445618
Weighted GeoSimCLR CNN 0.8730833530426025

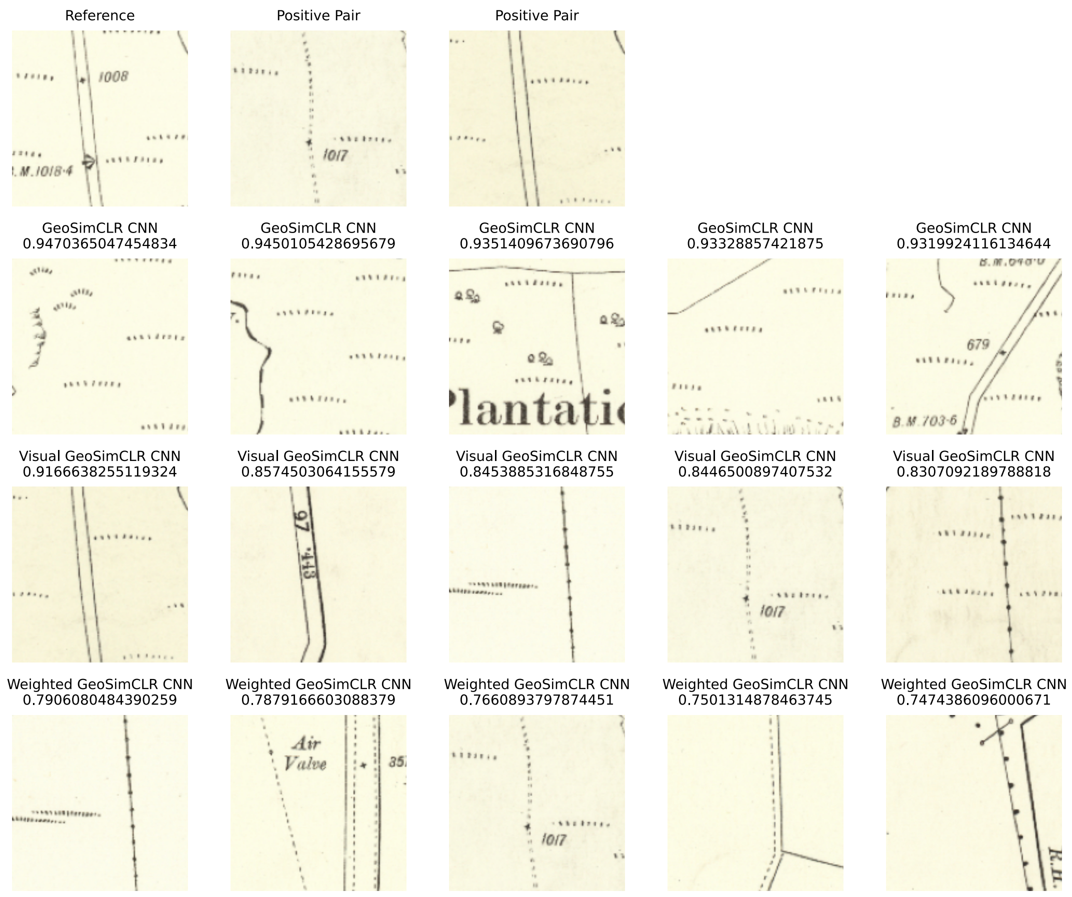
Reference
Positive Pair
Positive Pair
GeoSimCLR CNN 0.9470365047454834
GeoSimCLR CNN 0.9450105428695679
GeoSimCLR CNN 0.9351409673690796
GeoSimCLR CNN 0.93328857421875
GeoSimCLR CNN 0.9319924116134644
Visual GeoSimCLR CNN 0.9166638255119324
Visual GeoSimCLR CNN 0.8574503064155579
Visual GeoSimCLR CNN 0.8453885316848755
Visual GeoSimCLR CNN 0.8446500897407532
Visual GeoSimCLR CNN 0.8307092189788818
Weighted GeoSimCLR CNN 0.7906080484390259
Weighted GeoSimCLR CNN 0.7879166603088379
Weighted GeoSimCLR CNN 0.7660893797874451
Weighted GeoSimCLR CNN 0.7501314878463745
Weighted GeoSimCLR CNN 0.7474386096000671

D.2.2.2 Weight = 0.9

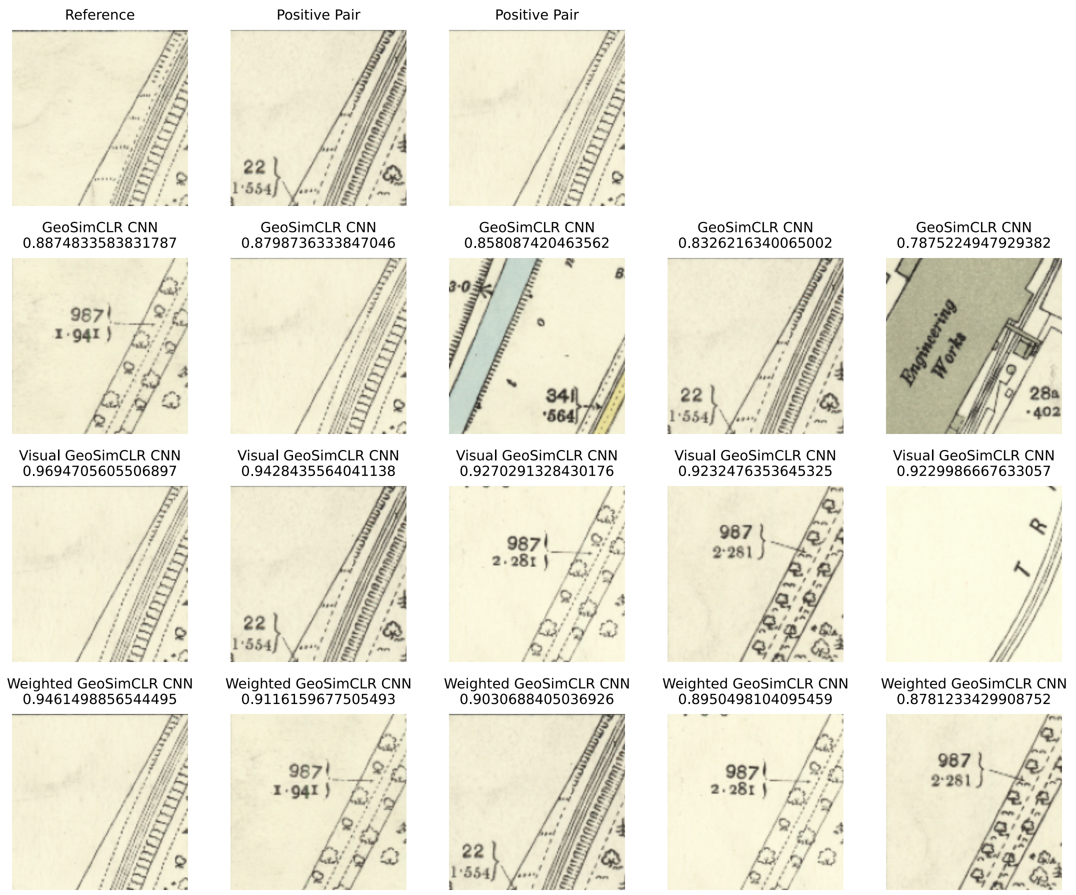
Reference
Positive Pair
Positive Pair
GeoSimCLR CNN 0.8874833583831787
GeoSimCLR CNN 0.8798736333847046
GeoSimCLR CNN 0.858087420463562
GeoSimCLR CNN 0.8326216340065002
GeoSimCLR CNN 0.7875224947929382
Visual GeoSimCLR CNN 0.9694705605506897
Visual GeoSimCLR CNN 0.9428435564041138
Visual GeoSimCLR CNN 0.9270291328430176
Visual GeoSimCLR CNN 0.9232476353645325
Visual GeoSimCLR CNN 0.9229986667633057
Weighted GeoSimCLR CNN 0.9461498856544495
Weighted GeoSimCLR CNN 0.9116159677505493
Weighted GeoSimCLR CNN 0.9030688405036926
Weighted GeoSimCLR CNN 0.8950498104095459
Weighted GeoSimCLR CNN 0.8781233429908752

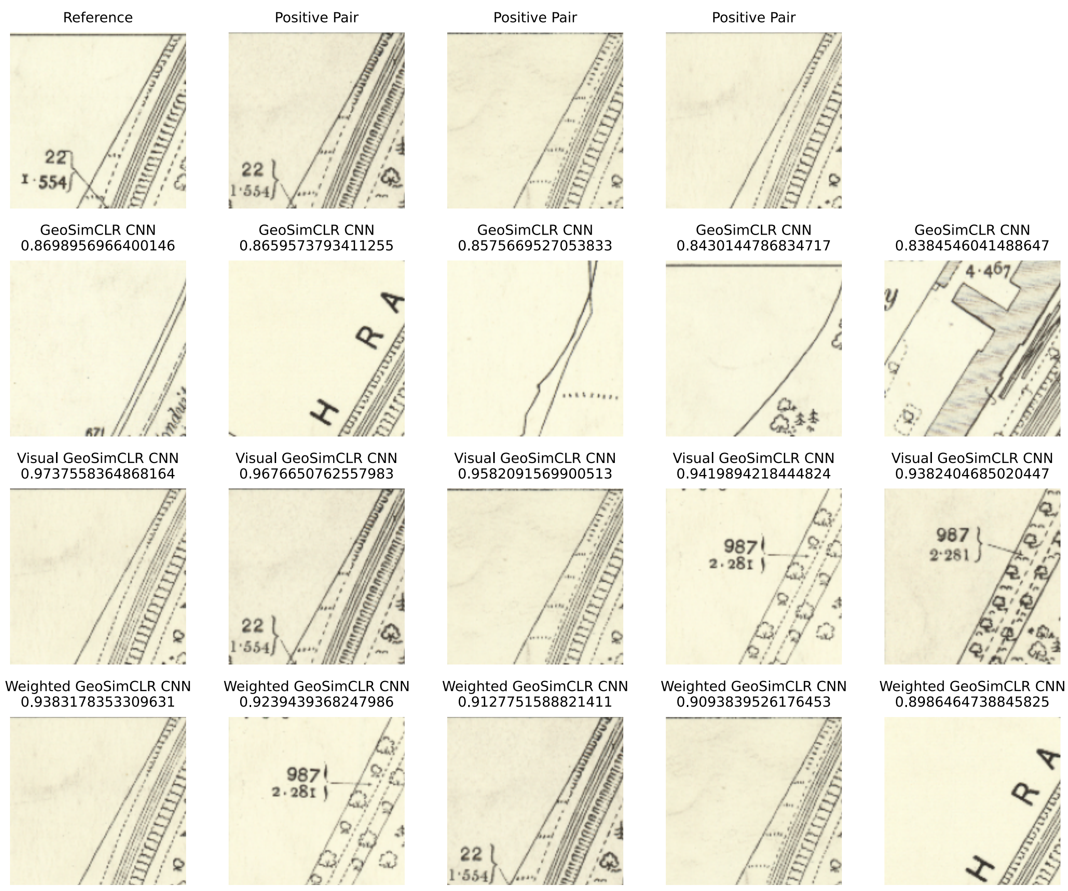
Reference
Positive Pair
Positive Pair
Positive Pair
GeoSimCLR CNN 0.8698956966400146
GeoSimCLR CNN 0.8659573793411255
GeoSimCLR CNN 0.8575669527053833
GeoSimCLR CNN 0.8430144786834717
GeoSimCLR CNN 0.8384546041488647
Visual GeoSimCLR CNN 0.9737558364868164
Visual GeoSimCLR CNN 0.9676650762557983
Visual GeoSimCLR CNN 0.9582091569900513
Visual GeoSimCLR CNN 0.9419894218444824
Visual GeoSimCLR CNN 0.9382404685020447
Weighted GeoSimCLR CNN 0.9383178353309631
Weighted GeoSimCLR CNN 0.9239439368247986
Weighted GeoSimCLR CNN 0.9127751588821411
Weighted GeoSimCLR CNN 0.9093839526176453
Weighted GeoSimCLR CNN 0.8986464738845825

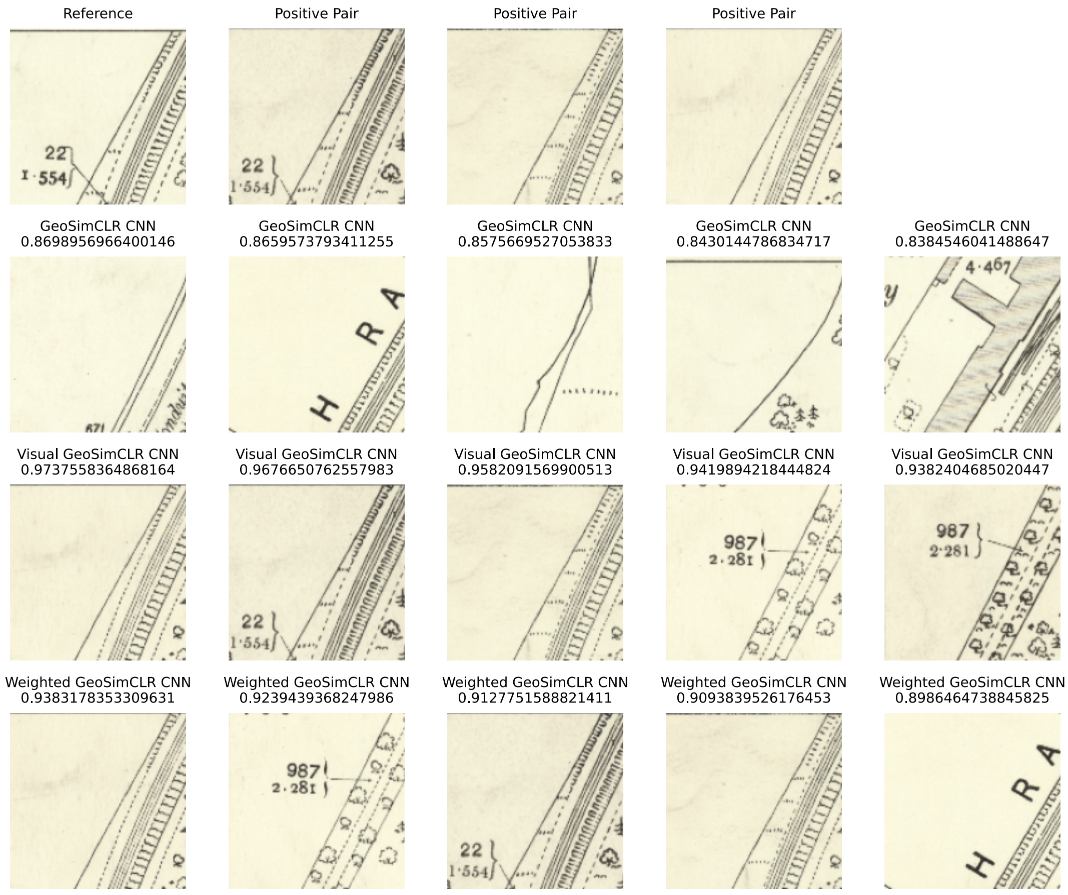
Reference
Positive Pair
Positive Pair
Positive Pair
GeoSimCLR CNN 0.8698956966400146
GeoSimCLR CNN 0.8659573793411255
GeoSimCLR CNN 0.8575669527053833
GeoSimCLR CNN 0.8430144786834717
GeoSimCLR CNN 0.8384546041488647
Visual GeoSimCLR CNN 0.9737558364868164
Visual GeoSimCLR CNN 0.9676650762557983
Visual GeoSimCLR CNN 0.9582091569900513
Visual GeoSimCLR CNN 0.9419894218444824
Visual GeoSimCLR CNN 0.9382404685020447
Weighted GeoSimCLR CNN 0.9383178353309631
Weighted GeoSimCLR CNN 0.9239439368247986
Weighted GeoSimCLR CNN 0.9127751588821411
Weighted GeoSimCLR CNN 0.9093839526176453
Weighted GeoSimCLR CNN 0.8986464738845825

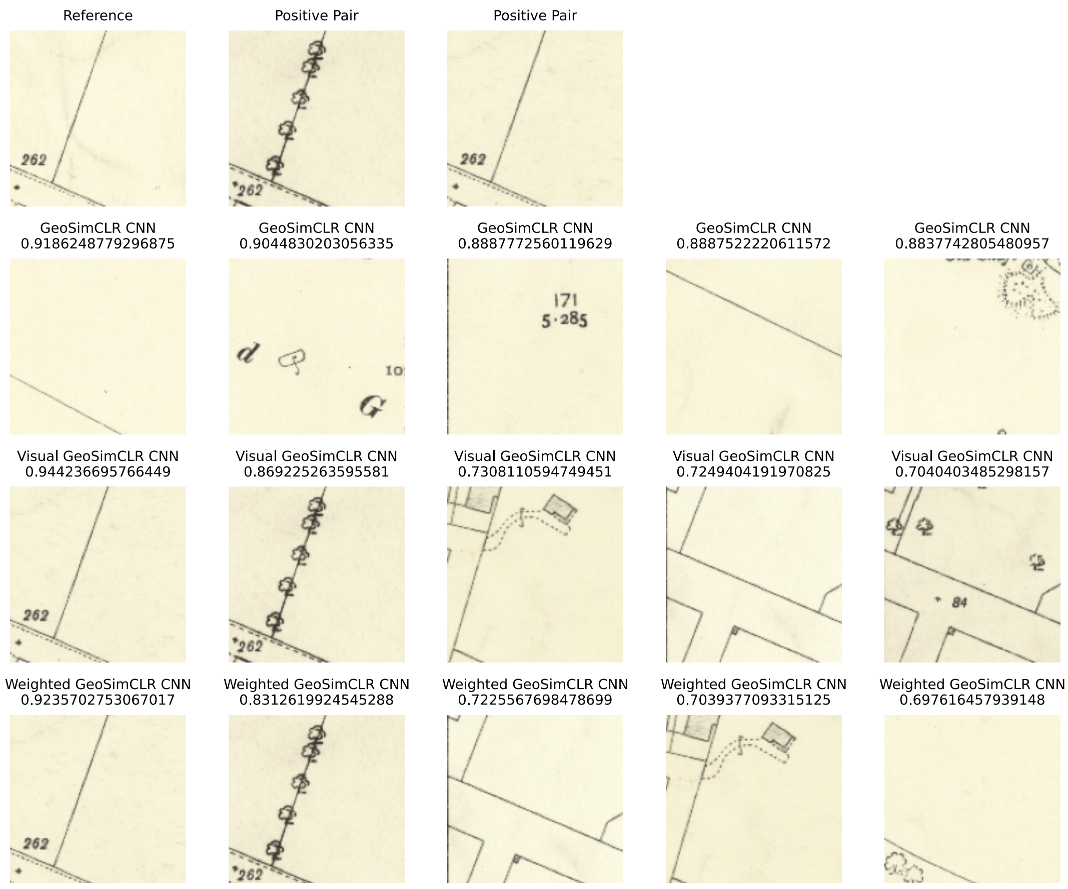
Reference
Positive Pair
Positive Pair
GeoSimCLR CNN 0.9186248779296875
GeoSimCLR CNN 0.9044830203056335
GeoSimCLR CNN 0.8887772560119629
GeoSimCLR CNN 0.8887522220611572
GeoSimCLR CNN 0.8837742805480957
Visual GeoSimCLR CNN 0.944236695766449
Visual GeoSimCLR CNN 0.869225263595581
Visual GeoSimCLR CNN 0.7308110594749451
Visual GeoSimCLR CNN 0.7249404191970825
Visual GeoSimCLR CNN 0.7040403485298157
Weighted GeoSimCLR CNN 0.9235702753067017
Weighted GeoSimCLR CNN 0.8312619924545288
Weighted GeoSimCLR CNN 0.7225567698478699
Weighted GeoSimCLR CNN 0.7039377093315125
Weighted GeoSimCLR CNN 0.697616457939148

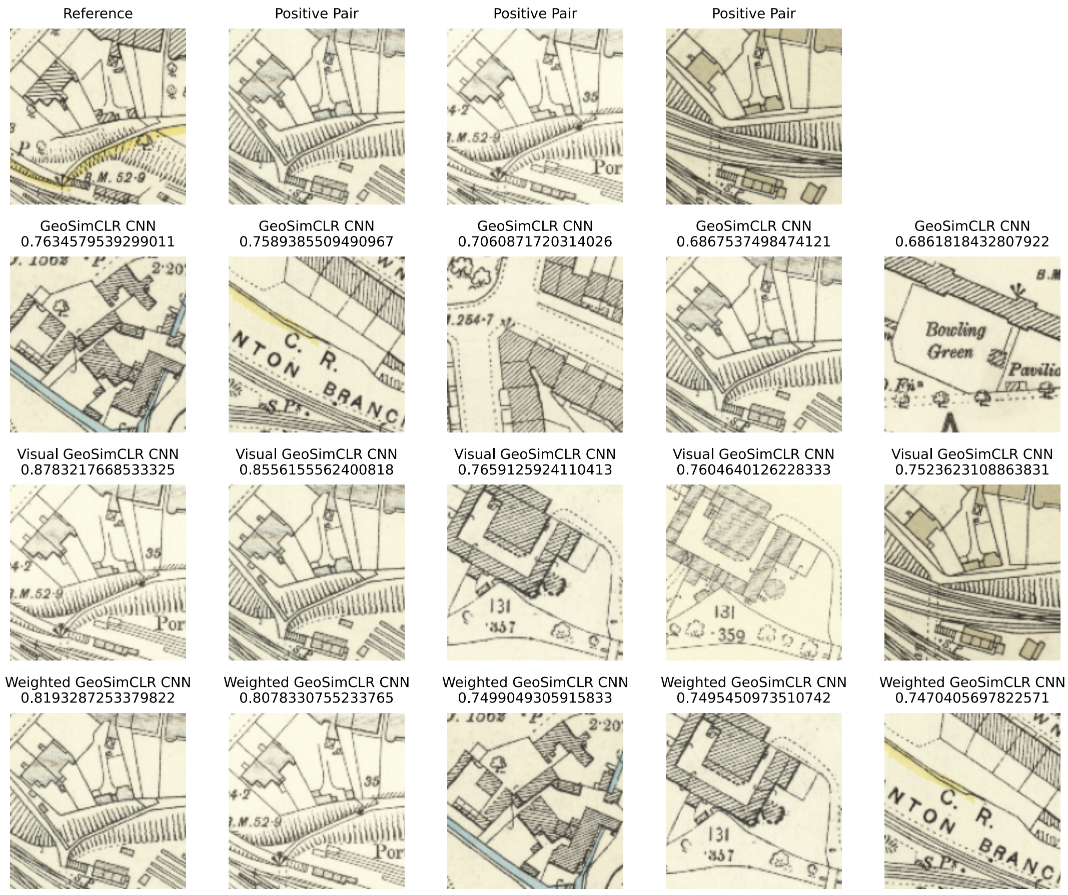
Reference
Positive Pair
Positive Pair
Positive Pair
GeoSimCLR CNN 0.7634579539299011
GeoSimCLR CNN 0.7589385509490967
GeoSimCLR CNN 0.7060871720314026
GeoSimCLR CNN 0.6867537498474121
GeoSimCLR CNN 0.6861818432807922
Visual GeoSimCLR CNN 0.8783217668533325
Visual GeoSimCLR CNN 0.8556155562400818
Visual GeoSimCLR CNN 0.7659125924110413
Visual GeoSimCLR CNN 0.7604640126228333
Visual GeoSimCLR CNN 0.7523623108863831
Weighted GeoSimCLR CNN 0.8193287253379822
Weighted GeoSimCLR CNN 0.8078330755233765
Weighted GeoSimCLR CNN 0.7499049305915833
Weighted GeoSimCLR CNN 0.7495450973510742
Weighted GeoSimCLR CNN 0.7470405697822571

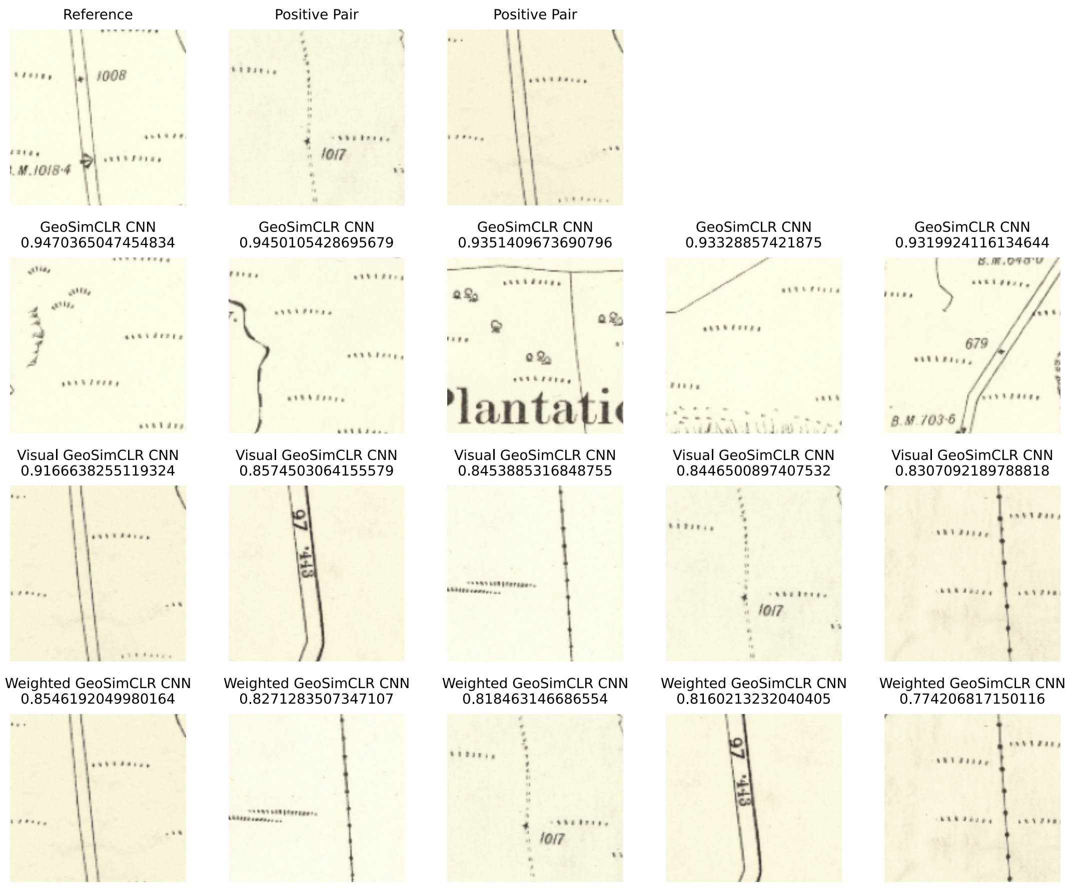
Reference
Positive Pair
Positive Pair
GeoSimCLR CNN 0.9470365047454834
GeoSimCLR CNN 0.9450105428695679
GeoSimCLR CNN 0.9351409673690796
GeoSimCLR CNN 0.93328857421875
GeoSimCLR CNN 0.9319924116134644
Visual GeoSimCLR CNN 0.9166638255119324
Visual GeoSimCLR CNN 0.8574503064155579
Visual GeoSimCLR CNN 0.8453885316848755
Visual GeoSimCLR CNN 0.8446500897407532
Visual GeoSimCLR CNN 0.8307092189788818
Weighted GeoSimCLR CNN 0.8546192049980164
Weighted GeoSimCLR CNN 0.8271283507347107
Weighted GeoSimCLR CNN 0.818463146686554
Weighted GeoSimCLR CNN 0.8160213232040405
Weighted GeoSimCLR CNN 0.774206817150116

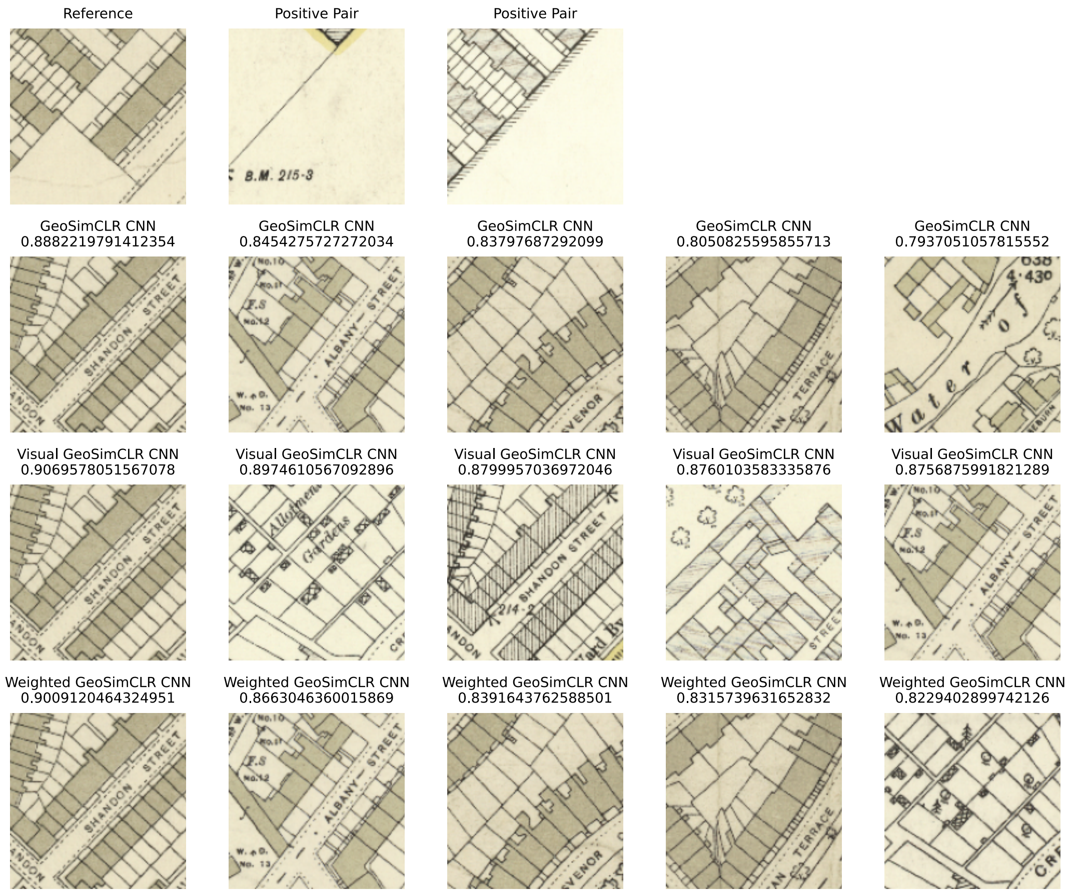
Reference
Positive Pair
Positive Pair
GeoSimCLR CNN 0.8882219791412354
GeoSimCLR CNN 0.8454275727272034
GeoSimCLR CNN 0.83797687292099
GeoSimCLR CNN 0.8050825595855713
GeoSimCLR CNN 0.7937051057815552
Visual GeoSimCLR CNN 0.9069578051567078
Visual GeoSimCLR CNN 0.8974610567092896
Visual GeoSimCLR CNN 0.8799957036972046
Visual GeoSimCLR CNN 0.8760103583335876
Visual GeoSimCLR CNN 0.8756875991821289
Weighted GeoSimCLR CNN 0.9009120464324951
Weighted GeoSimCLR CNN 0.8663046360015869
Weighted GeoSimCLR CNN 0.8391643762588501
Weighted GeoSimCLR CNN 0.8315739631652832
Weighted GeoSimCLR CNN 0.8229402899742126

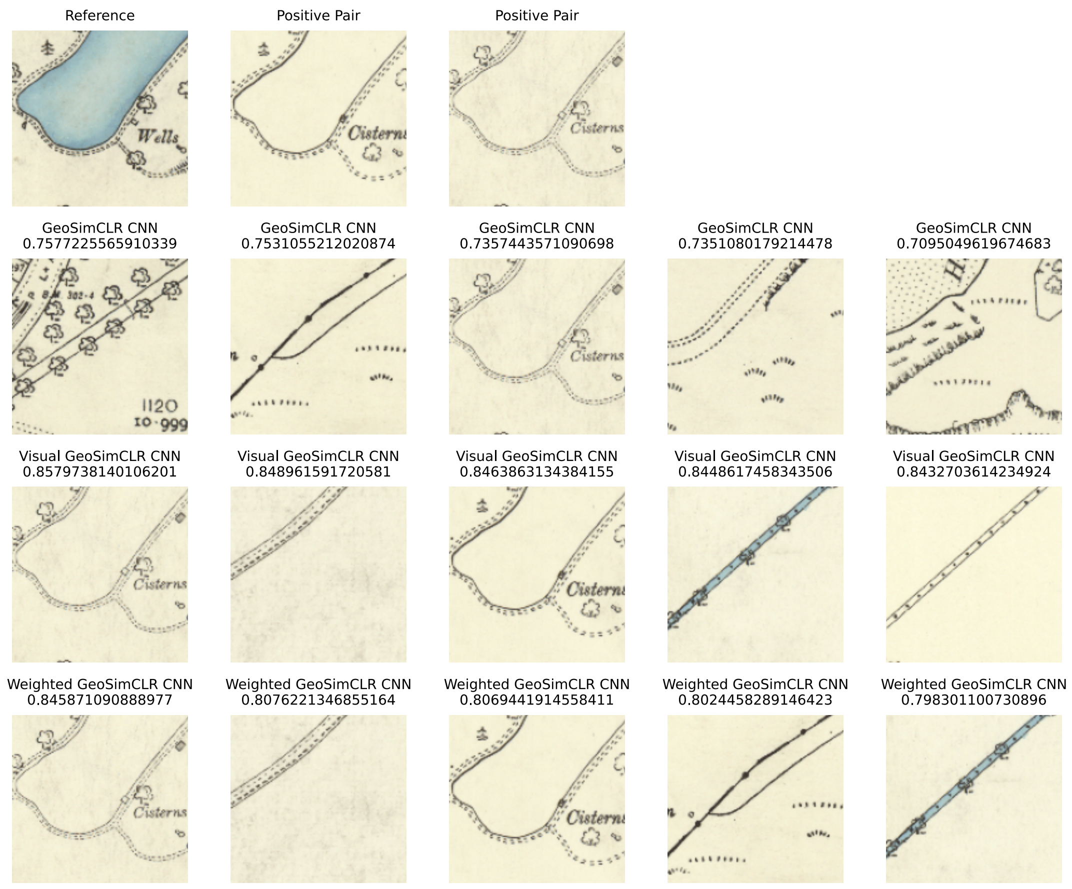
Reference
Positive Pair
Positive Pair
GeoSimCLR CNN 0.7577225565910339
GeoSimCLR CNN 0.7531055212020874
GeoSimCLR CNN 0.7357443571090698
GeoSimCLR CNN 0.7351080179214478
GeoSimCLR CNN 0.7095049619674683
Visual GeoSimCLR CNN 0.8579738140106201
Visual GeoSimCLR CNN 0.848961591720581
Visual GeoSimCLR CNN 0.8463863134384155
Visual GeoSimCLR CNN 0.8448617458343506
Visual GeoSimCLR CNN 0.8432703614234924
Weighted GeoSimCLR CNN 0.845871090888977
Weighted GeoSimCLR CNN 0.8076221346855164
Weighted GeoSimCLR CNN 0.8069441914558411
Weighted GeoSimCLR CNN 0.8024458289146423
Weighted GeoSimCLR CNN 0.798301100730896

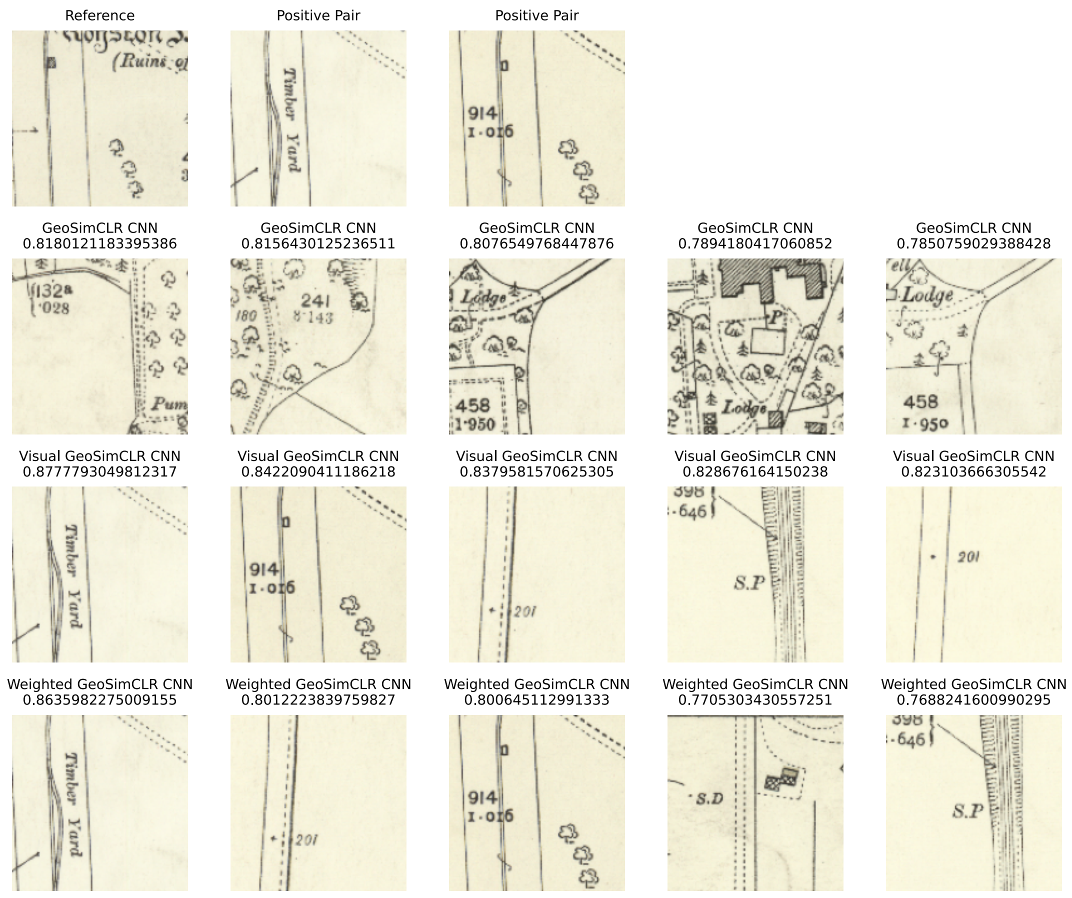
Reference
Positive Pair
Positive Pair
GeoSimCLR CNN 0.8180121183395386
GeoSimCLR CNN 0.8156430125236511
GeoSimCLR CNN 0.8076549768447876
GeoSimCLR CNN 0.7894180417060852
GeoSimCLR CNN 0.7850759029388428
Visual GeoSimCLR CNN 0.8777793049812317
Visual GeoSimCLR CNN 0.8422090411186218
Visual GeoSimCLR CNN 0.8379581570625305
Visual GeoSimCLR CNN 0.828676164150238
Visual GeoSimCLR CNN 0.823103666305542
Weighted GeoSimCLR CNN 0.8635982275009155
Weighted GeoSimCLR CNN 0.8012223839759827
Weighted GeoSimCLR CNN 0.800645112991333
Weighted GeoSimCLR CNN 0.7705303430557251
Weighted GeoSimCLR CNN 0.7688241600990295

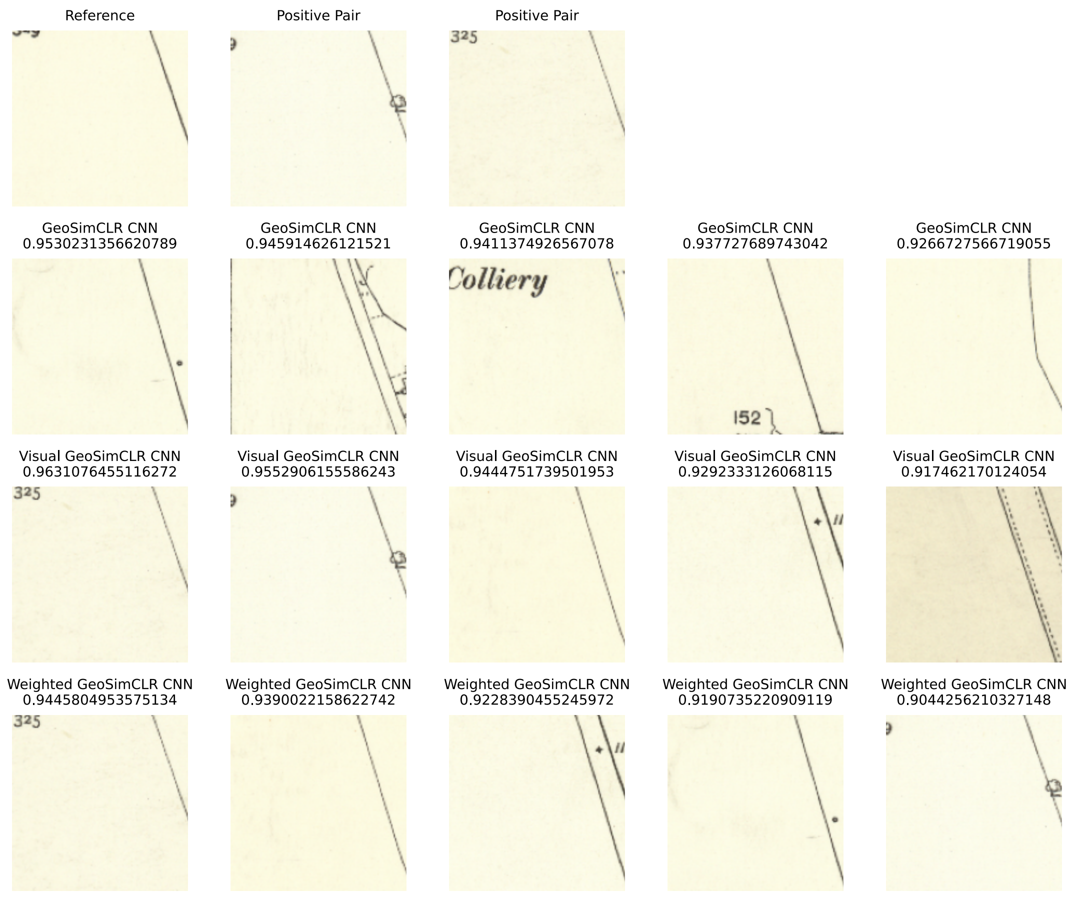
Reference
Positive Pair
Positive Pair
GeoSimCLR CNN 0.9530231356620789
GeoSimCLR CNN 0.945914626121521
GeoSimCLR CNN 0.9411374926567078
GeoSimCLR CNN 0.937727689743042
GeoSimCLR CNN 0.9266727566719055
Visual GeoSimCLR CNN 0.9631076455116272
Visual GeoSimCLR CNN 0.9552906155586243
Visual GeoSimCLR CNN 0.9444751739501953
Visual GeoSimCLR CNN 0.9292333126068115
Visual GeoSimCLR CNN 0.917462170124054
Weighted GeoSimCLR CNN 0.9445804953575134
Weighted GeoSimCLR CNN 0.9390022158622742
Weighted GeoSimCLR CNN 0.9228390455245972
Weighted GeoSimCLR CNN 0.9190735220909119
Weighted GeoSimCLR CNN 0.9044256210327148